

**Multi-metallic electrocatalysts as emerging class of materials  
opportunities and challenges in the synthesis, characterization, and applications**

Israr, Muhammad; Humayun, Muhammad; Suliman, Munzir H.; Abdinejad, Maryam; Rasheed, Tahir; Helal, Aasif; Khan, Iltaf; Bououdina, Mohamed; Wang, Chundong; Usman, Muhammad

**DOI**

[10.1080/01614940.2024.2347479](https://doi.org/10.1080/01614940.2024.2347479)

**Publication date**

2024

**Document Version**

Final published version

**Published in**

Catalysis Reviews - Science and Engineering

**Citation (APA)**

Israr, M., Humayun, M., Suliman, M. H., Abdinejad, M., Rasheed, T., Helal, A., Khan, I., Bououdina, M., Wang, C., & Usman, M. (2024). Multi-metallic electrocatalysts as emerging class of materials: opportunities and challenges in the synthesis, characterization, and applications. *Catalysis Reviews - Science and Engineering*. <https://doi.org/10.1080/01614940.2024.2347479>

**Important note**

To cite this publication, please use the final published version (if applicable).  
Please check the document version above.

**Copyright**

Other than for strictly personal use, it is not permitted to download, forward or distribute the text or part of it, without the consent of the author(s) and/or copyright holder(s), unless the work is under an open content license such as Creative Commons.

**Takedown policy**

Please contact us and provide details if you believe this document breaches copyrights.  
We will remove access to the work immediately and investigate your claim.

***Green Open Access added to TU Delft Institutional Repository***

***'You share, we take care!' - Taverne project***

**<https://www.openaccess.nl/en/you-share-we-take-care>**

Otherwise as indicated in the copyright section: the publisher is the copyright holder of this work and the author uses the Dutch legislation to make this work public.



# Catalysis Reviews

## Science and Engineering

ISSN: (Print) (Online) Journal homepage: [www.tandfonline.com/journals/lctr20](http://www.tandfonline.com/journals/lctr20)

## Multi-metallic electrocatalysts as emerging class of materials: opportunities and challenges in the synthesis, characterization, and applications

Muhammad Israr, Muhammad Humayun, Munzir H. Suliman, Maryam Abdinejad, Tahir Rasheed, Aasif Helal, Iltaf Khan, Mohamed Bououdina, Chundong Wang & Muhammad Usman

**To cite this article:** Muhammad Israr, Muhammad Humayun, Munzir H. Suliman, Maryam Abdinejad, Tahir Rasheed, Aasif Helal, Iltaf Khan, Mohamed Bououdina, Chundong Wang & Muhammad Usman (28 May 2024): Multi-metallic electrocatalysts as emerging class of materials: opportunities and challenges in the synthesis, characterization, and applications, *Catalysis Reviews*, DOI: [10.1080/01614940.2024.2347479](https://doi.org/10.1080/01614940.2024.2347479)

**To link to this article:** <https://doi.org/10.1080/01614940.2024.2347479>



Published online: 28 May 2024.



Submit your article to this journal [↗](#)



Article views: 82



View related articles [↗](#)













View Crossmark data [↗](#)

RESEARCH ARTICLE



# Multi-metallic electrocatalysts as emerging class of materials: opportunities and challenges in the synthesis, characterization, and applications

Muhammad Israr <sup>a#</sup>, Muhammad Humayun <sup>#</sup>, Munzir H. Suliman <sup>c</sup>,  
Maryam Abdinejad <sup>d</sup>, Tahir Rasheed <sup>e</sup>, Aasif Helal <sup>c</sup>, Iltaf Khan <sup>c</sup>,  
Mohamed Bououdina <sup>f</sup>, Chundong Wang <sup>b,f</sup>, and Muhammad Usman <sup>c</sup>

<sup>a</sup>Department of Chemistry, Tsinghua University, Beijing, China; <sup>b</sup>School of Integrated Circuits, Wuhan National Laboratory for Optoelectronics, Huazhong University of Science and Technology, Wuhan, P. R. China; <sup>c</sup>Interdisciplinary Research Center for Hydrogen Technologies and Carbon Management (IRC-HTCM), King Fahd University of Petroleum and Minerals (KFUPM), Dhahran, Saudi Arabia; <sup>d</sup>Materials for Energy Conversion and Storage (MECS), Department of Chemical Engineering, the Delft University of Technology, Delft, The Netherlands; <sup>e</sup>Interdisciplinary Research Center for Advanced Materials, King Fahd University of Petroleum and Minerals (KFUPM), Dhahran, Saudi Arabia; <sup>f</sup>Energy, Water, and Environment Lab, College of Humanities and Sciences, Prince Sultan University, Riyadh, Saudi Arabia

## ABSTRACT



Nowadays, extensive efforts have been devoted to the fabrication and design of metalbased catalysts with high activity, selectivity, and stability. Theoretical and experimental investigations have empowered the construction of a variety of techniques to tune the catalytic efficiency of catalysts by monitoring their size, morphology, composition, and crystal structure. Multimetal catalysts (MMCs) provide a revolutionary synergistic effect between metals, which is a promising strategy to tune and enhance the catalysts' productivity and product selectivity. The purpose of this article is to familiarize readers with the most up-to-date information regarding the synthesis and classification of MMCs. The key roles of MMCs electrocatalysts in a variety of applications such as CO<sub>2</sub> conversion via electrochemical CO<sub>2</sub> reduction reaction (ECO<sub>2</sub>RR), H<sub>2</sub> evolution reaction (HER), O<sub>2</sub> evolution reaction (OER), O<sub>2</sub> reduction reaction (ORR), N<sub>2</sub> reduction reaction (NRR), methanol oxidation reaction (MOR), ethanol oxidation reaction (EOR), formic acid oxidation reaction (FAOR), and urea oxidation reaction (UOR) are summarized. This review also addressed the challenges and prospects for multimetallic catalyst design, characterization, and applications. This review article will provide a clear roadmap for the research and progress of multimetallic catalysts for electrocatalytic applications.

## ARTICLE HISTORY

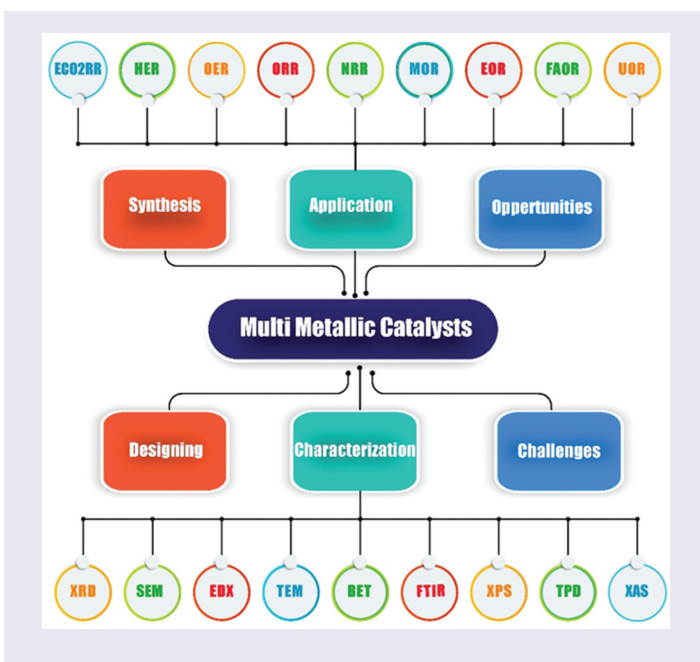
Received 10 June 2023  
Accepted 20 April 2024

## KEYWORDS

Bimetallic; catalysis; catalysts design; electrochemistry; multi-metallic

**CONTACT** Muhammad Usman  [muhammadu@kfupm.edu.sa](mailto:muhammadu@kfupm.edu.sa)  Interdisciplinary Research Center for Hydrogen Technologies and Carbon Management (IRC-HTCM), King Fahd University of Petroleum and Minerals (KFUPM), Dhahran 31261, Kingdom of Saudi Arabia

<sup>#</sup>These authors contributed equally to this work.



## 1. Introduction

The development of sustainable energy sources that could minimize our reliance on conventional fossil fuels relies heavily on electrocatalysis.<sup>[1–7]</sup> Electrocatalytic energy conversion techniques can only be applied effectively if catalysts with exceptional activity, selectivity, and stability are readily available.<sup>[8–11]</sup> Catalysts based on noble metal nanoparticles (i.e. Ru, Au, Ir, Pt, etc.) have been extensively used in electrocatalytic processes such as HER, CO<sub>2</sub>RR, NRR, OER, and ORR.<sup>[8–17]</sup> The weak activity, high cost, and limited availability of these metals make it difficult to find practical uses for them in industry. To combat these problems while maintaining optimal performance, researchers have concentrated heavily on creating highly efficient low-cost noble and non-noble metals-based electrocatalysts.<sup>[18–20]</sup> In this regard, monometallic catalysts have been utilized as the backbone of catalytic processes, providing unique reactivity depending on the type of metal used.<sup>[21]</sup> For instance, Dastafkan et al.<sup>[22]</sup> developed an interphasic synergy between Ni-N/Ni-C and Ni(OH)<sub>2</sub> phases for highly efficient alkaline HER, which decreased the energy barrier for adsorption and desorption of hydrogen and increased the hydroxyl intermediates. This resulted in the ready-to-serve Ni active sites that allocated a considerable number of Ni d-states at the Fermi level for allowing the co-adsorption of H<sub>ads</sub> and OH<sub>ads</sub> intermediates on the Ni-N/Ni-C moieties, and promoted the charge transfer from Ni(OH)<sub>2</sub> to Ni-N/Ni-C. In comparison to the monophasic Ni(OH)<sub>2</sub> catalyst, the Ni(OH)<sub>2</sub>@Ni-N/Ni-C catalyst

remarkably lowered the overpotentials to 102 and 113 mV to deliver  $-10$  and  $-100 \text{ mA cm}^{-2}$  current densities, respectively in alkaline electrolyte. However, monometallic catalysts often exhibit limitations in terms of selectivity, stability, and activity across different reaction environments.<sup>[23]</sup> These limitations have sparked interest into the design and fabrication of multimetallic catalysts, that perform more effectively due to synergistic interactions between various metals.<sup>[24,25]</sup>

Recently, multimetallic catalysts received considerable research interest in various electrocatalytic processes.<sup>[26–30]</sup> Due to their distinctive physicochemical features, multimetallic nanostructures could serve as cutting-edge catalysts. There has been substantial advancement in recent years toward the goal of tuning or regulating the surface strain of multimetallic nanostructures in order to increase their catalytic activity.<sup>[14–35]</sup> Multimetallic catalysts have a large number of catalytic active sites that can perform in various directions during electrocatalytic reactions, boosting the formation of the premium product, and thereby promoting the catalyst's performance.<sup>[36,37]</sup> Thus, compared to the single metal catalysts, the incorporation of multi-metal atoms in a single catalyst renders exceptional electrocatalytic performance toward various electrocatalytic processes such as HER,<sup>[38–41]</sup> OER,<sup>[15–44]</sup> ORR,<sup>[45,46]</sup> CO<sub>2</sub> RR,<sup>[26,47]</sup> etc.

It is crucial to use the parameters associated with the experiments rationally to produce multi-metallic catalysts with definite size, shape, structure, crystal phase, and composition to improve catalytic performance of multi-metallic catalysts significantly, because their catalytic performance mainly depends on these structural parameters.<sup>[48–55]</sup> Nevertheless, the fabrication process is challenging as the synthesis mechanism of multi-metallic particles is complex. Thus, highly complicated and advanced synthesis techniques have been widely developed to precisely control the structural features to achieve the desired properties. Generally, during the synthesis of multi-metallic catalysts, various ligands (surface-capping agents) are used to achieve controllable shape uniform size catalysts with good dispersion for superior electrocatalytic processes.<sup>[24,56]</sup>

As widely accepted, the performance discrepancies of catalysts could be attributed to the difference in atomic-scale characteristics such as atomic ordering, surface structuring, and spatial distribution of the elements. For instance, Zhang and coworkers<sup>[57]</sup> revealed that the ordered Pt<sub>3</sub>Mn intermetallic electrocatalysts exhibit exceptional ORR activity compared to their disordered counterpart's phase. Likewise, Li and coworkers<sup>[58]</sup> demonstrated that by altering the atomically disordered crystal phase of FePt catalyst to the ordered phase, the electrocatalyst performance and chemical stability toward ORR and HER processes could be considerably improved. Accordingly, it is inappropriate to use only the word “composition” to describe multi-metallic

catalysts. Hence, tremendous attention has been given to develop new formation protocols to modulate the multi-metallic catalysts with atomic-scale characteristics.<sup>[59–63]</sup>

A number of review articles on multi-metallic catalysts for various applications can be found in the literature.<sup>[13–68]</sup> Different from those reviews, this review is the first attempt, with a primary focus on current advances in the design, fabrication, characterization, and electrocatalytic applications of multi-metallic catalysts, as illustrated in Figure 1. Particularly, we summarize the most generally practiced synthesis approaches adopted in preparing multi-metallic catalysts with well-controlled and tunable properties. In addition, we emphasized on their standard characterization techniques and widespread electrochemical applications, including the CO<sub>2</sub>RR, HER, OER, ORR, NRR, ORR, and others. Finally, the existing challenges and future perspectives on the improvement of the electrocatalytic performance of MMCs have been well addressed.

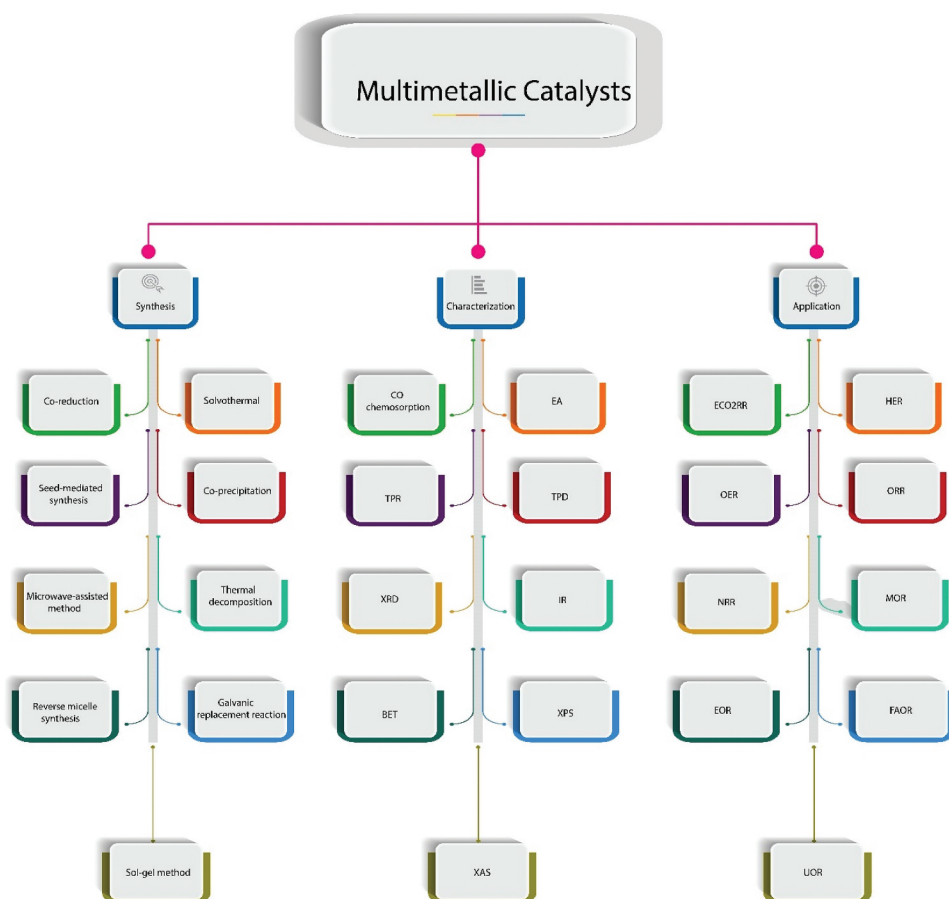


**Figure 1.** Multimetallic catalysts (MMCs) synthesis, characterization, and electrochemical applications.

## 2. Synthetic methods of multi-metallic catalysts

Multimetallic catalysts (MMCs) have been prepared using various synthetic approaches. Figure 2 summarizes the primarily used synthetic methods of MMCs.

### 2.1. Solvothermal method

The solvothermal method is a commonly employed method for synthesizing multi-metallic catalysts, which play a crucial role in diverse chemical processes and commercial applications. This technique entails the chemical transformation of metal precursors in a solvent under high temperatures and pressures, commonly within an autoclave or an enclosed vessel. Solvothermal synthesis offers a controlled atmosphere for producing nanoscale multi-metallic catalysts with precise compositions, structures, and features.<sup>[69]</sup> For instance, we fabricated a multimetallic electrocatalyst (PtNs/NiTe-Ns) through solvothermal method by decorating platinum (Pt) on nickel telluride and utilized in pH-universal and chloride tolerant HER.<sup>[70]</sup> The solvothermal approach for creating multi-metallic catalysts has both clear benefits and drawbacks. One advantage of this method is that it enables meticulous regulation of reaction conditions, leading to the formation of well-defined nanoscale structures characterized by an even distribution of particle sizes. The flexibility of this method allows for the specific fabrication of catalysts by utilizing numerous

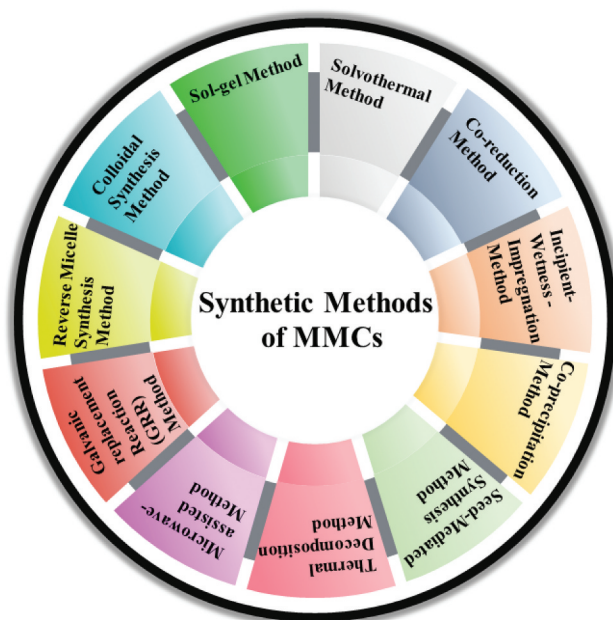


**Figure 2.** Schematic illustration of the synthetic methods of multi-metallic catalysts (MMCs).



metals to achieve synergistic effects and enhanced stability.<sup>[71,72]</sup> Solvothermal synthesis is well-suited for both research and industrial applications due to its capacity to produce products with high purity and uniformity, as well as its scalability. Nevertheless, the technique entails substantial energy consumption as a result of increased temperatures and pressures, hence reducing its environmental sustainability. The optimization of many reaction parameters, susceptibility to variations, and probable development of undesired phases pose limitations. Despite numerous disadvantages, the solvothermal method seems to be a useful technique to produce multi-metallic catalysts with specific features.<sup>[73,74]</sup> For instance, the preparation of PtCu<sub>3</sub> nanoparticles having a shape of rhombic dodecahedral can be achieved by the reaction of acetylacetonate precursors in a Teflon-lined autoclave in the existence of cetyltrimethylammonium chloride (CTAC) and n-butylamine (Figure 3a, b).<sup>[75]</sup> Along with the solvothermal method, nanomaterials could also be synthesized with metastable phases. The preparation of Pt – Ni multi pod structures with metastable close-packed hexagonal by means of Ni-rich precursor and formaldehyde (Figure 3c, d).<sup>[76]</sup>

## 2.2. Co-reduction method

The co-reduction method is a commonly used technique for producing multi-metallic catalysts. It involves the simultaneous reduction of metal precursors to produce alloyed or composites.<sup>[78]</sup> This approach has multiple benefits, such as its simple nature, low cost, and the capacity to regulate the composition by modifying the molar ratios of the metal precursors. The co-reduction approach frequently produces multi-metallic catalysts that exhibit improved catalytic activity as a result of synergistic interactions among several metals. In addition, the process generally takes place at lower temperatures in comparison to other processes, resulting in less energy use.<sup>[79]</sup> Nevertheless, there are certain limitations that arise in obtaining homogeneous dispersion of metal and controlling the size of particles. The simultaneous reduction of numerous metal ions can result in phase separation or the development of undesirable phases, which can have an impact on the catalytic efficiency.<sup>[80]</sup> Contrary to these drawbacks, the co-reduction approach is distinctive for its efficacy in yielding multi-metallic catalysts with specific compositions and features for diverse applications.<sup>[81]</sup> For instance, monomers supersaturation is prompted by the introducing suitable reducing agent, such as NaBH<sub>4</sub>, polyol, or hydrazine, into the provided precursor's solution, shadowed by the growth and nucleation methods.<sup>[26]</sup> As illustrated in Figure 3e the monodispersed nanoparticles of PtFe were achieved through co-reduction of Pt(acac)<sub>2</sub> (acac = acetylacetonate) and FeCl<sub>2</sub> by a reducer introducing, LiBEt<sub>3</sub>H, with stabilizing agents oleylamine and oleic acid (Figure 3f).<sup>[77]</sup> Additional example is the preparation of the Pd-derived alloy,<sup>[82]</sup> where a mixed metal solution of

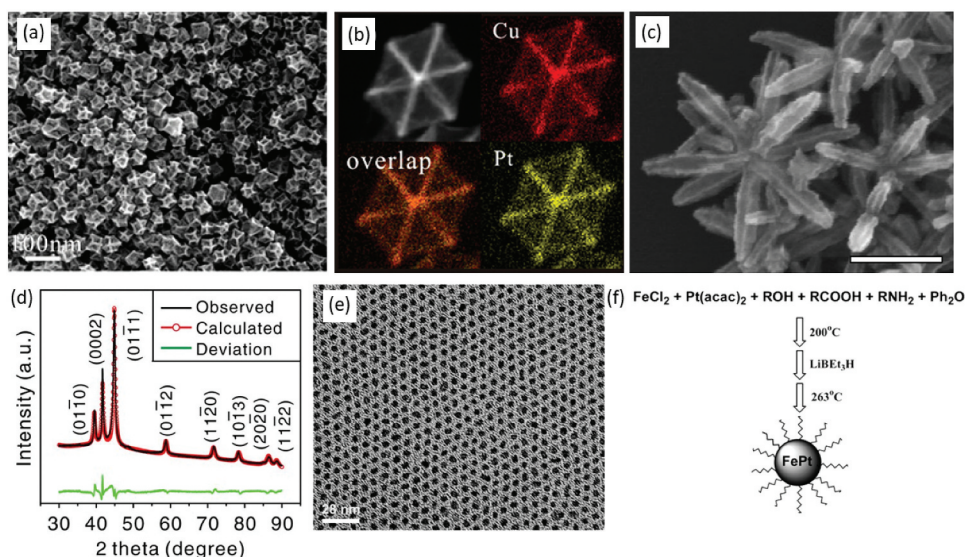


**Figure 3.** (a) SEM image, and (b) HAADF-STEM image and HAADF-STEM-EDS maps of a single ERD  $\text{PtCu}_3$  alloy nanoparticle<sup>[75]</sup> Copyright © 2014, American Chemical Society. (c) SEM image, and (d) XRD pattern of excavated  $\text{PtNi}$  nanomultipods<sup>[76]</sup> Copyright © 2017, Springer nature. (e) Bright field TEM image of a 2-D array of 4 nm  $\text{FePt}$  nanoparticles (f) Schematic representation of  $\text{FePt}$  nanoparticle preparation<sup>[77]</sup> Copyright © 2003, American Chemical Society.

acetylacetonate precursor was introduced in a heated solution comprising a borane tertbutylamine or borane morphine reductant, that reduces the precursor to  $\text{PdCu}$  and  $\text{PdCo}$  alloy NPs. Wang and coworkers<sup>[83]</sup> prepared  $\text{Pt}_3\text{Sn}$  alloy through co-reduction of  $\text{SnCl}_2$  and  $\text{PtCl}_4$  in a combined solution of oleic acid (OA) and oleylamine (OAM), using the borane tert-butylamine which works as a strong reducing agent. Another example is the synthesis of mixing mexene with Cu and Pd precursors followed by the reduction of the mixture by  $\text{NaBH}_4$  to yield Cu-Pd/Mxene for the efficient electroreduction of  $\text{CO}_2$  to formate.<sup>[84]</sup> Similar approach was used to synthesize Pd-Sn catalyst.<sup>[85]</sup>

### 2.3. Incipient wetness impregnation method

The incipient wetness impregnation process, commonly used for producing multi-metallic catalysts, entails depositing metal precursors onto a support material by leveraging the porous nature of the support to absorb the precursor solution.<sup>[86]</sup> This approach provides multiple benefits, including simplicity, the ability to easily scale-up, and an affordable cost. This technique enables precise modification of the metal loading as well as distribution over the support, thereby allowing the production of uniformly dispersed multi-metallic catalysts.<sup>[87]</sup> The impregnation method is very flexible, allowing for the incorporation of different types of metal and can

be used with a diverse array of support materials. Nevertheless, a few of the challenges that arise is the possibility of an uneven distribution of metals, which can result in the formation of clusters or the separation of different phases.<sup>[88]</sup> In addition, the potential to achieve a high metal loading might be regulated by the solubility of the metal precursors. Furthermore, the impregnation process may need to be repeated multiple times in order to adequately incorporate enough metal. Although there exist certain limitations, however, the incipient wetness impregnation approach is still frequently used and effective in developing multi-metallic catalysts with specific compositions.<sup>[89]</sup> For instance, Abruña et al.<sup>[90]</sup> described a generic synthesis method for RuM (where M = Ni, Co, Fe) particles that involved wet-impregnation of the precursor materials into a C-support followed by calcination. Furthermore, by employing three different metals as precursors, the approach could be expanded to the fabrication of tri-metallic nanoparticles.<sup>[91,92]</sup>

#### **2.4. Co-precipitation method**

The co-precipitation method is a frequently used technique for producing multi-metallic catalysts. It involves the simultaneous precipitation of metal ions onto a support material to produce nanoparticles or composite.<sup>[93]</sup> This approach provides numerous benefits, such as its ease, economical nature, and the ability to achieve substantial metal loadings. The procedure enables the integration of several metals, facilitating the development of synergistic effects in the catalyst that is produced.<sup>[94]</sup> The co-precipitation process is readily applicable to larger scales and is appropriate for producing catalysts with precise compositions and evenly distributed metal components.<sup>[95]</sup> Nevertheless, there are issues associated with the tendency for agglomeration or uneven distribution of metals, which might have an impact on the catalytic efficacy. Optimal precipitation conditions are essential for attaining the appropriate catalyst characteristics, and subsequent post-treatment procedures, such as calcination, may be required to improve the catalyst's activity and stability.<sup>[96,97]</sup> Although there exist certain limitations, yet, the co-precipitation method continues to be extensively used and flexible to synthesize multi-metallic catalysts, because in this approach, metal salts of aqueous solutions are mixed together at a specific temperature in presence of a base, which works as a precipitating agent. When the critical concentration of the solution is obtained, a burst of nucleation occurs and subsequently followed by a growth phase.<sup>[98–100]</sup> Zhou and coworkers<sup>[98]</sup> synthesized ultrathin Ni-Fe layered double-hydroxides (LDH) nanosheets through the coprecipitation method (Figure 4a). Wang and coworkers<sup>[101]</sup> reported Zr-Doped NiO nanoparticles by using this approach (Figure 4b).

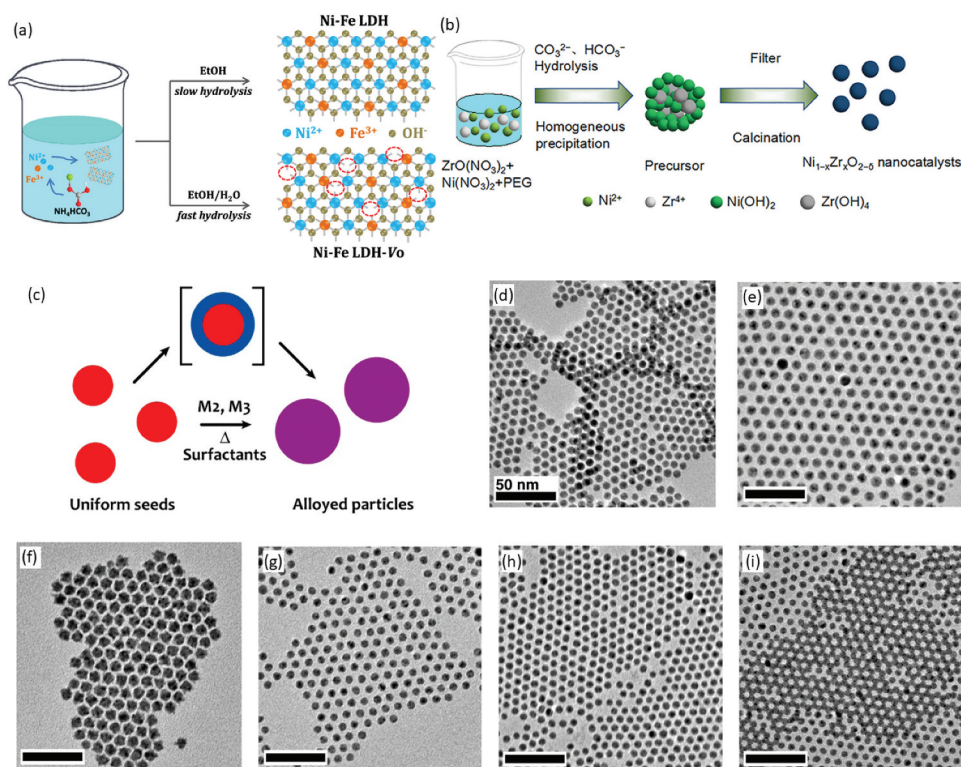


**Figure 4.** (a) Schematic illustration for synthesis of ultrathin Ni-Fe LDH-Vo nanosheets<sup>[98]</sup> Copyright © 2021 American Chemical Society and (b) Zr-doped NiO nanocatalysts ( $\text{Ni}_{1-x}\text{Zr}_x\text{O}_{2-\delta}$ )<sup>[101]</sup> Copyright © 2021 American Chemical Society. (c) synthesis mechanism of uniform bimetallic alloyed M/Au (M = Ag, Pt, Hg, Sn, and Cd) NCs and TEM images of prepared. (d) Au NC seeds, bimetallic particle, (e) Ag/Au 0.05, (f) Pt/Au 0.2, (g) Hg/Au 0.25, (h) Sn/Au 0.1, and (i) Cd/Au 0.1<sup>[102]</sup> Copyright © 2015 American Chemical Society.

## 2.5. Seed-mediated synthesis method

The seed-mediated synthesis technique is an effective approach for producing multi-metallic catalysts by precisely growing metallic nanoparticles on pre-synthesized seed particles.<sup>[103]</sup> This approach has significant benefits, such as rigorous control of particle dimensions, morphology, and composition, leading to catalysts with improved structural integrity as well as defined characteristics.<sup>[104]</sup> The step-by-step inclusion of several metal precursors enables the development of multi-metallic structures with unique compositions, promoting synergistic interactions among metals. The seed-mediated technique is very scalable and may be tuned to different support materials, allowing for the production of catalysts with precise and tailored characteristics.<sup>[105,106]</sup> Nevertheless, one of the limitations is the requirement for precise tuning of reaction conditions to avoid unregulated growth and aggregation. The synthesis can also involve many stages, hence amplifying the

complex nature and duration of the process. Considering these factors, the seed-mediated synthesis approach is unique for its ability to produce extremely precise and flexible multi-metallic catalysts with enhanced catalytic efficiency. Seed-mediated synthesis approaches consist of two types: direct secondary metals diffusion into seed particles. Core-shell nanoparticles conversion into the random alloys.<sup>[107,108]</sup> Sun et al. prepared PdCu NPs by adjusting the dispersion of Cu to Pd nanostructures at a 280°C.<sup>[109]</sup> Murray et al. fabricated a facile technique for thermal conversion of core/shell architectures to random-alloys initiated from gold particles (Figure 4c).<sup>[102]</sup> Interestingly, the temperature necessary for complete secondary metal (i.e. Pt, Ag, Hg, Cd, or Sn) diffusion varies from metal to metal (Figure 4d-i). Similarly, Au@Ag<sup>[110]</sup> and Ag@Au<sup>[111]</sup> core@shell nanoparticles are converted to randomly alloyed nanostructures.

## 2.6. Thermal decomposition

The thermal decomposition method is a flexible technique used for producing multi-metallic catalysts. It involves heating metal precursors to high temperatures, causing them to decompose and produce nanoparticles.<sup>[112]</sup> This approach provides multiple benefits, including as simplicity, fast production, and the possibility of reaching high levels of metal loading. This approach enables precise adjustment of particle size and content, hence facilitating the development of catalysts with tailored properties.<sup>[113]</sup> Thermal decomposition can be carried out using different support materials, which provides choice in the design of catalysts. Nevertheless, one of the drawbacks is the demand for precise regulation of reaction conditions to avoid the clustering of particles and to acquire an even dispersion of particles. In addition, the procedure may require the use of inert environments to avoid undesired oxidation of metal species.<sup>[114]</sup> Although this method has few limitations, yet, it remains to be an appealing technique for producing multi-metallic catalysts, especially where simplicity, speed, and variety are important factors to be considered.<sup>[79]</sup> In this method, the heat-up and hot injection processes come under the thermal decomposition category.<sup>[115]</sup> The main difference between the methods of these two procedures is the approach of accomplishing greater saturation of monomers for eruption nucleation. In the heat-up technique, precursors and other chemicals are mixed before heating up, and the continuous temperature elevation accomplishes the supersaturated monomers. On the other side, the rapid injection of organometallic complexes into an earlier heated reaction solution in the hot-injection technique prompts burst nucleation. Therefore, the hot-injection approach attributes flexibility for different preparation, including the usage of varying precursors. In contrast, the heat up procedure attributes accessibility by the lack of external process in the presence of reaction. As this method needs elevated temperatures, the increased boiling

points of organic solvents are characteristically employed. The merits in the collection of elements in this method are the basis on the use of the high temperature, allowing the metals use such as Fe, Co, and Ni, which possesses comparatively inferior reduction potentials compared to the precious metals. For example, sun's group synthesized PtFe NPs, which was accomplished by the disintegration of  $\text{Fe}(\text{CO})_5$  by adding it into a Pt precursor solution at a higher temperature and immediately reducing the Pt precursor by diol.<sup>[116-118]</sup>

## **2.7. Microwave-assisted method**

The microwave-assisted technique is an exciting methodology for producing multi-metallic catalysts, utilizing microwave irradiation to heat reaction mixtures and facilitate rapid and effective synthesis.<sup>[119]</sup> This approach has numerous benefits, such as considerably reduced reaction time, improved energy economy, and precise controlling of reaction conditions. The utilization of microwave heating facilitates precise and controlled heating, resulting in the production of evenly distributed and exceptionally crystalline multi-metallic nanoparticles with specific dimensions and compositions.<sup>[120]</sup> This approach is especially well-suited for synthesizing nanomaterials that have enhanced catalytic activity. Nevertheless, there exist some limitations, such as the possibility of improper heating and the requirement for precise parameter adjustment to avoid overheating. The microwave-assisted method's ease and performance render it an appealing choice for producing multi-metallic catalysts, particularly in applications in which fast and strictly controlled fabrication is required.<sup>[121,122]</sup> Synthesizing inorganic nanomaterials with this method gives larger quantum yields and more precision than the traditional heating process alone.<sup>[80]</sup> For instance, Armbruster and colleagues<sup>[81]</sup> created a Bi-Rh nanoplates structure with a hexagonal closed pack (hcp) arrangement of plates. BiRh nanoplates, coated with high-strength polyetherimide, were made in a Teflon-lined vessel heated to 250°C. The ethylene glycol suspension was then transferred to a microwave-safe vessel and heated to 250°C after the bismuth and rhodium acetates were added. The absence of a dispersal substance was found to cause potent aggregation. The typical size of the plate is 60 nm, and it is thinner than 20 nm, with a hexagonal closed pack assembly (Figure 5a, b).

## **2.8. Galvanic replacement reaction**

The Galvanic replacement reaction approach is a unique technique used for producing multi-metallic catalysts. It involves replacing metal ions in a sacrificial template with a different metal precursor.<sup>[127]</sup> This approach provides benefits such as ease, flexibility, and the capacity to control the

structure and form of the produced catalyst. The Galvanic replacement reaction enables the creation of complex structures with precisely controlled interfaces between various metals, resulting in synergistic effects that improve catalytic performance.<sup>[26]</sup> This approach is highly advantageous for producing catalysts that possess hierarchical or porous architectures. Nevertheless, there exist some limitations, such as the possible challenge in attaining an even distribution of metal and the demand for precise selection of the sacrificial templates.<sup>[128]</sup> Additionally, the procedure may require subsequent treatment measures to improve the stability as well as efficiency of the catalyst. Considering these factors, the Galvanic replacement reaction method remains to be a viable approach to fabricating multi-metallic catalysts with tailored features.<sup>[129]</sup> Interestingly, the obtained product usually achieves the shape of the template.<sup>[130,131]</sup> Li and coworkers<sup>[124]</sup> fabricated Pd@Pt core-shell uniform and ultrathin nanowires (Figure 5c) through this method which showed excellent activity for ORR. Another example is the preparation of Ag-Au-Pt cage like cubes, Ag@Ag-Au-Pt concave nanocubes (Figure 5d)<sup>[125]</sup> and Au/PtPd core/shell tri-metallic nanowires.<sup>[132]</sup>

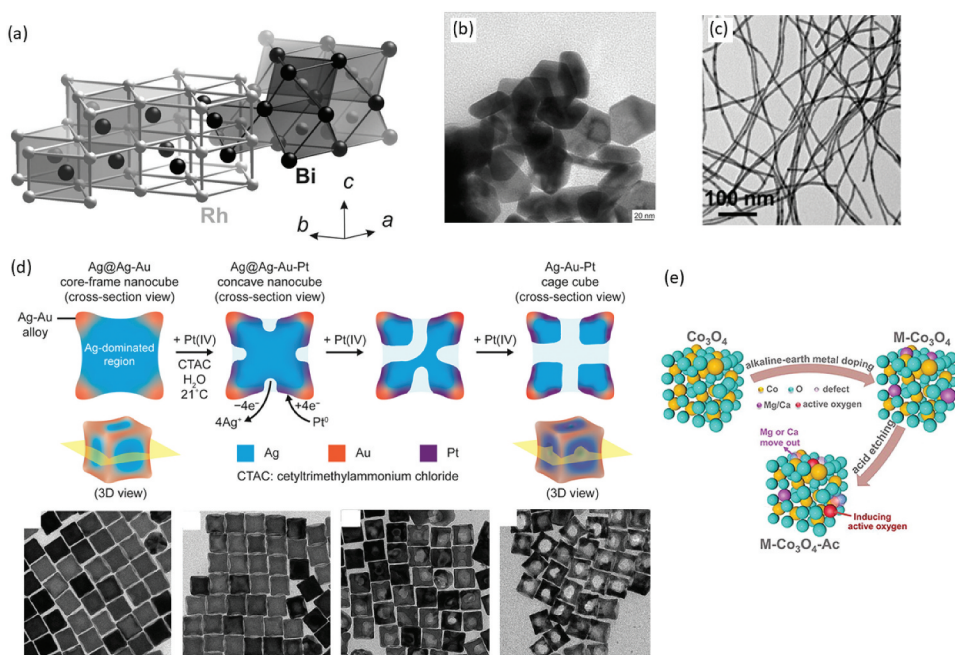


**Figure 5.** (a) Crystal structure and (b) TEM image of BiRh nanoplates.<sup>[123]</sup> Copyright © 2012 American Chemical Society. (c) TEM image of Pd@Pt (21.2%) NWS.<sup>[124]</sup> Copyright © 2015 American Chemical Society (d) Schematic illustrating of Ag@Ag–Au core–frame nanocube into Ag@Ag–Au–Pt concave cube and Ag–Au–Pt cage cube through a galvanic replacement reaction.<sup>[125]</sup> Copyright © 2019 American Chemical Society. (e) Synthesis procedure of M-Co<sub>3</sub>O<sub>4</sub> (M = Mg, Ca) and acetic acid etching (M-Co<sub>3</sub>O<sub>4</sub>-Ac) samples.<sup>[126]</sup> Copyright © 2022 Elsevier Inc. All rights reserved.

## 2.9. Reverse micelle synthesis

The reverse micelle synthesis method is an excellent and scalable technique for creating multi-metallic catalysts, which entails enclosing metal precursors within water-in-oil microemulsions. This approach provides numerous benefits, such as the capability to precisely regulate the size, shape, and composition of particles. The controlled reaction conditions within the reverse micelles enables the development of precise nanostructures, and the procedure can be used for various combinations of metals. Further, this approach enables the introduction of various metals, which enhances the synergistic effects in the catalysts.<sup>[133]</sup> Nevertheless, there are several challenges that exist, such as the potential complexity in scaling the synthesis production, and the need for precise fine-tuning of reaction parameters to get uniform distribution of metals. Additionally, further process may be required to eliminate surfactants and optimize the characteristics of the catalyst.<sup>[134]</sup> Despite these challenges, the reverse micelle synthesis process continues to be a potent technique for fabricating multi-metallic catalysts with precise structures and optimized functions.<sup>[135]</sup> Likewise, nanosized metallic materials are obtained by reduction of metal precursors using reducing agent (i.e.,  $\text{N}_2\text{H}_4$ ,  $\text{NaBH}_4$ ).<sup>[136]</sup> Supported catalysts are prepared by mixing metal precursor with aqueous solution and surfactant as well as reducing agent with a given oil phase solution. It is stirred until a clear solution is obtained, which denote the reverse micelles. To interrupt the micelles and allow adsorption to the specified support, a metal oxide support is introduced into the solution and determined by titration with acetone.<sup>[137]</sup> Through this technique, controlled size nanoparticles are obtained by regulating the surfactant to water ratio and amount of reducing agent.<sup>[136]</sup> Pt-Ni/ $\gamma$ - $\text{Al}_2\text{O}_3$  was fabricated through this method which revealed enhanced performance for hydrogenation of 1,3-butadiene.<sup>[138]</sup> In another report, Abazari and coworkers<sup>[139]</sup> also synthesized Pt/Pd/Fe trimetallic catalysts using this approach, which exhibited excellent performance for reductive hydrodehalogenation of aliphatic and Aryl halides. Melo-banda and coworkers<sup>[140]</sup> synthesized Ni:Co:Mo nanocatalysts through this method and employed in hydro-processing of heavy crude oil.

## 2.10. Colloidal synthesis

The colloidal synthesis method is a flexible and extensively employed technique for producing multi-metallic catalysts. It involves producing nanomaterials in a colloidal solution by reducing metal precursors.<sup>[141]</sup> This approach provides numerous benefits, such as precise regulation of particle dimensions, morphology, and chemical makeup, leading to the development of unique nanostructures with specific features.<sup>[142]</sup> The utilization of the colloidal technique enables the integration of different metal combinations, which



promotes synergistic effects and improves catalytic performance. The procedure is quite simple, and it can be readily extended for use in industrial applications.<sup>[143]</sup> Nevertheless, there are barriers to overcome, such as the possibility of particles aggregating during their growth and the demand for stabilizing materials or surfactants to avoid the aggregation of nanoparticles. In addition, it is necessary to carry out post-synthesis steps to eliminate any remaining stabilizers and enhance the catalyst's efficiency. Nevertheless, the colloidal synthesis process is a robust and efficient approach for synthesizing multi-metallic catalysts with precisely controlled features for a wide range of applications.<sup>[144]</sup> It is important to mention that the stabilizing agents utilized in this method may be surfactants, polymers and donor ligand, such as CTAC, poly (vinyl alcohol) (PVA), and PVP, which regulate the growth and prevent the agglomeration of nanoparticles.<sup>[145]</sup> For multi-metallic synthesis, metal precursors are mixed with a definite amount of surfactant, which form organic metal precursor by the interaction of anions of metal precursor with cations of surfactant in the present of aqueous solution. The solution is then stirred and heated to specific temperature along with addition of reducing agent. After the process is completed, the resulting product is centrifuged by washing with ethanol and distilled water, and dried in an oven.<sup>[24]</sup> For instance, Konuspayeva and coworkers<sup>[146]</sup> synthesized AuRh NPs on titania supported catalysts (AuRh/TiO<sub>2</sub>) via this method which were active for liquid-phase selective hydrogenation of cinnamaldehyde.

### **2.11. Sol-gel method**

The Sol-gel method is a widely used and flexible technique for producing multi-metallic catalysts. It involves converting a solution or colloidal system into a gel and then solidifying it to produce the desired material.<sup>[147]</sup> This approach offers multiple benefits, such as precise regulation of composition, exceptional uniformity, and the capacity to tailor the structure of the catalyst. The Sol-gel technique facilitates the integration of several metals, enabling the development of catalysts with distinctive characteristics and improved catalytic efficiency.<sup>[148]</sup> The resultant materials frequently display well-defined structures, homogeneous dispersion of metallic elements, and enhanced stability. Nevertheless, there are certain challenges to overcome, such as the possibility of gelation and variations in aging time, as well as the need for precise regulation of processing parameters to prevent undesired phase separation.<sup>[149]</sup> However, the sol-gel approach is still extensively utilized and effective in producing multi-metallic catalysts with high accuracy for diverse applications. The resultant product of sol-gel technique is calcined to achieve the respective materials.<sup>[150]</sup> For instance, Zhu and coworkers<sup>[126]</sup> prepared M-Co<sub>3</sub>O<sub>4</sub> (M = Mg, Ca, Co) nanostructure through citric acid sol-gel method (Figure 5e) which was employed to activate the surface lattice oxygen and

increase propane total oxidation. Casillas and coworkers<sup>[151]</sup> also synthesized  $\text{Al}_2\text{O}_3\text{-Nd}_2\text{O}_3\text{-ZnO}$  composites through this method which exhibited high photocatalytic activity for degradation of phenol.

### 3. Common characterization techniques for multi-metallic catalysts

Characterization of MMCs is critical in the identification of their structure which is definitely associated to the electrochemical properties. Hence, understanding the structure and configuration of MMCs are considerably important. In this part of the manuscript, we will discuss some common characterization techniques used for identification of MMCs (Figure 6).

#### 3.1. Chemisorption of carbon monoxide

One of the major aspects of multi-metallic catalysts is the number of active metal sites, which is usually achieved through CO chemisorption. Numerous specialized instruments are used to measure CO uptake, but Altamira Instruments (AMI-200ip) is a feasible choice. Investigations are accomplished via charging a definite amount of calcinated material to a given quartz based tube and then placed into a particular apparatus. Materials are abridged through a chosen mixture of hydrogen-helium gas at a certain room temperature and are chilled to a particular temperature. Once the substance has cooled to a certain temperature, a thermal conductivity detector is used to determine

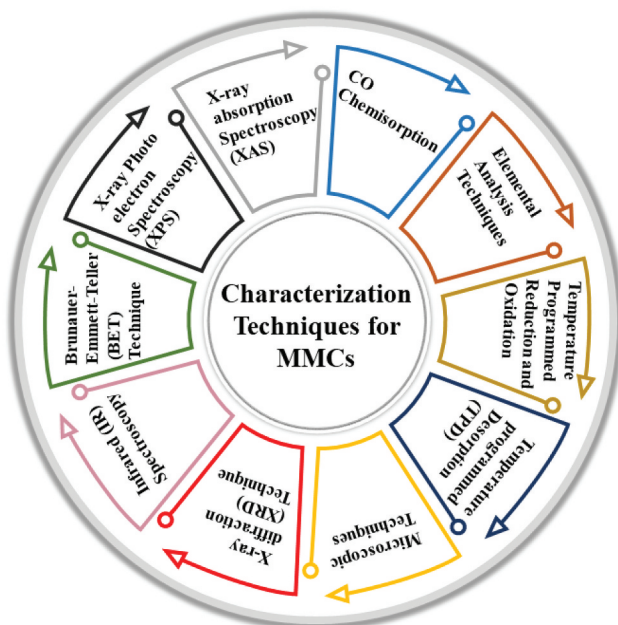


**Figure 6.** Characterization techniques used for identification of Multimetallic catalysts (MMCs).

how much CO was released during the cooling process.<sup>[152–154]</sup> Qi and coworkers employed this method to detect the surfaces active sites of the reduced bimetallic Pt–Ni, Pt–Cu, and Pt–Co catalysts.<sup>[152]</sup>

### **3.2. Elemental analysis techniques**

Two methods are generally employed for elemental concentration analysis of the catalysts. (i) Atomic absorption spectroscopy (AAS), and (ii) inductively coupled plasma atomic emission spectroscopy (ICP-AES) also known as inductively coupled plasma optical emission spectroscopy (ICP-OES). The AAS is an effective analytical method utilized for quantifying the concentration of particular elements in a sample by the measurement of the absorption of light at specific wavelengths. The AAS involves the atomization of a sample and its exposure to a beam of light with a particular wavelength that matches the electronic transition of the element being analyzed. The atoms within the sample absorb the light, and the degree of absorption is directly correlated to the concentration of existing elements. Subsequently, a detector detects the light that passes through, and the resultant absorption spectrum is employed to determine the concentration of the element. AAS is extensively utilized in different areas such as environmental science, medicine, and materials research, owing to its exceptional sensitivity, accuracy, and specificity. The flexibility of this device enables the examination of a broad spectrum of elements at very low concentrations, making it a vital tool used in modern chemical analysis.<sup>[155,156]</sup> In a typical AAS technique, a sample solution is prepared by dissolving a supported catalyst, and it is subsequently transformed into an aerosol using a nebulizer and isolated with a flame. The metal ions concentration in the solution is achieved after normalizing the strength of AAS using a reference compound.<sup>[157]</sup> For instance, Bisht et al. fabricated a nanocomposite of the Ag–Fe–Cu tri-metal with bismuth oxybromide for photocatalytic oxidation of alcohols under simulated sunlight and analyzed the metals concentration via the AAS technique.<sup>[158]</sup>

ICP-AES is a sophisticated and flexible analytical technology employed for elemental analysis. This technique utilizes inductively coupled plasma to atomize and activate the sample, and then measures the emitted light at specific wavelengths associated with each element.<sup>[159]</sup> The specimen, commonly in a liquid state, is incorporated into a high-temperature plasma containing argon gas. The sample is subjected to high temperatures, causing ionization and creating a high-energy environment in which atoms get excited. When these atoms return to their ground energy state, they release light, and the resulting spectral lines are analyzed to determine and measure the elements that are present in the sample.<sup>[160]</sup> ICP-AES provides numerous benefits, such as a broad linear dynamic range, exceptional sensitivity, and the capacity to investigate multiple elements simultaneously.<sup>[160]</sup> The ICP-AES

the technique is also used to measure the trace metals concentration within a multi-metallic catalyst.<sup>[161]</sup> Although ICP-AES is a more sophisticated and expensive equipment than AAS, its detection limit for most of the metals is higher.<sup>[155,162]</sup> For instance, Ding et al. prepared Pt–Ni nanostructure on a metal carbide ( $\text{Ni}_3\text{C@Pt}_3\text{Ni}$ ) and used the ICP-OES characterization technique to measure the Pt/Ni ratio, which is near to 3/1.<sup>[163]</sup> Zhang and coworkers<sup>[164]</sup> used this technique to measure the molar ratio of FeCoW (1:1.02:0.70) in gelled FeCoW oxyhydroxides catalysts.

### **3.3. Temperature-programmed reduction**

Temperature-programmed Reduction (TPR) is employed to predict the temperatures at which the catalyst is obtained by reducing metals and/or support materials. At a subsequent calcination, a particular catalyst is retained in the device's reactor under  $\text{H}_2$  flow and a steady ramp rate of temperature. By increasing the temperature, the provided catalysts are reduced by  $\text{H}_2$ , and oxygen is detached from the catalyst in the form of  $\text{H}_2\text{O}$ . The water concentration variation can be estimated using a TCD attached to the exhaust stream to determine the lowering temperatures. Temperature-programmed oxidation (TPO) is analogous to TPR concept in that it estimates the amount of deposited coke on the surface of the catalyst. During TPO estimation, a particular catalyst is retained in the device's reactor under  $\text{O}_2$  circulation and at a steady temperature. By increasing the temperature, the coke is oxidized via the  $\text{O}_2$  on the catalyst surface, and carbon is detached from the catalyst in the form of  $\text{CO}_2$ . The amount of surface carbon can be estimated by connecting a TCD to the exhaust stream and monitoring its composition using the  $\text{CO}_2$  intensity area vs temperature curve. Using this technique, the strength of the contact between the supported catalyst and the carbon surface is also determined because the higher the temperature of oxidation, the difficult to remove coke.<sup>[165,166]</sup> For example, Theofanidis and coworkers synthesized Fe–Ni–Pd supported on  $\text{MgAl}_2\text{O}_4$  and performed its TRP and TPO characterization.<sup>[167]</sup> Friberg and coworkers reported Ba modified Pd/ $\text{Al}_2\text{O}_3$  catalyst and demonstrated its TRP and TPO characterization.<sup>[168]</sup>

### **3.4. Temperature programmed desorption**

It is used to estimate the active site of the catalyst surface and understand catalytic reactions mechanisms containing adsorption, reaction and desorption. In a usual Temperature Programmed Desorption (TPD) experimental technique, catalyst of a small amount is loaded into a reactor. After the flow of inert gas in the presence of a catalyst, some gas is adsorbed on the catalyst surface. Then the catalyst is heated at a linear rate under a transporter gas flow. The change in the desorbed reaction gas from the catalyst surface upon the

given heating is measured through the downstream detector as a temperature function.<sup>[169]</sup> For instance, Chai and coworkers fabricated RuCo alloy nanosheets and measured its TPD characterization.<sup>[170]</sup> Likewise, BermejoLópez and coworkers reported Ru Na<sub>2</sub>CO<sub>3</sub>/Al<sub>2</sub>O<sub>3</sub> and Ru-CaO/Al<sub>2</sub>O<sub>3</sub> catalysts and measured its TPD characterization.<sup>[171]</sup>

### 3.5. Microscopic techniques

Crystal structural morphology and elemental chemical analysis of the materials are explored via the microscopic techniques such as SEM, TEM, HR-TEM, SAED, STEM, EDX spectroscopy, and HAADF-STEM technique. SEM is a highly effective scanning technique extensively employed in several scientific fields to provide highly detailed visualizations of surface structures at the micro- and nanoscale. SEM involves a focused beam of electrons for surface analysis of a material. The interactions between the electrons and the material create signals, which are subsequently gathered to produce specific 3-dimensional images with a high level of resolution.<sup>[172]</sup> TEM is an advanced scanning technique that enables the investigation of the internal structure of materials at the nanoscale. The HRTEM produces high-resolution images by transmitting electrons through an exceptionally thin material and interacting with its internal structures. The morphology and crystallography of nanomaterials can be observed via the TEM and HRTEM analysis.<sup>[173]</sup> SAED technique is employed in electron microscopy to explore the crystal structure of a specific target area in a material. The SAED pattern can be achieved by selectively diffracting electrons through a tiny aperture, resulting in a diffraction pattern which helps in determining the orientation and symmetry of the crystals within the particular area. The STEM is an imaging instrument that employs the quantum mechanical tunneling phenomenon to produce intricate, high-resolution images of surfaces at the atomic level. This allows researchers to explore the topography and electronic structure of nanomaterials with high precision.<sup>[174]</sup> EDX is an analytical technique employed in electron microscopy to identify and quantify the chemical composition and element distribution of a sample.<sup>[175]</sup> HAADF-STEM is an advanced imaging technique used in electron microscopy that enhances brightness by detecting variations in atomic number, enabling thorough analysis and imaging of the atomic structures of nanomaterials. This approach provides valuable information about the composition and crystallography of a material at the atomic level.<sup>[176]</sup> For instance, Liu and coworkers synthesized Au@PdPt porous nanowires (Au@PdPt pNWs) catalyst and investigated its morphology by using SEM (Figure 7a) which showed that catalyst has nanowire structures with high nanopore surface, which is also validated by TEM (Figure 7b). The SAED pattern corresponds to metallic face-centered cubic (fcc) crystals, indicating that the catalyst is polycrystalline (Figure 7b). The HRTEM image

showed lattice fringe and the lattice spacing of 0.23 nm, indexed to the (111) facet of PdPt alloy (Figure 7c). The nanoporous core-shell nanowire structural design further corroborated by the HAADF-STEM micrograph (Figure 7d). The subsequent EDX elemental mapping photos corroborated the Au, Pd, and Pt elemental distribution, with Au metal substantially distributed over the innermost core area and partially into the outer area, and Pd and Pt metals diffused around the Au metal core network in the current shell area (Figure 7e-h). Additionally, the Au, Pd, and Pt dispersion of the EDX line profiles thoroughly validates the core-shell nanostructure (Figure 7i).<sup>[177]</sup>

### 3.6. X-ray diffraction technique

It is a valuable technique to investigate various structural aspects in given crystalline samples. Typically, it provides attainable information about the crystalline shape, size, composition, the nature of phase, and lattice parameters. The crystal size is estimated through Scherrer's equation (Equation 1), taking the broadening of the high intense XRD peak for a given sample.<sup>[178]</sup>

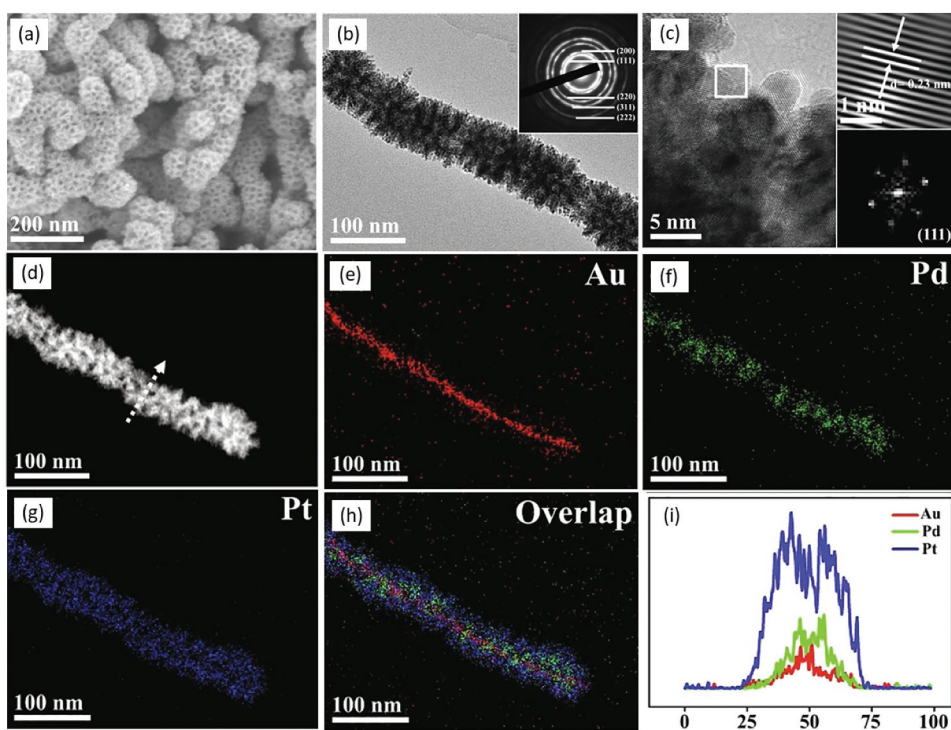


**Figure 7.** (a) SEM, (b) TEM (The inset displays the SAED image), (c) HRTEM images (insets lattice fringes and resultant FFT pattern), (d) HAADF-STEM image, (e-h) EDX mapping images, and (i) The corresponding compositional line profiles of Au@PdPt pNWs.<sup>[177]</sup> Copyright © 2021 Elsevier B.V. All rights reserved.

$$D_{hkl} = K\lambda/B_{hkl}\cos\theta \quad (1)$$

where  $D_{hkl}$  represents crystallite size,  $hkl$  Miller indices,  $K$  numerical factor such as crystallite-shape factor,  $\lambda$  X-rays wavelength,  $B_{hkl}$  the diffraction peak's full-width at half-maximum (FWHM), and the  $\theta$  Bragg angle.<sup>[179]</sup>

The material composition can also be obtained by comparing its various peak position and intensity with given standard-reference patterns of the International-Center for Diffraction-Data (ICDD, previous name as Joint-Committee on Powder-Diffraction-Standards, JCPDS) database. However, this technique is not applicable for amorphous materials and particles with 3 nm below size give very broad peaks.<sup>[178]</sup> Shah and coworkers performed X-ray diffraction (XRD) analysis for Co-SAC/RuO<sub>2</sub> catalysts to confirm their crystal structure. The RuO<sub>2</sub> main peaks are positioned and assigned as 28° (110), 35° (101), 40° (200), 54° (211), and 69.6° (301). The given XRD pattern well matched with the standard RuO<sub>2</sub> (JCPDS #43-1027). However, characteristic Peaks of cobalt nanoparticles were obtained, when a greater amount of cobalt salt was used during the preparation.<sup>[180]</sup> Wang and coworkers verified the crystal structure of prepared Three-dimensional PdAuRu nanospines (PdAuRu NSAs) by using XRD analysis. The PdAuRu NSAs XRD pattern showed peaks at 40.1 (111), 46.6 (200), 68.1 (220), 82.1 (311) and 86.6° (222) facets of fcc PdAuRu alloy structure (Figure 8a). Comparing these peaks to the standard Pd, it is clear that they move somewhat to the higher side, confirming lattice shrinkage due to other metal addition into Pd.<sup>[181]</sup> Moreover, Bimetallic Pt-Pd Symmetry-Broken Concave Nanocubes (Pt-Pd SBCNCs/C), PtPd NCs/C, and commercial TTK-Pt/C catalysts were all structurally verified by Wu and colleagues using XRD analysis (Figure 8b). The diffraction peak positions of face-centered-cubic (fcc) configuration were indexed to (111), (200), (220), (311), and (222) diffractions. The peak positions are slight shifts to a higher degree related to commercial Pt/C, which indicate the Pt-Pd alloy formation.<sup>[182]</sup>

### 3.7. Infrared spectroscopy

One of the most effective characterization techniques for catalytic systems is infrared (IR) spectroscopy. IR provides valuable information about a wide range of catalysts and specific catalytic processes. It is used to quantify the concentrations of specific reactants and products in the aqueous or gas phase and to identify the reaction intermediate bonding configuration as adsorbed on the surface of catalysts.<sup>[183,186]</sup> Many types of IR spectroscopy are employed in catalytic research. Fourier transform infrared (FTIR) spectroscopy is the most common. Chen and coworkers<sup>[183]</sup> reported PtBi@6.7%Pb nanoplates for methanol oxidation reaction (MOR) and used in situ FTIR spectra to elucidate the enhanced catalytic performance for active oxidation of CH<sub>3</sub>OH

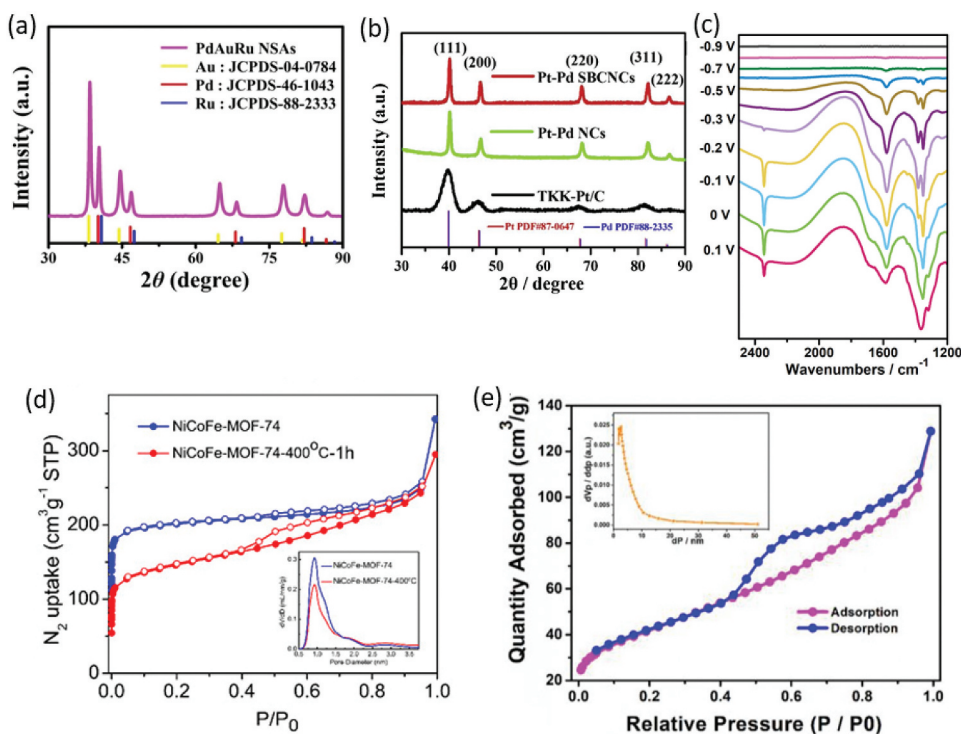


**Figure 8.** (a) XRD pattern of PdAuRu NSAs.<sup>[181]</sup> Copyright © 2022 Elsevier B.V. All rights reserved. (b) Commercial TKK-Pt/C, Pt-Pd NC and Pt-Pd SBCNC.<sup>[182]</sup> Copyright © 2019 Elsevier B.V. All rights reserved. (c) The in situ FTIR spectra of PtBi@6.7%Pb nanoplates.<sup>[183]</sup> Copyright © 2022 Wiley-VCH GmbH. (d) NiCoFe-MOF-74 and NiCoFe-MOF-74-400°C-1 h (NiCo/Fe<sub>3</sub>O<sub>4</sub>/MOF-74) at 77 K (insert: the pores size distribution).<sup>[184]</sup> Copyright © 2018 American Chemical Society. (e) The N<sub>2</sub> adsorption/desorption curves of Pt-FeP/C at 77 K (insert: the pores size distribution).<sup>[185]</sup> Copyright © 2021 Elsevier B.V. All rights reserved.

and intermediate HCOO<sup>-</sup>, along with the fast liberating of adsorbed CO<sub>2</sub> to make CO<sub>3</sub><sup>2-</sup>/HCO<sub>3</sub><sup>-</sup>. Figure 8c shows the in situ FTIR spectra of a PtBi@6.7% Pb catalyst for MOR. In the case of PtBi@6.7%Pb nanoplates, the HCOO<sup>-</sup> peaks (asymmetric stretching-vibration at 1585 cm<sup>-1</sup> and twin symmetric vibration at 1381 and 1348 cm<sup>-1</sup>) appeared at -0.7 V vs SCE, which appears to be lower than that of PtBi (-0.5 V) and Pt/C catalyst (-0.5 V). The vibration peaks of CO<sub>2</sub> (≈2345 cm<sup>-1</sup>) and CO<sub>3</sub><sup>2-</sup>/HCO<sub>3</sub><sup>-</sup> (≈1376 cm<sup>-1</sup>) appeared at -0.3 V that is inferior relative to the PtBi (-0.1 V). Following that, the HCOO<sup>-</sup> peak intensity slowly declines, while the indicated peak intensities of CO<sub>2</sub> and CO<sub>3</sub><sup>2-</sup>/HCO<sub>3</sub><sup>-</sup> gradually increase. As the input potential rises to -0.1 V, the CO<sub>2</sub> peak intensity rapidly declines while the CO<sub>3</sub><sup>2-</sup>/HCO<sub>3</sub><sup>-</sup> peak intensity increases, indicating the desorption of adsorbed CO<sub>2</sub> to form CO<sub>3</sub><sup>2-</sup>/HCO<sub>3</sub><sup>-</sup>. Because of these characteristics, PtBi@6.7%Pb nanoplates outperformed PtBi nanoplates and Pt/C catalysts in MOR.



### 3.8. Brunauer-Emmett-Teller technique

The Brunauer-Emmett-Teller (BET) approach is widely used for measuring the surface area, pore volume, and pore size distribution of nanoscale materials. It is worked on the principle of adsorption and desorption of gas molecules (e.g, N<sub>2</sub>) on a given solid surface under isothermal circumstances. Its name was derived from initials surname of its makers, Brunauer, Emmett and Teller. The explored materials are classed as microporous (< 2 nm pore size), mesoporous (2–50 nm pore size), and macroporous (> 50 nm pore size).<sup>[178,179]</sup> Shah and coworkers used BET analysis to measure the surface area of prepared Co-SAC/RuO<sub>2</sub> catalysts. According to the BET analysis, the specific surface area for Co-SAC/RuO<sub>2</sub> is 50.5 m<sup>2</sup>g<sup>-1</sup>, and 40.49 m<sup>2</sup>g<sup>-1</sup> for RuO<sub>2</sub> catalyst.<sup>[180]</sup> Wang and colleagues synthesized NiCo/Fe<sub>3</sub>O<sub>4</sub> hetero-particles in MOF-74 and assessed surface area using BET analysis, revealing that the calcined sample has a surface area of 558 m<sup>2</sup>g<sup>-1</sup> and the NiCoFe-MOF-74 precursor has a surface area of 820 m<sup>2</sup>g<sup>-1</sup> (Figure 8g). The MOF-74 microporous structure remained same after controlled pyrolysis (inset of Figure 8g).<sup>[184]</sup> Deng and colleagues also employed this method to determine the surface area as well as the pore size of a Pt-doped FeP/C hollow nanorod, which exhibited surface area of 148.7 cm<sup>2</sup> g<sup>-1</sup> (Figure 8f) and pore size in the range of 1.7–5 nm (inset of Figure 8f).<sup>[185]</sup>

### 3.9. X-ray photoelectron spectroscopy

X-ray Photoelectron Spectroscopy (XPS) is a powerful elemental-specific and surface sensitive technique. It is employed for nanoscale material (1–10 nm) characterization. It is useful in studying electronic structure, oxidation state and composition of elements in a heterogeneous catalyst.<sup>[178]</sup> It works on the basic physical principle of photoelectric effect, when a photon of high energy hit a material with the following releasing of photoelectrons with characteristic energies of the given elements inside of the sample. The photoelectron kinetic energy ( $E_k$ ) is demonstrated by Einstein's law (Equation 2).

$$E_k = h\nu - E_b \quad (2)$$

Where  $h\nu$  is the incident radiation energy and  $E_b$  is the electron binding energy at a certain level. When incident photon has sufficient energy, various levels may be ionized and obtained spectrum displaying all accessible energy levels as photoelectrons with regulated kinetic energies.<sup>[187]</sup> For example, Chen and coworkers used XPS to present composition and valence state of a prepared trimetallic PtNiCo hollow alloyed multipods (HAMPs). The survey spectrum of XPS shows the co-occurrence of Ni, Co and Pt metals (Figure 9a). The high-resolution Ni 2p XPS spectra (Figure 9b) reveals characteristic peaks of Ni<sup>0</sup> (i.e., 852.78 and 870.18 eV) and NiO (i.e., 856.00 and 873.75 eV).

Moreover, Co 2p XPS spectrum (Figure 9c) represents the Co<sup>0</sup> peaks (i.e., 778.28 and 793.33 eV) and CoO peaks (i.e., 780.93 and 796.43 eV). Figure 9d shows PtNiCo HAMPs with binding energies of 71.17 and 74.55 eV assigned to Pt<sup>0</sup>, and 72.01 and 75.75 eV assigned to Pt<sup>2+</sup>. Remarkably, the positive shift of the Pt 4f peaks in comparison to pure Pt (70.9 eV) indicates electron transport between Co, Ni, and Pt.<sup>[188]</sup>

### 3.10. X-ray absorption spectroscopy

It is a synchrotron-based working technique for describing the constrained atomic and electronic configurations of a given catalyst specimen under certain catalyst reaction conditions.<sup>[190,191]</sup> The monochromatic X-ray beam of X-ray is used to perform X-ray Absorption Spectroscopy (XAS) measurements and assemble the coefficient of absorption,  $\mu$ , as an X-ray energy function. Once the instance energy ( $h\nu$ ) focuses on the core level electron binding energy  $E_0$ , a distinct jump in  $\mu$  is observed, which is referred to as the absorption edge. The X-ray absorption near-edge structure (XANES) zone is the scan region that commences earlier at the absorption edge and extends up to 50–100 eV above the absorption edge.<sup>[192,193]</sup> The enlarged X-ray absorption fine structure (EXAFS) area begins at 50–100 eV just above the edge (next to the particular region of XANES) and extends up to 1000 eV above the edge.<sup>[192]</sup> The white line is a prominent characteristic of the XANES region, induced by a rapid increase in absorption. This characteristic exists in L-edges due to electron excitation from lower energy p-orbitals toward higher energy unoccupied d-states.<sup>[194]</sup> The white line's primary function is the oxidation state characterization of metal in the presence and afterward H<sub>2</sub> treatment, along with the company of catalytic reactions. For instance, a decrease in the intensity of white light after H<sub>2</sub> treatment indicates that concern metal is reduced. Coordination number data may also be assessed using further XANES region analysis.<sup>[190,191]</sup> The EXAFS area is made up of fine structure concerning the constrained coordination environment. The EXAFS region differs from the XANES region in that the ejected photoelectron of the EXAFS region has enough energy to scatter electrons from all nearby atoms and then backscatter to the specific absorbing atoms.<sup>[190]</sup> Due to the wave-particle duality of the expelled photoelectron, the electrons of leaving and backscattered might interact constructively or destructively with one another, providing information about the catalytic coordination environment. For example, the intensity of oscillations increases as the coordination number increases, yet the frequency of oscillations is inversely proportional to interatomic distances.<sup>[191]</sup> For example, Jia and colleagues<sup>[189]</sup> investigated the oxidation states as well as the local chemical environments of Pd-based catalysts using XANES and FT-EXAFS spectra. Figure 9e depicts XANES at the Pd Kedge, where the curvature point (X) position and inset derived peak

indicate the oxidation state of a specified catalyst. Similarly with Pd foil, a strong oxidation state of Pd is observed for Pd/C, as evidenced by the massive inset black line. The oxidation state of Pd was marginally decreased due to Cu addition in the PdCu<sub>0.2</sub>/C Catalyst, indicating a metallic state of Pd and suppression of oxidation by the creation of hydride. Furthermore, as shown in Figure 9e, the two absorption peaks led to the transition of electrons from the 1s to 5p and 1s to 4f, respectively, and modification in conjunction with the addition of Cu or Pd oxidation. Figure 9f depicts the Fourier-transformed extended X-ray absorption fine structure (FT-EXAFS) spectra near the Pd K-edge. Pd-O, Pd-Pd, and Pd-Cu bonds are represented by peaks A, B, and C, respectively. Pd/C is largely made up of Pd oxide, with a prominent Pd-O peak at 2.0 Å and peaks at 2.25 Å representing PdCu<sub>0.2</sub> and PdCu<sub>0.2</sub>H<sub>0.43</sub> catalysts.

#### 4. Electrocatalytic applications

MMCs have received significant attention in the catalysis field due to their structure, size, higher surface/volume ratios, and excellent catalytic performances. MMCs of various sizes and shapes have several advantages over monometallic catalysts in terms of catalytic performance, selectivity, and physical/chemical stability. The commonly recognized approach is that multi-metallic catalysts provide enhanced physicochemical properties developing from the synergy of the multicomponent. The

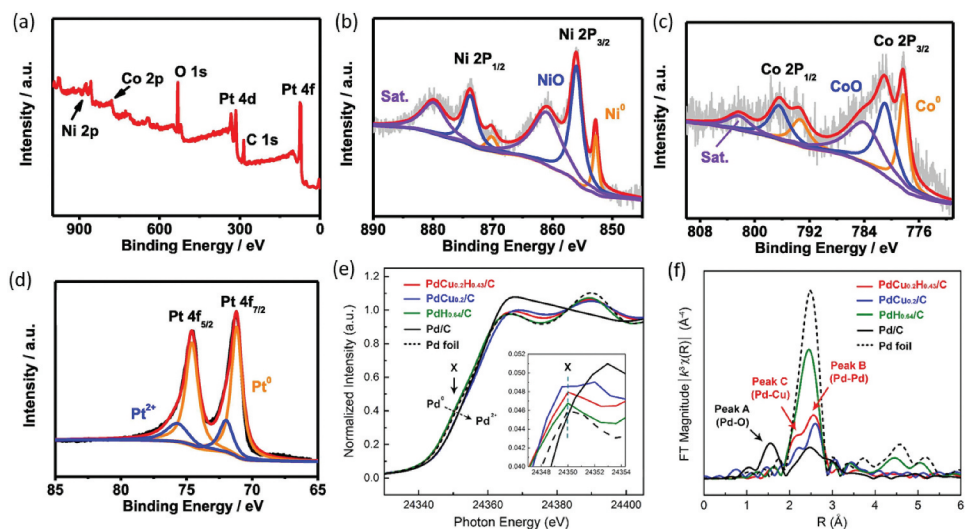


**Figure 9.** XPS spectra of the PtNiCo HAMPs (a) Survey, high-resolution (b) Ni2p, (c) Co2p and (d) Pt 4f.<sup>[188]</sup> Copyright © 2020 Elsevier Inc. All rights reserved XAS characterization of Pd-based catalysts: (e) XANES, and (f) FT-EXAFS spectra.<sup>[189]</sup> Copyright © 2022 American Chemical Society.

mechanism of multifunctional, geometrical effects, electronic effects, or lattice strains prompted owing to lattice disparity are commonly emphasized as the main factors beyond their synergistic effect, which displays a more significant role in catalysis.<sup>[195]</sup> To Date, MMCs have been extensively studied in CO<sub>2</sub> RR, HER, OER, ORR, NRR, and others. The given part of the review will explain their applications in these fields individually.

#### 4.1. MMCs for CO<sub>2</sub> reduction reaction

Fossil fuel burning produces a large amount of CO<sub>2</sub>, which is primarily responsible for air pollution and global warming.<sup>[196–198]</sup> Electrochemical CO<sub>2</sub> reduction transformation to C<sub>1</sub> products (i.e., CO, HCOOH, CH<sub>4</sub>) or C<sub>2</sub> products (i.e., C<sub>2</sub>H<sub>5</sub>OH and C<sub>2</sub>H<sub>4</sub>) is the most attractive approach to produce renewable fuels to address the escalating environmental contamination problem.<sup>[12,199–201]</sup> Nevertheless, because of the relatively stable C = O chemical bond of 806 KJ mol<sup>-1</sup> and the competitive HER side reaction, the direct production of liquid fuels from CO<sub>2</sub> reduction still has a very low transformation efficiency.<sup>[202]</sup> Thus, developing highly efficient and selective catalysts to reduce CO<sub>2</sub> with high yield products and low overpotential is urgently required. MMCs have shown promising catalytic performance, efficiency, and selectivity for CO<sub>2</sub> reduction reaction (CO<sub>2</sub> RR)<sup>[85]</sup> applications owing to their tunability through the synergic effects between the metals in a catalytic complex. The mechanism of CO<sub>2</sub>RR often relies on the synergistic interactions among various metals, with each metal providing distinct catalytic features. MMCs offer several advantages over single-metal catalysts, such as enhanced catalytic activity, selectivity, and stability. The utilization of several metals enables the fine-tuning of binding energies for key intermediates in the CO<sub>2</sub>RR, resulting in improved overall performance.<sup>[26]</sup> For instance, Zhu and coworkers<sup>[203]</sup> developed an Au<sub>94</sub>Pd<sub>6</sub> core-shell catalyst that shown exceptional activity for CO<sub>2</sub>RR to CO with a significant Faradaic efficiency (FE<sub>CO</sub>) of 96.7% at -0.6 V vs RHE. At an overpotential of 390 mV, the electrocatalyst had a maximum mass activity of 99.8 Ag<sub>Pd+Au</sub><sup>-1</sup> for CO production.<sup>[204]</sup> The in situ infrared absorption spectroscopy and DFT calculations demonstrated that the adsorption scaling relation of \*COOH/\*CO could be broken on the core-shell catalyst surface, which is responsible for catalytic performance. Recently, Cheng and coworkers<sup>[205]</sup> developed bimetallic Ni/Cu-N-C electrocatalysts (Figure 10a) for electrocatalytic CO<sub>2</sub> conversion (Figure 10b). The catalyst demonstrated 99.2% FE<sub>CO</sub> at -0.79 V vs RHE (Figure 10c), a partial current density ( $J_{CO}$ ) of 29.9 mA cm<sup>-2</sup>, and long-term stability for 60 h (Figure 10d). DFT simulations demonstrated that the synergetic effect of Ni and Cu, in which Ni centers charge

redistribution driven by neighboring  $\text{CuN}_4$  moieties increases  $^*\text{COOH}$  adsorption and facilitates CO generation, boosts  $^*\text{COOH}$  adsorption, and facilitates CO generation. Pei and Coworkers<sup>[207]</sup> demonstrated that N-bridged bimetallic sites Co-N-Ni anchored on N-doped porous carbon nanosheets (Co-N-Ni/NPCNSs) had a best performance for CO generation, with an FE<sub>CO</sub> of 96.4% at  $-0.48$  V against RHE and a TOF of  $2049 \text{ h}^{-1}$  at  $370 \text{ mV}$ . The catalyst demonstrated good stability for up to 20 h at  $-0.48$  V versus RHE with an FE<sub>CO</sub> of more than 90%. Among the several products of  $\text{CO}_2\text{RR}$ , formate is considered as an appreciated fuel with a greater volumetric density of hydrogen and relatively appropriate transportability. Recently, Yang and coworkers<sup>[206]</sup> reported that bimetallic CuBi, has a high reactivity toward electroreduction of  $\text{CO}_2$  to formate. Among all the synthesized catalysts, bimetallic CuBi75 showed the highest performance with FE<sub>formate</sub> of 100% at  $-0.77$  V vs RHE (Figure 10e-g).

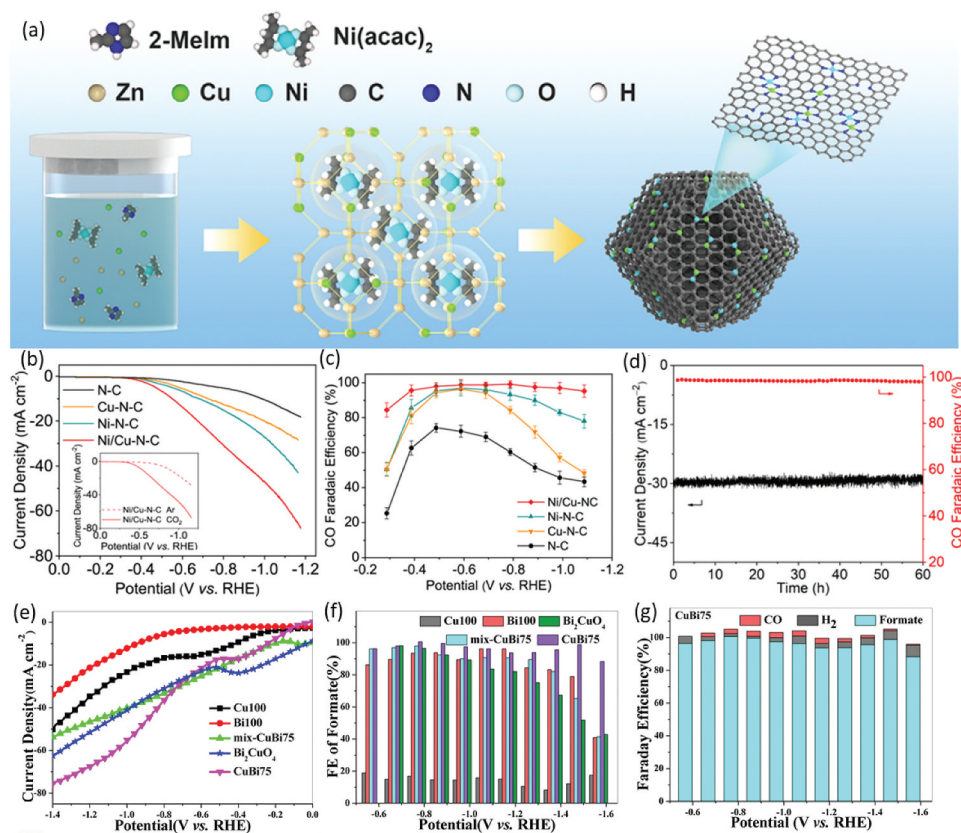


**Figure 10.** (a) Schematic synthesis of Ni/Cu-N-C catalysts. (b) LSV curves of Ni/Cu-N-C. Inset: LSV curves achieved in 0.5 M KHCO<sub>3</sub> electrolyte saturated with Ar- and CO<sub>2</sub>, (c) FE<sub>CO</sub> and (d) stability of Ni/Cu-N-C.<sup>[205]</sup> Copyright © 2021 American Chemical Society. (e) LSV curves, (f) FE<sub>formate</sub> of CuBi75 and along with different catalysts. (g) FE<sub>formate</sub> of CuBi75 at various potentials.<sup>[206]</sup> Copyright © 2021 Elsevier B.V. All rights reserved.

Moreover, bimetallic CuBi75 catalysts showed long-term continuous electrolysis stability for 24h. Because of the significant CO<sub>2</sub> adsorption and charge transfer capabilities on the catalyst surface, *in-situ* FT-IR and DFT measurements revealed that the HCOO\* pathway was dominant. Likewise, Chen and coworkers<sup>[208]</sup> used hydrothermal method to fabricate Cu-doped SnS<sub>2</sub> nanoflowers, which demonstrated excellent efficiency and selectivity of the CO<sub>2</sub>RR transformation to formate with a Faradaic efficiency > 80% and a potential range of -0.8 to -1.3 V versus RHE, with the highest Faradaic efficiency of 90.5% at 1.0 VRHE with a -23.8 mA cm<sup>-2</sup> partial current density. The three at.% Cu-doped SnS<sub>2</sub> demonstrated outstanding stability with the current density of -16.5 mA cm<sup>-2</sup> at -0.9 V vs RHE over 120 h.

The conversion of CO<sub>2</sub> via electrocatalysis into high-value multicarbon (C<sub>2+</sub>) products offers an inspiring opportunity to liberate the current chemical industry from its reliance on fossil-resources and, eventually, close the anthropogenic carbon cycle, but it is severely hampered by the lack of high-performance electrocatalysts.<sup>[209]</sup> Xiong and coworkers<sup>[210]</sup> fabricated Cu<sub>3</sub>-Ag<sub>3</sub>Au nanoframes catalyst for CO<sub>2</sub> RR to C<sub>2</sub>H<sub>4</sub>, which exhibited high FE<sub>C<sub>2</sub>H<sub>4</sub></sub> of 69 ± 5% and 77 ± 2% in the given H-cell and flow cell, correspondingly. The catalyst demonstrated outstanding electrocatalytic stability and durability. In-situ IR and DFT experiments revealed that C<sub>2</sub>H<sub>4</sub> is produced by two opposing processes, with direct dimerization of CO being the more energetically favorable. The given work provides an example of a catalyst design that break the CO<sub>2</sub>RR linear scaling connection toward improved C<sub>2</sub>H<sub>4</sub> production by merging defect engineering, tandem effect, and electronic modulation. In addition, many other MMCs have been synthesized; their catalytic performances for CO<sub>2</sub> RR are summarized in Table 1.

**Table 1.** CO<sub>2</sub>RR performance of Multi-metallic catalysts.

Catalysts	Electrolyte (M)	Faradaic efficiency (FE) [%]	Stability (h)	Ref.
Pd <sub>5</sub> @Au <sub>95</sub>	KHCO <sub>3</sub> (0.1)	80 (FE <sub>CO</sub> )	>24	[211]
Sn <sub>0.8</sub> Bi <sub>0.2</sub> @Bi-SnO <sub>x</sub>	KHCO <sub>3</sub> (0.5)	96 (FE <sub>formate</sub> )	>50	[212]
Ag-Zn dendritics	CsHCO <sub>3</sub> (0.1)	> 90 (FE <sub>CO</sub> )	>40	[213]
Au@Cu	KHCO <sub>3</sub> (0.1)	47 (FE <sub>C<sub>2</sub>H<sub>4</sub></sub> )	>9	[214]
Cu/Ni(OH) <sub>2</sub>	NaHCO <sub>3</sub> (0.5)	92 (FE <sub>CO</sub> )	>22	[215]
diatomic Ni-Fe sites	KHCO <sub>3</sub> (0.5)	98 (FE <sub>CO</sub> )	>30	[216]
Cu <sub>4</sub> Zn	KHCO <sub>3</sub> (0.1)	29 (FE <sub>ethanol</sub> )	>5	[217]
Ag/Cu <sub>2</sub> O	KHCO <sub>3</sub> (0.1)	65 (FE <sub>C<sub>2+</sub></sub> )	>12	[218]
Bi@Sn Core-Shell	KHCO <sub>3</sub> (0.5)	91 (FE <sub>HCOOH</sub> )	>31	[219]
	KOH (2.0)	92 (FE <sub>HCOOH</sub> )	>6	
Pd/SnO <sub>2</sub>	NaHCO <sub>3</sub> (0.1)	55 (FE <sub>methanol</sub> )	>24	[220]

## 4.2. MMCs for hydrogen evolution reaction

Hydrogen ( $H_2$ ) is a renewable and environmentally friendly energy source. Electrochemical water ( $H_2O$ ) splitting produces hydrogen, which is a green, efficient, and sustainable technology.<sup>[221–225]</sup> For high purity of  $H_2$  production, the HER through the electrocatalytic process in both acidic and alkaline mediums have recently attracted increasing consideration. The HER has a 0  $V_{RHE}$  equilibrium potential. The electrocatalysts activity is evaluated by given parameters, including Tafel slope,  $E_{10}$  (or  $\eta_{10}$ ), and the onset potential. During the reaction of hydrogen evolution processes, intermediates ( $H^*$ ) adsorb on the active sites. Therefore, active material for HER is selected based on the adsorption energy of hydrogen and catalyst of zero adsorption free energy  $H^*$  ( $\Delta G_{H^*}$ ) is considered as an excellent catalyst.<sup>[226]</sup> Among the most reported materials for HER, Pt-based electrocatalysts are accepted to be the best active catalysts for HER with an onset overpotential of near zero. Most precious metal-free materials for HER consist of (1) W- and Mo-based materials; (2) materials are other than hydroxides and oxides, such as chalcogenides, nitrides, and phosphides. In this portion, we will discuss MMCs electrocatalysts for HER. MMCs enhance the reaction kinetics and minimize overpotential in the HER by utilizing metals with favorable features, such as hydrogen binding strength and electronic structure. This optimization makes the HER energetically more favorable.<sup>[39]</sup> For instance, Liu and coworkers<sup>[227]</sup> reported a multilayered nanosheets alloy of RuNi nanostructures (RuNi NSs) for HER (Figure 11a). The catalysts had a remarkable HER performance in an alkaline environment, with a specific low overpotential of 15 mV at 10  $mA\ cm^{-2}$  current density and a relatively small Tafel slope of 28  $mV\ dec^{-1}$ , which was significantly greater than commercial Pt/C and Ru/C catalysts (Figure 11b, c). Furthermore, the RuNi NSs showed best catalytic stability (Figure 11d). This high activity is attributed to the electrochemically active high surface area of 154  $m^2\ g^{-1}$ , the influence of alloying Ni atoms, which allows water dissociation and enhances water adsorption and desorption. However, Nobel metals are recognized as the best catalysts for enhancing the cathode dynamic process in devices electrolysis of water. Because of their large surface areas and low coordination surface atoms, 1D nanowires, and 2D ultrathin nanosheets are frequently studied, though stacking issues do affect their performance and durability. Recently, Lu and coworkers<sup>[228]</sup> synthesized three-dimensional worm-like S-doped RhNi alloy (S-RhNi) through the hydrothermal method (Figure 11e), which showed excellent HER activity (Figure 11f). This catalyst exhibited Pt liked HER performance regarding its 0 mV overpotential, and a 24.61  $mV\ dec^{-1}$  Tafel slope in acidic medium. Furthermore, it demonstrated outstanding stability over 1,000

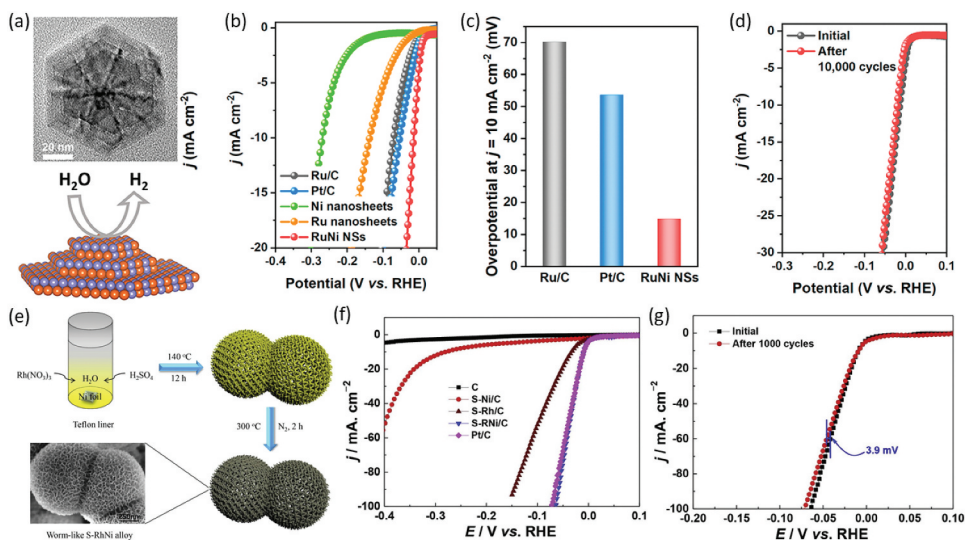


**Figure 11.** (a) TEM image and schematic representation of RuNi NS for HER. (b) Polarization curves of HER and (c) Overpotentials at current density of  $10 \text{ mA cm}^{-2}$  for RuNi NSs along with other catalysts, (d) RuNi NSs stability test<sup>[227]</sup> Copyright © 2019 Elsevier Ltd. All rights reserved. (e) Schematic synthesis diagram of the worm-like S-RhNi alloys, (f) Polarization curves and (g) stability test of S-RhNi/C<sup>[228]</sup> Copyright © 2019 Elsevier B.V. All rights reserved.

cycles (Figure 11g) and maintained a current density of  $-20 \text{ mA cm}^{-2}$  for 10 h. This enhanced activity of the catalyst is assumed to be initiated by the combining of the S doped atoms, a worm-like alloy of RhNi, and the present three-dimensional structure.

Transition metal phosphides (TMPs) are considered as a best catalyst for HER, in which phosphorus atom acts as site for a proton-ophile that enhances HER activity through electron withdrawing from present transitional metals. The H adsorption-free energy ( $\Delta G_{\text{H}}$ ), is commonly used to define the adsorption strength of H at the present P-atom, which is further altered by doping or alloying with another transition metals. For instance, Shin and coworkers<sup>[229]</sup> developed  $\text{Fe}_{0.5}\text{Ni}_{1.5}\text{P}$  catalysts with significant HER activity, a low overpotential of 0.163 V at  $50 \text{ mA cm}^{-2}$ , a small tafel slope of  $65 \text{ mV dec}^{-1}$ , and outstanding stability. The XPS and XANES measurements show that the P-atom in the  $\text{Fe}_{0.5}\text{Ni}_{1.5}\text{P}$  electrocatalyst has a high electron vacancy. The EXAFS results demonstrated that minor distortions in metal-metal (M-M) bonds significantly restrict charge transport from M-to-P and increase electron vacancy in the P atom, which is correlated with strong HER activity in acidic solution media.

In addition to simple metal alloys, transition metal selenides (TMSs) with tunable characteristics have been examined as high efficiency electrocatalysts for H<sub>2</sub> generation, owing to the lower intrinsic electrical resistance which facilitate charge transport in electrocatalysis. However,



related to the precious metal electrocatalysts, the TMSs catalytic performance is still needs more enhancements. Hence, Wang and coworkers<sup>[230]</sup> fabricated trimetallic Mo-Ni-Co selenide consisting of nanorod arrays on Ni-Co foam treated with plasma (MoSe<sub>2</sub>-NiSe<sub>2</sub>-CoSe<sub>2</sub>/PNCF), which exhibited high HER activity in alkaline mediums with the low overpotential of 38 mV at 10 mA cm<sup>-2</sup>. The generation amount of H<sub>2</sub> is 2.6 mmol h<sup>-1</sup>, greater than other already reported transition metals consisting electrocatalyst. Moreover, The MoSe<sub>2</sub>-NiSe<sub>2</sub>-CoSe<sub>2</sub>/PNCF showed superior catalytic stability. Its outstanding catalytic activity and stability are attributed to synergetic effects and the catalysts' tailored morphology.

Non-noble Fe, Co, and Ni metal-based catalysts have been widely explored as promising HER electrocatalysts alternatives. But these catalysts have some limitations, containing low performance and durability in alkaline medium. Hence, Pt alloying with different transition metals is a brilliant strategy to enhance HER activity as well as reduce the catalyst cost. Hence, Zheng and coworkers<sup>[231]</sup> developed a 1-PtNiMg-900 alloy with a low Pt concentration of about 1% and demonstrated outstanding HER performance in an alkaline medium. With a specific current density of 10 mA cm<sup>-2</sup>, the 1-PtNiMg catalysts had an overpotential of 22 mV and a smaller Tafel slope of 30.9 mV dec<sup>-1</sup>. Furthermore, the 1-PtNiMg catalysts shown good stability of 1–2000 mA cm<sup>-2</sup> current density after 100 h. As a result, the high HER performance of 1-PtNiMg-900 can be credited to its highly porous 3D uniform surface, ideal Ni and Pt synergistic effect, increased exposure of available active sites, and good conductivity. Furthermore, some other MMCs have been published; their catalytic performances for HER are given in Table 2.

**Table 2.** HER performance of multi-metallic catalysts.

Catalysts	Electrolyte(M)	Overpotential [mV <sub>RHE</sub> ]at 10 mA cm <sup>-2</sup>	Stability	Ref.
PtW NWS/C	KOH (1.0)	18	10, 000 cycles	[232]
F-SnO <sub>2</sub> @Pt	H <sub>2</sub> SO <sub>4</sub> (0.5)	42	10,000 cycles	[233]
RuRh <sub>2</sub>	H <sub>2</sub> SO <sub>4</sub> (0.5)KOH (1.0)PBS (1.0)	172412	30,000 cycles	[234]
PdCu <sub>0.2</sub> H <sub>0.43</sub> /C	H <sub>2</sub> SO <sub>4</sub> (0.5)	28	5000 cycles	[189]
NiFeI <sup>3+</sup> -LDH	KOH (1)	19	80 h@500 mA cm <sup>-2</sup>	[235]
Pt-MoS <sub>2</sub>	H <sub>2</sub> SO <sub>4</sub> (0.5)	67.4	24 h @-0.3 V	[236]
Ru <sub>2</sub> P/CCG-800	KOH (1)PBS (1)H <sub>2</sub> SO <sub>4</sub> (0.5)	21.83113.3849.42	5000 cycles	[237]
2DPC-RuMo	KOH (1)	18	2000 cycles	[238]
RuCo@NC-600	KOH (1.0)H <sub>2</sub> SO <sub>4</sub> (0.5)PBS (1.0)	34660	120 h@10 mA cm <sup>-2</sup>	[239]
CoP@Ni <sub>2</sub> P	KOH (1)PBS (1)H <sub>2</sub> SO <sub>4</sub> (0.5)	162029	48 h@500 mA cm <sup>-2</sup>	[240]

### 4.3. MMCs for oxygen evolution reaction

The Oxygen Evolution Reaction (OER) is a critical anodic half-reaction occurring in numerous energy storage and conversion devices, such as water splitting, fuel cells, and metal-air batteries.<sup>[241–244]</sup> It is now known that the formation of O<sub>2</sub> during OER was composed of many electron/proton-coupled stages with different reaction pathways in alkaline and acidic environments. The OER is a slow 4-electron transfer reaction kinetics that needs a relatively high overpotential (extra energy) to overcome the water oxidation barrier, prompting innovative advancement of advanced MMCs.<sup>[202,245]</sup> The process commonly utilizes synergistic interactions among metals to enhance catalytic activity, conductivity, and stability during the OER. MMCs offer several benefits, such as the capacity to fine-tune electronic structures, binding energies, and reaction kinetics. This results in reduced overpotentials and enhanced efficiency in the process of oxygen evolution.<sup>[43]</sup> For instance, Zhang and coworkers synthesized NiO/Co<sub>3</sub>O<sub>4</sub> heterostructures (Figure 12a), which demonstrated good performance with a 262 mV overpotential at 10 mA cm<sup>-2</sup> and a small Tafel slope of 58 mV dec<sup>-1</sup> in 1.0 M KOH electrolyte (Figure 12b-c). DFT calculation demonstrated that NiO/Co<sub>3</sub>O<sub>4</sub> catalyst shows a definite metallic nature, and the Co d-band centers at the given interface are shifted down, hence promoting the reaction kinetics and enhancing its OER activity.<sup>[246]</sup>

Among various combinations, current studies expose that the Cobalt (Co) and molybdenum (Mo) based bimetallic catalysts can significantly boost catalytic performance, due to their superior electronic and atomic correlations. Consequently, further increase of the exposure of active site and assist mass transportation are carried out by the optimization of structure and morphology. The catalysts with quasi 2D structure are recognized as ideal electrocatalysts. For example, Zhao and coworkers<sup>[247]</sup> prepared quasi 2D Co-Mo-O (2:1) ultrathin nanosheets (NSs) catalysts through ionic layer epitaxy (ILE) approach, which exhibited ~2.5 nm uniform thickness and a quadrangle shape. The synthesized catalysts with a 2:1 ratio of Co-to-Mo showed excellent catalytic OER activity of 273 mV overpotential at 10 mA cm<sup>-2</sup> (Figure 12d). Additionally, it possessed a lower Tafel slope of 69.6 mV dec<sup>-1</sup> and excellent stability up to 12 h (Figure 12e). They revealed that the Co-Mo-O (2:1) catalyst had the optimum OER performance due to its appropriate electronic surface structure and asymmetric electron distribution, potentially offering the optimal energy barrier for given OER intermediates. Ru is considered as a promising electrocatalyst for OER in acidic environment. Therefore, it is compulsory to prepare Ru-based catalysts of outstanding catalytic performance and durability. Commonly, heteroatom doping is considered as excellent approaches to decrease the cost and alter the electronic configuration to increase the OER activity. Hence, Qiu and coworkers<sup>[248]</sup> synthesized a Sn-

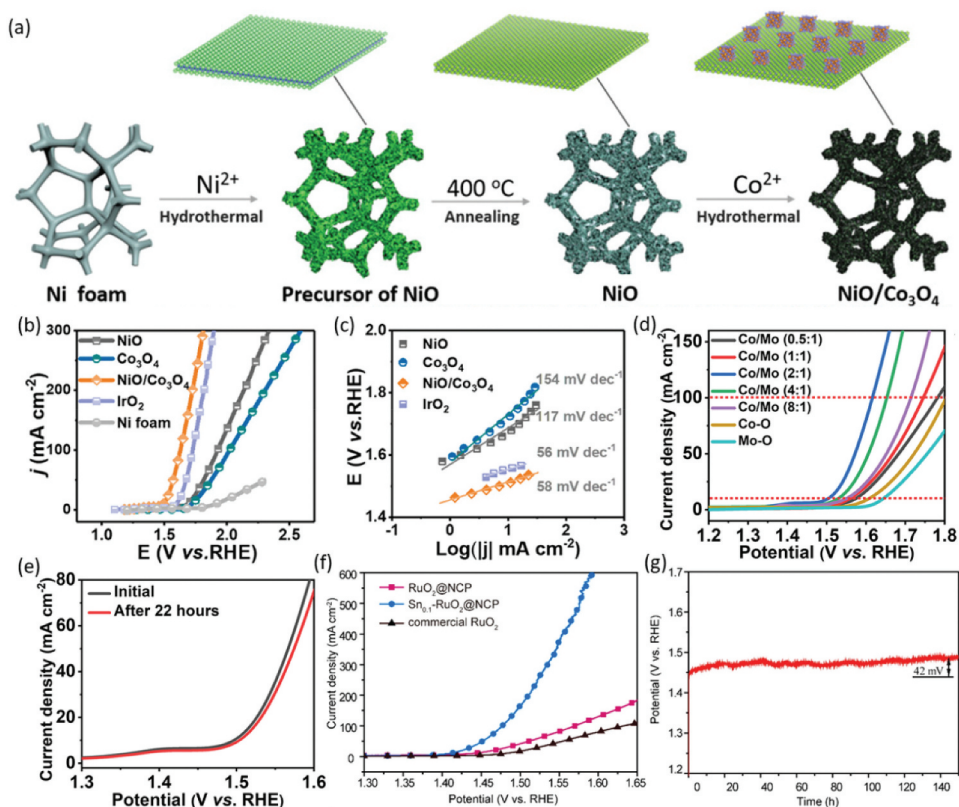


**Figure 12.** (a) Schematic synthesis process of NiO/ $\text{Co}_3\text{O}_4$  heterostructures, (b) Polarization curves, and (c) Tafel slopes of NiO/ $\text{Co}_3\text{O}_4$  catalyst.<sup>[246]</sup> Copyright © 2020 American Chemical Society. (d) LSV of Co-Mo-O NSs with different Co and Mo ratios, and (e) stability test.<sup>[247]</sup> Copyright © 2021 American Chemical Society. (f) LSV curves and (g) stability test of  $\text{Sn}_{0.1}\text{RuO}_2$ @NCP Copyright © 2020 Elsevier B.V. All rights reserved.<sup>[248]</sup>

doped  $\text{RuO}_2$  catalyst on N-doped carbon polyhedral shape support for OER. The catalyst demonstrated outstanding OER activity, with an overpotential of only 178 mV at  $10 \text{ mA cm}^{-2}$  (Figure 12f), a Tafel slope of  $60.6 \text{ mV dec}^{-1}$ , and strong durability (Figure 12g). DFT calculations revealed that Sn doping into the given  $\text{RuO}_2$  could efficiently enhance adjacent Ru sites OER activity, reducing the provided rate-determining steps' Gibbs free energy. Furthermore, analysis using the crystal-orbital Hamilton-population (COHP) approach revealed that the incorporation of Sn lowered the binding capacity among Ru active sites and reactive intermediate products ( $^*\text{O}$ ), allowing  $^*\text{OOH}$  intermediate to form easily and therefore enhancing OER performance.

Bi-metallic NiFe catalysts were investigated for OER. Core-shell  $\text{Ni}_3\text{Fe}/\text{NiFe}_2\text{O}_4$  dispersed on conductive polyaniline (PANI) was prepared using benzyl alcohol (BA) as reducing agent and was utilized as efficient OER electrocatalyst.<sup>[249]</sup> BA was also used to prepare bi metallic (NiFe) layered

double hydroxide (NiFe-LDH) as an excellent catalyst for OER.<sup>[250]</sup> In additional report, tri-metallic (Co, Fe and Ni) as the core-shell Co(OH)F@FeOOH nanorod arrays on NF was also investigated for the OER.<sup>[251]</sup> Trimetallic catalysts also show excellent catalytic performance. Huang and colleagues, for example, developed trimetallic NiCo<sub>2-x</sub>Fe<sub>x</sub>O<sub>4</sub> nanoboxes (x = 0.117) catalyst with a 274 mV overpotential at 10 mA cm<sup>-2</sup> and a small Tafel slope of 42 mVdec<sup>-1</sup> in alkaline medium, leading to the considerable electrocatalytic activity and long-term durability for OER.<sup>[252]</sup> Solomon and coworkers synthesized NiMoO<sub>4</sub>@Co<sub>3</sub>O<sub>4</sub> catalyst through the hydrothermal method of NiMoO<sub>4</sub> nanorods and followed Co<sub>3</sub>O<sub>4</sub> thin layer coating, by atomic layer deposition (ALD). The NiMoO<sub>4</sub>@Co<sub>3</sub>O<sub>4</sub> catalyst demonstrated exceptional OER activity with a modest overpotential of 120 mV at 10 mA cm<sup>-2</sup>, a Tafel slope of 58 mV dec<sup>-1</sup>, and exceptional stability.<sup>[253]</sup> Table 3 summarizes some MMCs and their OER performances.

#### 4.4. MMCs for oxygen reduction reaction

The Oxygen Reduction Reaction (ORR) takes place at the cathode of metal-air batteries and fuel cells via either 4-electron (4e<sup>-</sup>) pathway where O<sub>2</sub> molecule reduces directly to H<sub>2</sub>O or a 2-electron (2e<sup>-</sup>) pathway where the given O<sub>2</sub> molecule first reduces to H<sub>2</sub>O<sub>2</sub> molecule and then convert to H<sub>2</sub>O.<sup>[221,265]</sup> The entire ORR process is typically combination of 4e<sup>-</sup> and 2e<sup>-</sup> reactions pathway. The 4e<sup>-</sup> reaction pathway is generally chosen in maximum cases since it is considered more efficient. The H<sub>2</sub>O<sub>2</sub> formed in the 2e<sup>-</sup> reaction pathway may damage the different parts of the present electrochemical cell. Hence, the number of electron transfers is an essential estimate the definite catalytic performance. The described ORR process comprises of many stages of O<sub>2</sub> intermediates adsorbed on the

**Table 3.** OER performance of multi-metallic catalysts.

Catalysts	Electrolyte (M)	Overpotential [mV vs RHE]at 10 mA cm <sup>-2</sup>	Stability	Ref.
Ni <sub>3</sub> FeN-HC/NF	KOH (1)	219	72 h@10 mA cm <sup>-2</sup>	[254]
S-RuFeO <sub>x</sub>	HClO <sub>4</sub> (0.1)	187	5000 cycles	[255]
NiFe-PBA/Ni3C(B)	KOH (1)	196	22 h@100 mA cm <sup>-2</sup>	[256]
NiFe(OH) <sub>x</sub> /(Ni,Fe)Se <sub>2</sub> /CC	KOH (1)	180	3000 cycles	[257]
NiCo <sub>2</sub> O <sub>3</sub> @OMC	KOH (1)	281	230 h@1.15 V	[258]
CoMoP <sub>2</sub>	KOH (1)	270	6000 cycles	[259]
Ni/Ni <sub>0.2</sub> Mo <sub>0.8</sub> N@N-C	KOH (1)	260	2000 cycles	[260]
CeO <sub>2</sub> @CoS/MoS <sub>2</sub>	KOH (1)	247	12h@10 mA cm <sup>-2</sup>	[261]
RuRh@(RuRh)O <sub>2</sub> NSs	HClO <sub>4</sub> (1.0)	245	8000 s@5 mA cm <sup>-2</sup>	[262]
Mn-RuO <sub>2</sub>	H <sub>2</sub> SO <sub>4</sub> (0.5)	158	5000 cycles	[263]
Ru@Ir-O	H <sub>2</sub> SO <sub>4</sub> (0.5)	238	40 h@10 mA cm <sup>-2</sup>	[264]

electrocatalyst binding sites. As a result, the ORR performance of catalysts is mostly determined by the strength of the connection between the total active sites and the  $O_2$  intermediates, in other words, the adsorption potential of the  $O_2$  intermediates on the specified active sites. The adsorption energy correlates to the electron cloud of the binding sites in the catalysts and can be adjusted by the electrocatalyst composition and structural design.<sup>[221]</sup> Until now, great efforts have been devoted to prepare MMCs materials to accomplish high ORR catalytic performance. MMCs reveal several advantages such as the ability to customize electronic structures, regulate active sites, and optimize reaction pathways. This leads to the reduced overpotentials and enhanced overall performance for ORR in comparison to their counterparts.<sup>[39]</sup> For instance, Ge and coworkers<sup>[266]</sup> reported 2H-Pd-based alloy catalysts, i.e., 2H-PdCu nanoparticles of various contents of copper (Cu), through the definite seeded path. Moreover, the Pt incorporation into the given 2H-PdCu nanoparticles has been accomplished through the Cu galvanic replacement, followed to the 2H-PdCuPt NPs synthesis (Figure 13a). The 2H-Pd<sub>67</sub>Cu<sub>33</sub> nanoparticles possessed high ORR activity compared to fcc-Pd<sub>69</sub>Cu<sub>31</sub> nanoparticles and

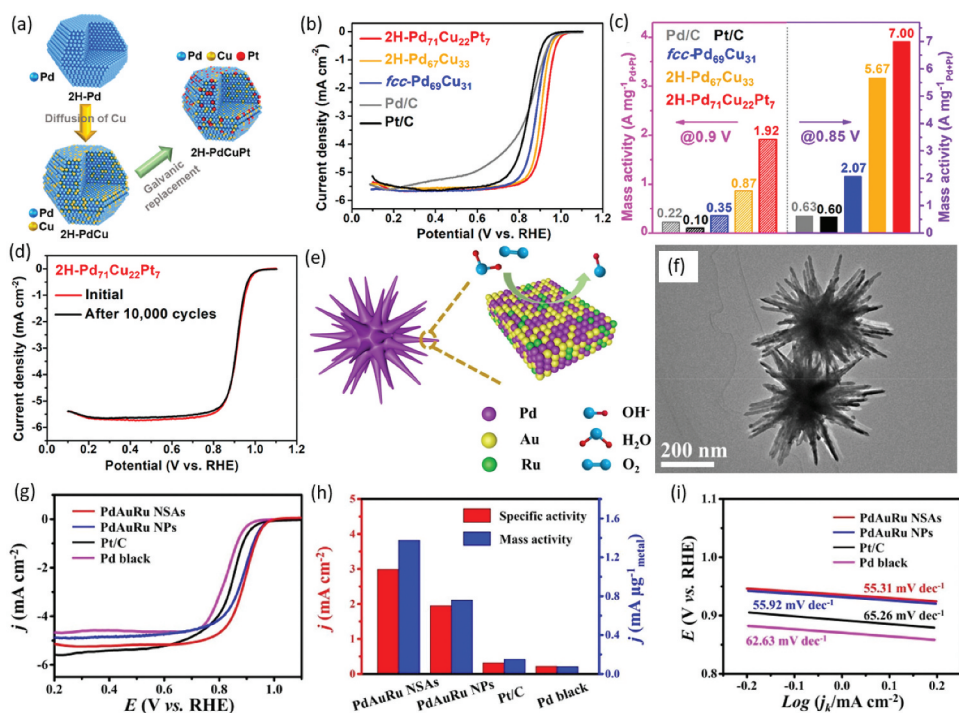


**Figure 13.** (a) Schematic preparation, (b) ORR polarization curves, (c) Mass activity, and (d) stability of 2H-Pd<sub>71</sub>Cu<sub>22</sub>Pt<sub>7</sub> nanoparticles.<sup>[266]</sup> Copyright © 2021 American Chemical Society. (e) Schematic representation, (f) TEM image, (g) ORR polarization curves, (h) specific activity and mass activity, (i) Tafel slopes of PdAuRu nanospines.<sup>[181]</sup> Copyright © 2022 Elsevier B.V. All rights reserved.

given commercial Pd/C, correspondingly. Notably, a small quantity of Pt incorporation into the 2H-Pd<sub>67</sub>Cu<sub>33</sub> nanoparticles to obtain 2H-Pd<sub>71</sub>Cu<sub>22</sub>Pt<sub>7</sub> catalyst could further improve their ORR activity (Figure 13b, c). Furthermore, the obtained catalysts possessed excellent catalytic stability (Figure 11d). Platinum (Pt)-based catalysts are regarded to be the most efficient ORR electrocatalysts. However, Pt has serious limitations, such as low availability in nature, high costs, and sluggish kinetics which make limit their applications. Hence, Sanad and coworkers<sup>[267]</sup> synthesized CoCu bimetallic metal-organic framework (MOF) catalysts through a hydrothermal method of Low temperature, which possessed excellent catalytic performance for ORR in alkaline solutions. The catalyst exhibited an onset potential ( $E_{\text{onset}}$ ) of 1.06 V<sub>RHE</sub>, a half-wave potential ( $E_{1/2}$ ) of 0.95 V<sub>RHE</sub>, and good durability of  $\Delta E_{1/2} = 30$  mV after 1000 cycles of ORR. The XPS analysis and DFT simulations confirmed that the strong Co and Cu electronic coupling generated an effective electron transfer process of interatomic, which is the significant factor to showed excellent catalytic activity for ORR. Pd-based catalysts exhibit exceptional activity and durability for ORR. Nevertheless, the incorporation of additional metals in the Pd lattice can control the electron localization and produce lattice strain, which improves catalytic performance.<sup>[80,181]</sup> For instance, Wang and coworkers<sup>[181]</sup> fabricated PdAuRu nanospines assemblies for ORR (Figure 13e, f), which displayed superior catalytic performance (Figure 13g) and stability under an alkaline environment with specific activity (SA) of 2.99 mA cm<sup>-2</sup> and a Mass activity (MA) of 1.376 mA  $\mu\text{g}_{\text{Pd}}^{-1}$  (Figure 13h). The PdAuRu NSAs showed  $E_{\text{onset}}$  of 1.0336 V,  $E_{1/2}$  of 0.8935 V, and Tafel slopes of 55.92 mV dec<sup>-1</sup> (Figure 13i). They discovered that strong ORR activity is often caused by Au and Cu introduction, which reduces adsorption energy of O<sub>2</sub> due to Pd d-band center downshift. Wang and coworkers<sup>[80]</sup> fabricated trimetallic PdCuAu nanothorn through the one-step method, which possessed a highly branched

**Table 4.** ORR performance of multi-metallic catalysts.

Catalysts	Electrolyte (M)	$E_{\text{onset}}$ [V <sub>RHE</sub> ]	$E_{1/2}$ [V <sub>RHE</sub> ]	Stability (cycles)	Ref.
AuPd NWs	KOH (0.1)	1.01	0.90	5000	[268]
Fe <sub>1</sub> Se <sub>1</sub> -NC	KOH (0.1)	1.0	0.88	5000	[269]
AuPd-SB <sub>67</sub> A <sub>33</sub> aerogels	KOH (0.1)	1.067	0.970	30,000	[270]
Au@PdPt pNWs	HClO <sub>4</sub> (0.1)	1.02	0.95	5000	[177]
Pt <sub>1</sub> Rh <sub>1</sub> @BmimBF <sub>4</sub> /CNBs	H <sub>2</sub> SO <sub>4</sub> (0.5)	0.99	0.85	5000	[271]
N-GT(FeCoNi)	NaOH (0.1)	1.01	0.89	1000	[272]
AuPd@TA LCs	KOH (0.1)	1.01	0.90	5000	[273]
PdNi TNWs	KOH (0.1)	1.05	0.95	200,000	[274]
Au@Ir CSNWs	KOH (0.1)	1.038	0.883	5000	[275]

shape, self-supported structure, and superior ORR activity. The PdCuAu NAs catalyst showed the  $E_{\text{onset}}$  of 0.96 V and  $E_{1/2}$  of 0.86 V. the catalyst exhibited a Tafel slope of  $64 \text{ mV dec}^{-1}$  and outstanding catalytic stability.

Furthermore, some other types of MMCs have been demonstrated to possess high catalytic activity for ORR, as described in Table 4.

#### 4.5. MMCs for nitrogen reduction reaction

Nitrogen reduction reaction (NRR) via atmospheric  $\text{N}_2$  conversion into ammonia ( $\text{NH}_3$ ) is an important industrial conversion reaction because ammonia shows a significant role in forming fertilizer and serves as an alternative fuel and green energy carrier.<sup>[16,276]</sup> Currently, industrial  $\text{NH}_3$  is mostly formed through the Haber–Bosch approach using Fe-based catalysts at high pressure of 150–200 atm and given high temperature of 300–500°C, which carries in huge consumption of energy.<sup>[277]</sup> In recent times, electrochemical techniques applying heterogeneous catalysts at room temperature to accomplish  $\text{N}_2$  reduction and fixation have concerned increasing attention.<sup>[278–280]</sup> The H-type electrochemical cell is mostly an adopted reactor for  $\text{N}_2$  converting into ammonia. On the anode,  $\text{H}_2\text{O}$  undergoes an oxidation process, while on the cathode,  $\text{N}_2$  is reduced to ammonia. The given reaction process is suppressed by a high overpotential, low FE, slow  $\text{N}_2$  adsorption kinetics, sluggish  $\text{N} \equiv \text{N}$  bond splitting, and low yield of ammonia production is the main NRR challenges.<sup>[277]</sup> Developing electrocatalysts, which possess high activity and stability, possess advantages in accomplishing high ammonia yield, low overpotential, and high FE is of extraordinary significance.<sup>[281]</sup> Recently, MMCs received tremendous attention and are widely utilized in the electrochemical NRR due to its high efficiency of converting nitrogen into ammonia by the synergistic effect of various metal components. MMCs exhibit several advantages in NRR, such as more appealing electrocatalytic efficiency, optimized binding for nitrogen intermediates, and exceptional durability. Through the combination of metals having favorable features, such as diverse electronic structures and strong affinities for binding nitrogen, these catalysts can overcome the challenges associated with single-metal counterparts and provide electrochemical nitrogen reduction that is both more efficient and sustainable.<sup>[282]</sup>

Gold (Au)-based catalysts have been extensively used for NRR, owing to their inattention for hydrogen, however they affect from unconvinced formation of ammonia owing to their low capability for activation of nitrogen. Modifying their morphology, size, electronic configuration and composition is an effective technique to boost their catalytic performance. For instance, Wang and colleagues<sup>[283]</sup> fabricated mesoporous film of bimetallic  $\text{Au}_3\text{Rh}$  catalyst on Ni foam ( $\text{mAu}_3\text{Rh/NF}$ ) via a micelle-assisted replacement approach. In 0.1 M  $\text{Na}_2\text{SO}_4$  electrolyte,

the  $\text{mAu}_3\text{Rh}/\text{NF}$  demonstrated outstanding activity and stability for NRR with a high  $\text{NH}_3$  yield of  $26.29 \mu\text{g h}^{-1} \text{mgcat}^{-1}$  and a FE of 23.84% (Figure 14a-c). Wang and coworkers demonstrated that the superior performance and durability of the  $\text{mAu}_3\text{Rh}/\text{NF}$  is due to the synergistic effect and regular mesoporous structure. Wang and coworkers<sup>[284]</sup> synthesized CuAu alloys with ultra-thin layers Cu skins (CuAu@2LCS) through a one-pot solvothermal process (Figure 14d). Particularly, the CuAu@2LCS catalysts demonstrated excellent NRR activity, with a maximal  $\text{NH}_3$  yield rate of  $33.9 \mu\text{g h}^{-1} \text{mgcat}^{-1}$ , FE of 24.1% at  $-0.2 \text{ V}$  versus RHE in 0.1 M HCl acidic solution, and long-term stability (Figure 14e and f). Theoretical results validated that the synergistic effect of ligand and strain engineering improved the CuAu@2LCS electrocatalytic performance concerning NRR owing to the stronger adsorption of  $\text{N}_2$  species and inhibited Hydrogen evolution reaction (HER). Palladium (Pd)-based materials also showed excellent performance for NRR, However, their performance is further enhanced by making it alloy with other metals and modulating their morphology. Hence, Wang and coworkers<sup>[286]</sup> fabricated nanoporous intermetallic  $\text{Pd}_3\text{Bi}$  (np- $\text{Pd}_3\text{Bi}$ ) catalysts, Which had exceptional activity and stability for NRR. In 0.05 M  $\text{H}_2\text{SO}_4$  medium, the np- $\text{Pd}_3\text{Bi}$  had a high  $\text{NH}_3$  production of  $59.05 \pm 2.27 \mu\text{g h}^{-1} \text{mgcat}^{-1}$  and a FE of  $21.52 \pm 0.71\%$  at  $-0.2 V_{\text{RHE}}$ . The Operando XAS and computational results revealed that robust orbital interaction among Pd and adjacent Bi atom sites resulted in a high electrostatic interaction in the given intermetallic  $\text{Pd}_3\text{Bi}$ , lowering the energy barrier and stabilizing the reaction transition state for excellent NRR.

Some oxide and sulfate based MMCs also reported, which showed high performance for NRR. For example, Tong and coworkers<sup>[287]</sup> fabricated Fe-doped  $\text{W}_{18}\text{O}_{49}$  nanowires on carbon fibers papers by hydrothermal approach, which exhibited high electrocatalysis of NRR. Significantly, the catalysts showed  $\text{NH}_3$  yielding rate of  $24.7 \mu\text{g h}^{-1} \text{mgcat}^{-1}$ , FE of 20.0% at low overpotential of  $-0.15 V_{\text{RHE}}$ , and remarkable stability. The experimental characterization and DFT calculations revealed Fe atoms interaction doping in the  $\text{W}_{18}\text{O}_{49}$  structure, exposing higher W active sites by increasing the vacancy of oxygen. Liu and coworkers<sup>[285]</sup> fabricated  $\text{FeNi}_2\text{S}_4/\text{NiS}/\text{CC-2}$  (FNS/CC-2) electrocatalysts for NRR. Notably, the catalysts performed admirably, with an  $\text{NH}_3$  yield of  $128.398 \pm 1.32 \mu\text{g h}^{-1} \text{cm}^{-2}$ , a FE of  $28.64 \pm 0.18\%$ , and exceptional stability (Figure 14g and h). The experimental investigation and theoretical findings revealed that the improved catalytic activity and selectivity are ascribed to D-band center modifications and catalyst surface electronic arrangement. Additionally, some other MMCs for NRR are have been published and exhibited good catalytic performance, are given in Table 5.



**Table 5.** NRR performance of multi-metallic catalysts.

Catalysts	Electrolyte (M)	Faradaic efficiency (FE) [%]	NH <sub>3</sub> yield rate ( $\mu\text{g h}^{-1} \text{mg}_{\text{cat}}^{-1}$ )	Stability (V vs RHE)	Ref.
mAu <sub>3</sub> Rh/NF	Na <sub>2</sub> SO <sub>4</sub> (0.1)	23.84	26.29	20 h@ -0.1	[283]
Li-TiO <sub>2</sub> (B)	LiClO <sub>4</sub> (0.5)	18.2	8.7	17 h@-0.4	[288]
Au <sub>25</sub> -Cys-Mo	HCl (0.1)	26.5	34.5	15 h@-0.2	[289]
FeMo/NC	PBS (0.1)	11.8 ± 0.8	26.5 ± 0.8	100,000 s@-0.25	[290]
Rh <sub>0.6</sub> Ru <sub>0.4</sub> NAs/CP	Na <sub>2</sub> SO <sub>4</sub> (0.1)	3.39	57.75	12 h@-0.2	[291]
BCC PdCu	LiCl (0.5)	11.5	35.7	45 h@-0.1	[292]
Au-Fe <sub>3</sub> O <sub>4</sub>	KOH (0.1)	10.54	21.42	12 h@ -0.2	[293]
Fe <sub>0.4</sub> Ni <sub>1.6</sub> P	HCl (0.1)	7.92	88.51	20 h@ -0.3	[294]

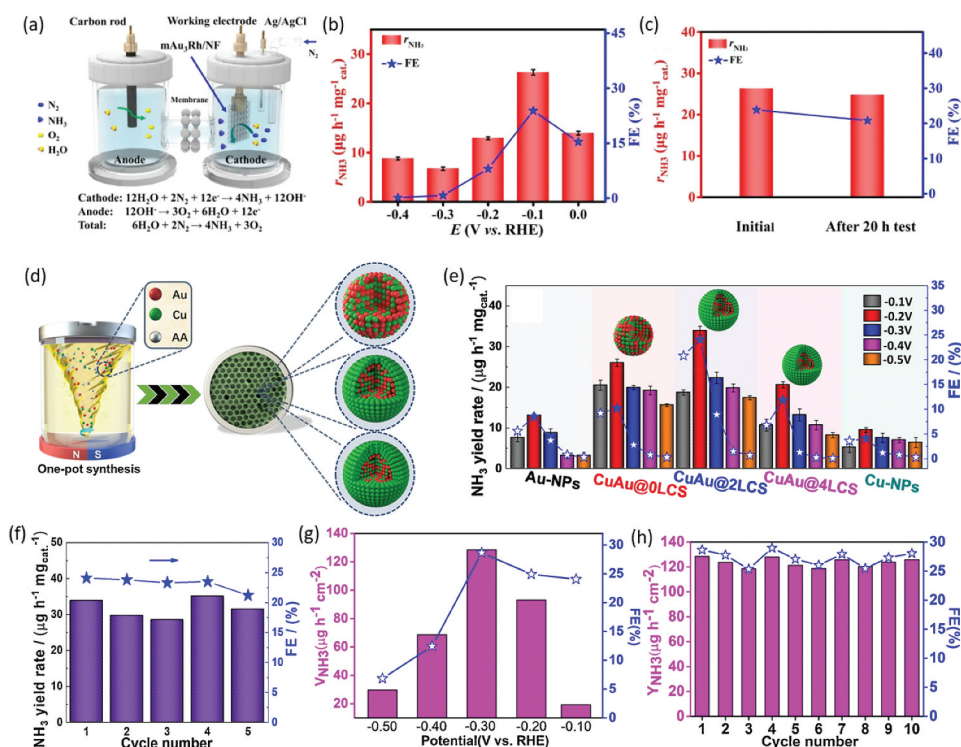


**Figure 14.** (a) Schematic representation of NRR process, (b) EF and NH<sub>3</sub> production at various potential, (c) stability test for mAu<sub>3</sub>Rh/NF.<sup>[283]</sup> Copyright © 2021 Elsevier B.V. All rights reserved. (d) Schematic synthesis, (e) NH<sub>3</sub> production and FE at various potential, (f) stability test for CuAu@xLCS.<sup>[284]</sup> Copyright © 2021 Elsevier B.V. All rights reserved. (g) NH<sub>3</sub> yield and FE at each potential, (h) stability test FeNi<sub>2</sub>S<sub>4</sub>/NiS catalysts.<sup>[285]</sup> Copyright © 2021 Elsevier B.V. All rights reserved.

#### 4.6. Other applications of multi-metallic catalysts

In addition, the electrochemical applications discussed above, MMCs are also used for some other kind of electrochemical application.<sup>[295]</sup> For example, Chen and Coworkers reported PtBi@6.7%Pb nanocatalyst for

methanol oxidation reaction (MOR). Compared to the commercial Pt/C in alkaline solution, the PtBi@6.7%Pb catalyst displayed 4 and 7.4-times greater mass activity of  $13.93 \text{ A mg}_{\text{Pt}}^{-1}$  at  $30^\circ\text{C}$  and  $51.07 \text{ A mg}_{\text{Pt}}^{-1}$  at  $60^\circ\text{C}$ , respectively. Furthermore, it was extremely durable and resistant to CO poisoning. DFT simulations showed that introducing Pb oxyhydroxide on the surface boosts the efficiency of electron transport while decreasing the poisoning impact of CO, and effective p-d coupling promotes the PtBi@6.7%Pb electrochemical performance further toward the MOR with a reduced energy barrier.<sup>[183]</sup> Qiu and coworkers presented PdZn/NC@ZnO catalysts for Ethanol oxidation reaction (EOR), which possessed higher mass activity of  $18.14 \text{ A mg}_{\text{Pd}}^{-1}$ , specific activity of  $54.60 \text{ mA cm}^{-2}$  and high catalytic stability. DFT analyses revealed that dual Pd-Zn sites enhance ethanol and OH adsorption more than individual Pd sites and dual Pd-Pd sites, allowing the EOR reaction path to operate more effectively with lower energy constraints.<sup>[296]</sup> Luo and coworkers synthesized Intermetallic PtSnBi Nanoplates, which exhibited excellent activity for formic-acid oxidation reaction (FAOR). The  $\text{Pt}_{45}\text{Sn}_{25}\text{Bi}_{30}$  nanoplates possessed ultrahigh mass activity ( $4394 \text{ mA mg}^{-1} \text{ Pt}$ ) and long-term stability, which is preserved 78% activity after 4000 potential cycles and chronopotentiometry (CA) test evaluated at 0.3 V versus SCE for 3600 s. The enhanced FAOR activities of the  $\text{Pt}_{45}\text{Sn}_{25}\text{Bi}_{30}$  nanoplates catalysts mostly ascribed due to the synergic effect of the ternary metals.<sup>[297]</sup> Incorporating extra metallic components is another design method to improve Ni-based catalysts for Urea Oxidation reaction (UOR) through bimetallic synergistic effects which was described by Yu and coworkers.<sup>[298]</sup> For instance, Li et al. developed a heteroporous  $\text{MoS}_2/\text{Ni}_3\text{S}_2$  catalyst that delivered 1.45 V cell voltage to achieve  $20 \text{ mA cm}^{-2}$  in an electrochemical cell with a 1 M KOH and 0.33 M urea solution.<sup>[299]</sup> Aside from the Ni-Mo systems, other bimetallic incorporations may also provide comparable catalytic efficiency in urea electrolysis. For instance,  $\text{Ni}_{0.9}\text{Fe}_{0.1}\text{O}$  porous hollow microspheres reported by Wu et al. demonstrated a 1.455 V cell voltage to achieve  $10 \text{ mA cm}^{-2}$ .<sup>[300]</sup> Likewise, Rh-Ni electrode with a  $50 \text{ mA cm}^{-2}$  current density at the 1.4 V cell voltage was fabricated by King et al. by electrodepositing Rh on Ni foil.<sup>[301]</sup>

## 5. Summary and outlook

As described in this review, multi-metal catalysts are applied for various applications owing to their unique property and stability which can be tuned through their particle size, shape, structure, composition, and crystal phase that can all be precisely optimized and controlled. However, despite significant accomplishments in several fields using MMCs, much more research and fundamental studies are required to develop a reproducible and robust

catalytic system. Among all, reproducibility is one of the most frequent problems for MMC synthesis, which is necessary to advance the quality of the current chemicals at this stage to reproduce the MMCs.

Furthermore, because some MMC syntheses are extremely sensitive to changes in experimental conditions, given experimental observations can lead to incorrect or ambiguous conclusions. As a result, the main syntheses parameters may be misinterpreted. Typically, qualitative research evaluations are based on precise experiments in which one or two given parameters in previous MMCs synthesis reports are purposefully varied. In certain practical syntheses, separating each parameter's effects on the product can be challenging, leading to speculative conclusions about the preparation mechanism. Therefore, in terms of qualitative research evaluation, the emphasis is shifting toward more accurate and reliable quantitative estimation in order to achieve significant success in MMCs synthesis.

Although significant research struggles have been dedicated to the preparation and electrochemical applications, the improvement of MMCs is quiet in its early stages. There is no uncertainty that the novel synthetic approaches perform a critical part in the development of MMCs from basics to applications, mainly depend on the developments in nano-materials and given nanotechnologies. When it originates to the synthesis and design of highly active and efficient electrocatalysts, increasing the number of active sites, improving the active sites' reactivity, controlling the composition and increasing stability are our last goals that we all search for. These approaches should be focused into concerns for the synthesis of advanced MMCs (Figure 15). Moreover, future research must include emphasis on the overwhelming giving challenges in the advancement of MMCs electrocatalysts.



**Figure 15.** Development approaches of advanced MMCs and challenges with the synthesis, characterization and theoretical study.

1-The composition, active sites, and electronic structure must be precisely controlled. Optimizing the catalytic synthesis conditions and novel preparation methods are needed to obtain well-controlled composition/morphology/active sites.

2-More advanced experimental and situ/operando studies require to explicate the catalytic physicochemical properties. During the electrocatalysis, the active species and electronic configuration of Catalysts undergo vigorous changes; the observing of these given changes will be useful for organizing the exact structure–property–relationship performance.

3-Combination with advanced techniques for characterization, theoretical modeling is required for deeper understanding of the MMCs nature. theoretical DFT measurements has conveyed unprecedented visions into the active sites identification and given electrocatalytic mechanism. Meanwhile, the supremacy of the theoretical calculation also lies in their valuable estimation in terms of catalytic activity in the definite electrochemical system, permitting for the manufacture of targeted MMCs.

4-The performance requires further improvement. Most of MMCs have exhibited superior performance compared to mono-metallic catalysts. However, the MMCs corrosion resistance requires to be increased to improve their cycling stability for long time, which is additional need for their wide-spread application.

5-Future commercial uses typically require MMCs on the kg scale, which is frequently required. To achieve a high yield, new synthetic techniques must be developed. In general, the majority of current methods for making MMCs involve milligram-scale production and a reaction volume range of 1–100 mL. Yields cannot be enhanced simply by raising the volume of the reaction solution while keeping the equivalent molar ratios of all the reagents constant. To accomplish this, modern technologies based on droplet-based reaction processes and continuous flow have been established. In comparison to the current traditional batch methods, these methods have the ability to identify mechanization, achieve accurate product quality control, and considerably lower overall costs. It still needs to be done more research on reliability production's rational application of the experimental reaction parameters.











## Disclosure statement

No potential conflict of interest was reported by the author(s).

## Funding

This work was supported by the Saudi Aramco [ORCP2390].

## ORCID

Muhammad Israr  <http://orcid.org/0000-0003-3854-9683>  
Muhammad Humayun  <http://orcid.org/0000-0003-3504-3935>  
Munzir H. Suliman  <http://orcid.org/0009-0000-0358-6025>  
Maryam Abdinejad  <http://orcid.org/0000-0002-9279-3815>  
Tahir Rasheed  <http://orcid.org/0000-0001-9265-6303>  
Aasif Helal  <http://orcid.org/0000-0003-2013-5327>  
Iltaf Khan  <http://orcid.org/0000-0001-8045-697X>  
Mohamed Bououdina  <http://orcid.org/0000-0001-8770-7129>  
Chundong Wang  <http://orcid.org/0000-0001-6728-0519>  
Muhammad Usman  <http://orcid.org/0000-0002-9451-3696>

## Acknowledgments

The author would like to acknowledge the support provided by the Saudi Aramco ChairProgram (ORCP2390), KFUPM Consortium for Sustainable Future, and Prince Sultan University for a Sustainable Future.

## References

- [1] Wu, L.; Ning, M.; Xing, X.; Wang, Y.; Zhang, F.; Gao, G.; Song, S.; Wang, D.; Yuan, C.; Yu, L., et al. Boosting Oxygen Evolution Reaction of (Fe,Ni)OOH via Defect Engineering for Anion Exchange Membrane Water Electrolysis Under Industrial Conditions. *Adv. Mater.* **2023**, *35*(44), 2306097. DOI: [10.1002/adma.202306097](https://doi.org/10.1002/adma.202306097).
- [2] Yang, M.; Wang, X.; Gómez-García, C. J.; Jin, Z.; Xin, J.; Cao, X.; Ma, H.; Pang, H.; Tan, L.; Yang, G., et al. Efficient Electron Transfer from an Electron-Reservoir Polyoxometalate to Dual-Metal-Site Metal-Organic Frameworks for Highly Efficient Electroreduction of Nitrogen. *Adv. Funct. Mater.* **2023**, *33*(28), 2214495. DOI: [10.1002/adfm.202214495](https://doi.org/10.1002/adfm.202214495).
- [3] Wulan, B.; Cao, X.; Tan, D.; Shu, X.; Zhang, J. Atomic Bridging of Metal-Nitrogen-Carbon toward Efficient Integrated Electrocatalysis. *Adv. Funct. Mater.* **2022**, *32*(33), 2203842. DOI: [10.1002/adfm.202203842](https://doi.org/10.1002/adfm.202203842).
- [4] Yaseen, M.; Shakirullah, M.; Ahmad, I.; Rahman, A. U.; Rahman, F. U.; Usman, M.; Razzaq, R. Simultaneous Operation of Dibenzothiophene Hydrodesulfurization and Methanol Reforming Reactions over Pd Promoted Alumina Based Catalysts. *J. Fuel Chem. Technol.* **2012**, *40*(6), 714–720. DOI: [10.1016/S1872-5813\(12\)60027-9](https://doi.org/10.1016/S1872-5813(12)60027-9).
- [5] Helal, A.; Cordova, K. E.; Arafat, M. E.; Usman, M.; Yamani, Z. H. Defect-engineering a metal-organic Framework for CO<sub>2</sub> Fixation in the Synthesis of Bioactive Oxazolidinones. *Inorg. Chem. Front.* **2020**, *7*(19), 3571–3577. DOI: [10.1039/D0QI00496K](https://doi.org/10.1039/D0QI00496K).
- [6] Usman, M.; Recent Progress of SAPO-34 Zeolite Membranes for CO<sub>2</sub> Separation: A Review. *Membranes.* **2022**, *12*(5), 507. DOI: [10.3390/membranes12050507](https://doi.org/10.3390/membranes12050507).
- [7] Ala'a, F. E.; Qaroush, A. K.; Hasan, A. K.; Assaf, K. I.; Feda'a, M.; Melhem, M. E.; Al-Maythaly, B. A.; Usman, M. Cross-linked, porous imidazolium-based poly(ionic liquid)s for CO<sub>2</sub> capture and utilisation. *New J. Chem.* **2021**, *45*(36), 16452–16460. DOI: [10.1039/D1NJ02946K](https://doi.org/10.1039/D1NJ02946K).

- [8] Rasheed, T.; 3D MXenes as Promising Alternatives for Potential Electrocatalysis Applications: Opportunities and Challenges. *J. Mater. Chem. C*. **2022**, *10*(26), 9669–9690. DOI: [10.1039/D2TC01542K](https://doi.org/10.1039/D2TC01542K).
- [9] Rasheed, T.; Ahmad Hassan, A.; Ahmad, T.; Khan, S.; Sher, F. Organic Covalent Interaction-based Frameworks as Emerging Catalysts for Environment and Energy Applications: Current Scenario and Opportunities. *Chem. Asian J.* **2023**, *18*(13), e202300196. DOI: [10.1002/asia.202300196](https://doi.org/10.1002/asia.202300196).
- [10] Rasheed, T.; Anwar, M. T. Metal Organic Frameworks as self-sacrificing Modalities for Potential Environmental Catalysis and Energy Applications: Challenges and Perspectives. *Coord. Chem. Rev.* **2023**, *480*, 215011. DOI: [10.1016/j.ccr.2022.215011](https://doi.org/10.1016/j.ccr.2022.215011).
- [11] Su, J. F.; Ahmad, M. S.; Kuan, W.-F.; Chen, C.-L.; Rasheed, T. Electrochemical Nitrate Reduction over Bimetallic Pd–Sn Nanocatalysts with Tunable Selectivity toward Benign Nitrogen. *Chemosphere*. **2024**, *350*, 141182. DOI: [10.1016/j.chemosphere.2024.141182](https://doi.org/10.1016/j.chemosphere.2024.141182).
- [12] Abdinejad, M.; Irtem, E.; Farzi, A.; Sassenburg, M.; Subramanian, S.; Iglesias van Montfort, H.-P.; Ripepi, D.; Li, M.; Middelkoop, J.; Seifitokaldani, A., et al. CO<sub>2</sub> Electrolysis via Surface-Engineering Electrografted Pyridines on Silver Catalysts. *ACS Catal.* **2022**, *12*(13), 7862–7876. DOI: [10.1021/acscatal.2c01654](https://doi.org/10.1021/acscatal.2c01654).
- [13] Afonso, R. V.; Gouveia, J. D.; Gomes, J. R. B. Catalytic Reactions for H<sub>2</sub> Production on Multimetallic Surfaces: A Review. *J. Phys.* **2021**, *3*, 032016.
- [14] Fajín, J. L. C.; Cordeiro, M. N. D. S.; Gomes, J. R. B. Water Dissociation on Multimetallic Catalysts. *Appl. Catal. B Environ.* **2017**, *218*, 199–207. DOI: [10.1016/j.apcatb.2017.06.050](https://doi.org/10.1016/j.apcatb.2017.06.050).
- [15] Marwat, M. A.; Humayun, M.; Afridi, M. W.; Zhang, H.; Abdul Karim, M. R.; Ashtar, M.; Usman, M.; Waqar, S.; Ullah, H.; Wang, C., et al. Advanced Catalysts for Photoelectrochemical Water Splitting. *ACS Appl. Energy Mater.* **2021**, *4*(11), 12007–12031. DOI: [10.1021/acsaem.1c02548](https://doi.org/10.1021/acsaem.1c02548).
- [16] Minteer, S. D.; Christopher, P.; Linic, S. Recent Developments in Nitrogen Reduction Catalysts: A Virtual Issue. *ACS Energy Lett.* **2018**, *4*(1), 163–166. DOI: [10.1021/acsenergylett.8b02197](https://doi.org/10.1021/acsenergylett.8b02197).
- [17] Rezki, M.; Septiani, N. L. W.; Iqbal, M.; Adhika, D. R.; Wenten, I. G.; Yulianto, B. Review—Recent Advance in Multi-Metallic Metal Organic Frameworks (MM-MOFs) and Their Derivatives for Electrochemical Biosensor Application. *J. Electrochem. Soc.* **2022**, *169*(1), 017504. DOI: [10.1149/1945-7111/ac3713](https://doi.org/10.1149/1945-7111/ac3713).
- [18] Lyu, F.; Wang, Q.; Choi, S. M.; Yin, Y. Noble-Metal-Free Electrocatalysts for Oxygen Evolution. *Small*. **2019**, *15*(1), 1804201. DOI: [10.1002/sml.201804201](https://doi.org/10.1002/sml.201804201).
- [19] Gong, Y.-N.; Jiao, L.; Qian, Y.; Pan, C.-Y.; Zheng, L.; Cai, X.; Liu, B.; Yu, S.-H.; Jiang, H.-L. Regulating the Coordination Environment of MOF-Templated Single-Atom Nickel Electrocatalysts for Boosting Co<sup>2+</sup> Reduction. *Angew. Chem. Int. Ed.* **2020**, *59*(7), 2705–2709. DOI: [10.1002/anie.201914977](https://doi.org/10.1002/anie.201914977).
- [20] Tan, D.; Xiong, H.; Zhang, T.; Fan, X.; Wang, J.; Xu, F. Recent Progress in noble-metal-free Electrocatalysts for Alkaline Oxygen Evolution Reaction. *Front. Chem.* **2022**, *10*, 1071274. DOI: [10.3389/fchem.2022.1071274](https://doi.org/10.3389/fchem.2022.1071274).
- [21] Han, L.; Cheng, H.; Liu, W.; Li, H.; Ou, P.; Lin, R.; Wang, H.-T.; Pao, C.-W.; Head, A. R.; Wang, C.-H. A single-atom Library for Guided Monometallic and concentration-complex Multimetallic Designs. *Nat. Mater.* **2022**, *21*(6), 681–688. DOI: [10.1038/s41563-022-01252-y](https://doi.org/10.1038/s41563-022-01252-y).
- [22] Dastafkan, K.; Shen, X.; Hocking, R. K.; Meyer, Q.; Zhao, C. Monometallic Interphasic Synergy via nano-hetero-interfacing for Hydrogen Evolution in Alkaline Electrolytes. *Nat. Commun.* **2023**, *14*(1), 547. DOI: [10.1038/s41467-023-36100-3](https://doi.org/10.1038/s41467-023-36100-3).

- [23] Toan, T. T. T.; Dao, A. Q.; Vasseghian, Y. Latest Insights on metal-based Catalysts in the Electrocatalysis Processes: Challenges and Future Perspectives. *Mol. Catal.* **2023**, *538*, 113001. DOI: [10.1016/j.mcat.2023.113001](https://doi.org/10.1016/j.mcat.2023.113001).
- [24] Kim, H.; Yoo, T. Y.; Bootharaju, M. S.; Kim, J. H.; Chung, D. Y.; Hyeon, T. Noble Metal-based Multimetallic Nanoparticles for Electrocatalytic Applications. *Adv. Sci.* **2022**, *9*(1), 2104054. DOI: [10.1002/advs.202104054](https://doi.org/10.1002/advs.202104054).
- [25] Yusuf, B. A.; Yaseen, W.; Xie, J.; Babangida, A. A.; Muhammad, A. I.; Xie, M.; Xu, Y. Rational Design of Noble metal-based Multimetallic Nanomaterials: A Review. *Nano Energy.* **2022**, *104*, 107959.
- [26] Chen, Z.; Zhang, G.; Chen, H.; Prakash, J.; Zheng, Y.; Sun, S. Multi-metallic Catalysts for the Electroreduction of Carbon Dioxide: Recent Advances and Perspectives. *Renewable Sustainable Energy Rev.* **2022**, *155*, 111922. DOI: [10.1016/j.rser.2021.111922](https://doi.org/10.1016/j.rser.2021.111922).
- [27] Zhang, N.; Amorim, I.; Liu, L. Multimetallic transition metal phosphide nanostructures for supercapacitors and electrochemical water splitting. *Nanotechnol.* **2022**, *33*(43), 432004. DOI: [10.1088/1361-6528/ac8060](https://doi.org/10.1088/1361-6528/ac8060).
- [28] Ullah, L.; Zhao, G.; Ma, J.-X.; Usman, M.; Khan, R.; Hedin, N. Pd-promoted Heteropolyacid on Mesoporous Zirconia as a Stable and Bifunctional Catalyst for Oxidation of Thiophenes. *Fuel.* **2022**, *310*, 122462. DOI: [10.1016/j.fuel.2021.122462](https://doi.org/10.1016/j.fuel.2021.122462).
- [29] Usman, M.; Helal, A.; Abdelnaby, M. M.; Alloush, A. M.; Zeama, M.; Yamani, Z. H. Trends and Prospects in UiO-66 Metal-Organic Framework for CO<sub>2</sub> Capture, Separation, and Conversion. *Chem. Rec.* **2021**, *21*(7), 1771–1791. DOI: [10.1002/tcr.202100030](https://doi.org/10.1002/tcr.202100030).
- [30] Afewerki, S.; Edlund, U. Unlocking the Power of Multicatalytic Synergistic Transformation: Toward Environmentally Adaptable Organohydrogel. *Adv. Mater.* **2024**, *36*(3), 2306657. DOI: [10.1002/adma.202306657](https://doi.org/10.1002/adma.202306657).
- [31] Luo, M.; Guo, S. Strain-controlled electrocatalysis on multimetallic nanomaterials. *Nat. Rev. Mater.* **2017**, *2*(11), 17059. DOI: [10.1038/natrevmats.2017.59](https://doi.org/10.1038/natrevmats.2017.59).
- [32] Khan, N. A.; Humayun, M.; Usman, M.; Ghazi, Z. A.; Naeem, A.; Khan, A.; Khan, A. L.; Tahir, A. A.; Ullah, H. Structural Characteristics and Environmental Applications of Covalent Organic Frameworks. *Energies.* **2021**, *14*(8), 2267. DOI: [10.3390/en14082267](https://doi.org/10.3390/en14082267).
- [33] Garba, M. D.; Usman, M.; Khan, S.; Shehzad, F.; Galadima, A.; Ehsan, M. F.; Ghanem, A. S.; Humayun, M. CO<sub>2</sub> Towards Fuels: A Review of Catalytic Conversion of Carbon Dioxide to Hydrocarbons. *J. Environ. Chem. Eng.* **2021**, *9*(2), 104756. DOI: [10.1016/j.jece.2020.104756](https://doi.org/10.1016/j.jece.2020.104756).
- [34] Khan, I.; Usman, M.; Imran, M.; Saeed, K. Nanoclay-mediated Photocatalytic Activity Enhancement of Copper Oxide Nanoparticles for Enhanced Methyl Orange Photodegradation. *J. Mater. Sci: Mater. Electron.* **2020**, *31*, 8971–8985.
- [35] Ehsan, M. F.; Fazal, A.; Hamid, S.; Arfan, M.; Khan, I.; Usman, M.; Shafiee, A.; Ashiq, M. N. CoFe<sub>2</sub>O<sub>4</sub> Decorated g-C<sub>3</sub>N<sub>4</sub> Nanosheets: New Insights into Superoxide Anion Mediated Photomineralization of Methylene Blue. *J. Environ. Chem. Eng.* **2020**, *8*(6), 104556. DOI: [10.1016/j.jece.2020.104556](https://doi.org/10.1016/j.jece.2020.104556).
- [36] Shen, S.; Han, C.; Wang, B.; Du, Y.; Wang, Y. Dual Active sites-dependent Syngas Proportions from Aqueous CO<sub>2</sub> Electroreduction. *Appl. Catal. B.* **2020**, *279*, 119380. DOI: [10.1016/j.apcatb.2020.119380](https://doi.org/10.1016/j.apcatb.2020.119380).
- [37] Usman, M.; Li, D.; Razaq, R.; Latif, U.; Muraza, O.; Yamani, Z. H.; Al-Maythalony, B. A.; Li, C.; Zhang, S. Poly Aromatic Hydrocarbon (Naphthalene) Conversion into Value Added Chemical (Tetralin): Activity and Stability of MoP/AC Catalyst. *J. Environ. Chem. Eng.* **2018**, *6*(4), 4525–4530. DOI: [10.1016/j.jece.2018.06.053](https://doi.org/10.1016/j.jece.2018.06.053).
- [38] Zhao, Z.; Liu, H.; Gao, W.; Xue, W.; Liu, Z.; Huang, J.; Pan, X.; Huang, Y. Surface-engineered PtNi-O Nanostructure with record-high Performance for Electrocatalytic

- Hydrogen Evolution Reaction. *J. Am. Chem. Soc.* **2018**, *140*(29), 9046–9050. DOI: [10.1021/jacs.8b04770](https://doi.org/10.1021/jacs.8b04770).
- [39] Du, R.; Jin, W.; Hübner, R.; Zhou, L.; Hu, Y.; Eychmüller, A. Engineering Multimetallic Aerogels for pH-Universal HER and ORR Electrocatalysis. *Adv. Energy Mater.* **2020**, *10* (12), 1903857. DOI: [10.1002/aenm.201903857](https://doi.org/10.1002/aenm.201903857).
- [40] Park, J.; Choi, S.; Oh, A.; Jin, H.; Joo, J.; Baik, H.; Lee, K. Hemi-core@frame AuCu@IrNi nanocrystals as active and durable bifunctional catalysts for the water splitting reaction in acidic media. *Nanoscale Horiz.* **2019**, *4*(3), 727–734. DOI: [10.1039/C8NH00520F](https://doi.org/10.1039/C8NH00520F).
- [41] Usman, M.; Zeb, Z.; Ullah, H.; Suliman, M. H.; Humayun, M.; Ullah, L.; Shah, S. N. A.; Ahmed, U.; Saeed, M. A Review of metal-organic frameworks/graphitic Carbon Nitride Composites for solar-driven Green H<sub>2</sub> Production, CO<sub>2</sub> Reduction, and Water Purification. *J. Environ. Chem. Eng.* **2022**, *10*(3), 107548. DOI: [10.1016/j.jece.2022.107548](https://doi.org/10.1016/j.jece.2022.107548).
- [42] Jiang, S.; Chen, F.; Zhu, L.; Yang, Z.; Lin, Y.; Xu, Q.; Wang, Y. Insight into the Catalytic Activity of Amorphous Multimetallic Catalysts under a Magnetic Field toward the Oxygen Evolution Reaction. *ACS Appl. Mater. Interfaces.* **2022**, *14*(8), 10227–10236. DOI: [10.1021/acsami.1c19936](https://doi.org/10.1021/acsami.1c19936).
- [43] Borisov, G.; Bachvarov, V.; Penchev, H.; Rashkov, R.; Slavcheva, E. Multi-metallic Electrodeposited Catalysts Applicable for Oxygen Evolution Reaction in AEM Water Electrolysis. *Mater. Lett.* **2021**, *286*, 129248. DOI: [10.1016/j.matlet.2020.129248](https://doi.org/10.1016/j.matlet.2020.129248).
- [44] Kim, T.; Kim, B.; Kwon, T.; Kim, H. Y.; Kim, J. Y.; Lee, K. Multimetallic nanostructures for electrocatalytic oxygen evolution reaction in acidic media. *Mater. Chem. Front.* **2021**, *5*(12), 4445–4473. DOI: [10.1039/D1QM00138H](https://doi.org/10.1039/D1QM00138H).
- [45] Fang, H.; Bian, H.; Hu, B.; Liu, J.; Li, S.; Wang, M.; He, L.; Zhang, Z. Multimetallic Electrocatalysts of FeCoNi Nanoalloy Embedded in Multilayered Carbon Nanotubes for Oxygen Reduction Reaction and Flexible Zn-air Battery. *Appl. Surf. Sci.* **2022**, *604*, 154590. DOI: [10.1016/j.apsusc.2022.154590](https://doi.org/10.1016/j.apsusc.2022.154590).
- [46] Wang, W.; Lei, B.; Guo, S. Engineering Multimetallic Nanocrystals for Highly Efficient Oxygen Reduction Catalysts. *Adv. Energy Mater.* **2016**, *6*(17), 1600236. DOI: [10.1002/aenm.201600236](https://doi.org/10.1002/aenm.201600236).
- [47] Suliman, M. H.; Yamani, Z. H.; Usman, M. Electrochemical Reduction of CO<sub>2</sub> to C<sub>1</sub> and C<sub>2</sub> Liquid Products on Copper-Decorated Nitrogen-Doped Carbon Nanosheets. *Nanomater.* **2023**, *13*(1), 47. DOI: [10.3390/nano13010047](https://doi.org/10.3390/nano13010047).
- [48] Huang, L.; Zhang, X.; Wang, Q.; Han, Y.; Fang, Y.; Dong, S. Shape-Control of Pt-Ru Nanocrystals: Tuning Surface Structure for Enhanced Electrocatalytic Methanol Oxidation. *J. Am. Chem. Soc.* **2018**, *140*(3), 1142–1147. DOI: [10.1021/jacs.7b12353](https://doi.org/10.1021/jacs.7b12353).
- [49] Chen, S.; Su, H.; Wang, Y.; Wu, W.; Zeng, J. Size-Controlled Synthesis of Platinum–Copper Hierarchical Trigonal Bipyramid Nanoframes. *Angew. Chem. Int. Ed.* **2015**, *54* (1), 108–113. DOI: [10.1002/anie.201408399](https://doi.org/10.1002/anie.201408399).
- [50] Ruditskiy, A.; Peng, H. C.; Xia, Y. Shape-Controlled Metal Nanocrystals for Heterogeneous Catalysis, Annual Review of Chemical and Biomolecular Engineering. *Annu Rev Chem Biomol Eng.* **2016**, *7*, 327–348.
- [51] Wang, Q.; Chen, S.; Shi, F.; Chen, K.; Nie, Y.; Wang, Y.; Wu, R.; Li, J.; Zhang, Y.; Ding, W., et al. Structural Evolution of Solid Pt Nanoparticles to a Hollow PtFe Alloy with a Pt-Skin Surface via Space-Confined Pyrolysis and the Nanoscale Kirkendall Effect. *Adv. Mater.* **2016**, *28*(48), 10673–10678. DOI: [10.1002/adma.201603509](https://doi.org/10.1002/adma.201603509).
- [52] Humayun, M.; Ullah, H.; Usman, M.; Habibi-Yangjeh, A.; Tahir, A. A.; Wang, C.; Luo, W. Perovskite-type lanthanum ferrite based photocatalysts: Preparation, properties, and applications. *J. Energy Chem.* **2022**, *66*, 314–338. DOI: [10.1016/j.jechem.2021.08.023](https://doi.org/10.1016/j.jechem.2021.08.023).



- [53] Usman, M.; Li, D.; Razzaq, R.; Yaseen, M.; Li, C.; Zhang, S. Novel MoP/HY Catalyst for the Selective Conversion of Naphthalene to Tetralin. *J. Ind. Eng. Chem.* **2015**, *23*, 21–26. DOI: [10.1016/j.jiec.2014.08.033](https://doi.org/10.1016/j.jiec.2014.08.033).
- [54] Usman, M.; Li, D.; Li, C.; Zhang, S. Highly Selective and Stable Hydrogenation of Heavy aromatic-naphthalene over Transition Metal Phosphides. *Sci. China Chem.* **2015**, *58*(4), 738–746. DOI: [10.1007/s11426-014-5199-3](https://doi.org/10.1007/s11426-014-5199-3).
- [55] Razzaq, R.; Li, C.; Usman, M.; Suzuki, K.; Zhang, S. A Highly Active and Stable Co<sub>4</sub>N/γ-Al<sub>2</sub>O<sub>3</sub> Catalyst for CO and CO<sub>2</sub> Methanation to Produce Synthetic Natural Gas (SNG). *Chem. Eng. J.* **2015**, *262*, 1090–1098. DOI: [10.1016/j.ccej.2014.10.073](https://doi.org/10.1016/j.ccej.2014.10.073).
- [56] Helal, A.; Sanhoob, M. A.; Hoque, B.; Usman, M.; Zahir, M. H. Bimetallic Metal-Organic Framework Derived Nanocatalyst for CO<sub>2</sub> Fixation through Benzimidazole Formation and Methanation of CO<sub>2</sub>. *Catalysts*. **2023**, *13*(2), 357. DOI: [10.3390/catal13020357](https://doi.org/10.3390/catal13020357).
- [57] Zhang, B.; Fu, G.; Li, Y.; Liang, L.; Grundish, N. S.; Tang, Y.; Goodenough, J. B.; Cui, Z. General Strategy for Synthesis of Ordered Pt 3 M Intermetallics with Ultrasmall Particle Size. *Angew. Chem. Int. Ed.* **2020**, *59*(20), 7857–7863. DOI: [10.1002/anie.201916260](https://doi.org/10.1002/anie.201916260).
- [58] Li, Q.; Wu, L.; Su, D.; Lv, H.; Zhang, S.; Zhu, W.; Casimir, A.; Zhu, H.; Mendoza-Garcia, A.; Sun, S. New Approach to Fully Ordered fct-FePt Nanoparticles for Much Enhanced Electrocatalysis in Acid. *Nano Lett.* **2015**, *15*(4), 2468–2473.
- [59] Dionigi, F.; Weber, C. C.; Primbs, M.; Gocyla, M.; Bonastre, A. M.; Spöri, C.; Schmiehs, H.; Hornberger, E.; Köhl, S.; Drnec, J., et al. Controlling Near-Surface Ni Composition in Octahedral PtNi(Mo) Nanoparticles by Mo Doping for a Highly Active Oxygen Reduction Reaction Catalyst. *Nano Lett.* **2019**, *19*(10), 6876–6885. DOI: [10.1021/acs.nanolett.9b02116](https://doi.org/10.1021/acs.nanolett.9b02116).
- [60] Pedersen, A.; Barrio, J.; Li, A.; Jervis, R.; Brett, D. J. L.; Titirici, M. M.; Stephens, I. E. L. Dual-Metal Atom Electrocatalysts: Theory, Synthesis, Characterization, and Applications. *Adv. Energy Mater.* **2022**, *12*(3), 2102715. DOI: [10.1002/aenm.202102715](https://doi.org/10.1002/aenm.202102715).
- [61] Zeng, J.; Fiorentin, M. R.; Fontana, M.; Castellino, M.; Risplendi, F.; Sacco, A.; Cicero, G.; Farkhondeh, M. A.; Drago, F.; Pirri, C. F. Novel Insights into Sb-Cu Catalysts for Electrochemical Reduction of CO<sub>2</sub>. *Appl. Catal. B Environ.* **2022**, *306*, 121089. DOI: [10.1016/j.apcatb.2022.121089](https://doi.org/10.1016/j.apcatb.2022.121089).
- [62] Maity, R.; Birenheide, B. S.; Breher, F.; Sarkar, B. Cooperative Effects in Multimetallic Complexes Applied in Catalysis. *ChemCatChem*. **2021**, *13*(10), 2337–2370. DOI: [10.1002/cctc.202001951](https://doi.org/10.1002/cctc.202001951).
- [63] Grefe, L.; Mejía, E. Earth-abundant Bimetallic and Multimetallic Catalysts for Epoxide/CO<sub>2</sub> ring-opening Copolymerization. *Tetrahedron*. **2021**, *98*, 132433. DOI: [10.1016/j.tet.2021.132433](https://doi.org/10.1016/j.tet.2021.132433).
- [64] Shoshani, M. M. Cooperative Heterometallic Platforms Enabling Selective C–H Bond Activation and Functionalization of Pyridines. *Cell Rep. Phys. Sci.* **2023**, *4*(4), 101213.
- [65] Shibasaki, M.; Kanai, M.; Matsunaga, S.; Kumagai, N. Recent Progress in Asymmetric Bifunctional Catalysis Using Multimetallic Systems. *Acc. Chem. Res.* **2009**, *42*(8), 1117–1127. DOI: [10.1021/ar9000108](https://doi.org/10.1021/ar9000108).
- [66] Pietrzak, M.; Ivanova, P. Bimetallic and Multimetallic Nanoparticles as Nanozymes. *Sens. Actuators B Chem.* **2021**, *336*, 129736. DOI: [10.1016/j.snb.2021.129736](https://doi.org/10.1016/j.snb.2021.129736).
- [67] Ning, C.; Bai, S.; Wang, J.; Li, Z.; Han, Z.; Zhao, Y.; O’Hare, D.; Song, Y.-F. Review of photo- and electro-catalytic multi-metallic layered double hydroxides. *Coord. Chem. Rev.* **2023**, *480*, 215008. DOI: [10.1016/j.ccr.2022.215008](https://doi.org/10.1016/j.ccr.2022.215008).
- [68] Kobylarczyk, J.; Kuzniak, E.; Liberka, M.; Chorazy, S.; Sieklucka, B.; Podgajny, R. Modular approach towards functional multimetallic coordination clusters. *Coord. Chem. Rev.* **2020**, *419*, 213394.

- [69] Han, Z.; Wang, A.-J.; Zhang, L.; Wang, Z.-G.; Fang, K.-M.; Yin, -Z.-Z.; Feng, -J.-J. 3D Highly Branched PtCoRh Nanoassemblies: Glycine-assisted Solvothermal Synthesis and Superior Catalytic Activity for Alcohol Oxidation. *J. Colloid Interface Sci.* **2019**, *554*, 512–519. DOI: [10.1016/j.jcis.2019.07.030](https://doi.org/10.1016/j.jcis.2019.07.030).
- [70] Sun, H.; Chen, M.; Xiao, B.; Zhou, T.; Humayun, M.; Li, L.; Lu, Q.; He, T.; Zhang, J.; Bououdina, M. Interface Engineering Induced Electron Redistribution at Pt Ns/NiTe-Ns Interfaces for Promoting pH-Universal and Chloride-Tolerant Hydrogen Evolution Reaction. *Small.* **2023**, *19*(49), 2303974. DOI: [10.1002/sml.202303974](https://doi.org/10.1002/sml.202303974).
- [71] Li, F.; Tian, Y.; Su, S.; Wang, C.; Li, D.-S.; Cai, D.; Zhang, S. Theoretical and Experimental Exploration of tri-metallic Organic Frameworks (t-MOFs) for Efficient Electrocatalytic Oxygen Evolution Reaction. *Appl. Catal. B Environ.* **2021**, *299*, 120665. DOI: [10.1016/j.apcatb.2021.120665](https://doi.org/10.1016/j.apcatb.2021.120665).
- [72] Ren, G.; Zhang, Z.; Liu, Y.; Liang, Y.; Zhang, X.; Wu, S.; Shen, J. One-pot Solvothermal Preparation of Ternary PdPtNi Nanostructures with Spiny Surface and Enhanced Electrocatalytic Performance during Ethanol Oxidation. *J. Alloys Compd.* **2020**, *830*, 154671. DOI: [10.1016/j.jallcom.2020.154671](https://doi.org/10.1016/j.jallcom.2020.154671).
- [73] Lai, J.; Niu, W.; Luque, R.; Xu, G. Solvothermal Synthesis of Metal Nanocrystals and Their Applications. *Nano Today.* **2015**, *10*(2), 240–267. DOI: [10.1016/j.nantod.2015.03.001](https://doi.org/10.1016/j.nantod.2015.03.001).
- [74] Broge, N. L. N.; Bertelsen, A. D.; Søndergaard-Pedersen, F.; Iversen, B. B. Facile Solvothermal Synthesis of Pt–Ir–Pd–Rh–Ru–Cu–Ni–Co High-Entropy Alloy Nanoparticles. *Chem. Mater.* **2023**, *35*(1), 144–153. DOI: [10.1021/acs.chemmater.2c02842](https://doi.org/10.1021/acs.chemmater.2c02842).
- [75] Jia, Y.; Jiang, Y.; Zhang, J.; Zhang, L.; Chen, Q.; Xie, Z.; Zheng, L. Unique Excavated Rhombic Dodecahedral PtCu<sub>3</sub> Alloy Nanocrystals Constructed with Ultrathin Nanosheets of High-Energy {110} Facets. *J. Am. Chem. Soc.* **2014**, *136*(10), 3748–3751. DOI: [10.1021/ja413209q](https://doi.org/10.1021/ja413209q).
- [76] Cao, Z.; Chen, Q.; Zhang, J.; Li, H.; Jiang, Y.; Shen, S.; Fu, G.; Lu, B.-A.; Xie, Z.; Zheng, L. Platinum-nickel alloy excavated nano-multipods with hexagonal close-packed structure and superior activity towards hydrogen evolution reaction. *Nat. Commun.* **2017**, *8*(1), 1–7. DOI: [10.1038/ncomms15131](https://doi.org/10.1038/ncomms15131).
- [77] Sun, S.; Anders, S.; Thomson, T.; Baglin, J.; Toney, M. F.; Hamann, H. F.; Murray, C.; Terris, B. D. Controlled Synthesis and Assembly of FePt Nanoparticles. *J. Phys. Chem. B.* **2003**, *107*(23), 5419–5425. DOI: [10.1021/jp027314o](https://doi.org/10.1021/jp027314o).
- [78] Li, X.; Zhang, C.; Cai, S.; Lei, X.; Altoe, V.; Hong, F.; Urban, J. J.; Ciston, J.; Chan, E. M.; Liu, Y. Facile transformation of imine covalent organic frameworks into ultrastable crystalline porous aromatic frameworks. *Nat. Commun.* **2018**, *9*(1), 2998. DOI: [10.1038/s41467-018-05462-4](https://doi.org/10.1038/s41467-018-05462-4).
- [79] Kaya, S.; Caglar, A.; Kivrak, H. CNT-Supported Multi-Metallic (Ga@PdAgCo) Anode Catalysts: Synthesis, Characterization, and Glucose Electrooxidation Application. *J. Electron. Mater.* **2023**, *52*(2), 887–895. DOI: [10.1007/s11664-022-10079-x](https://doi.org/10.1007/s11664-022-10079-x).
- [80] Wang, H.; Yin, S.; Li, Y.; Yu, H.; Li, C.; Deng, K.; Xu, Y.; Li, X.; Xue, H.; Wang, L. One-step Fabrication of tri-metallic PdCuAu Nanothorn Assemblies as an Efficient Catalyst for Oxygen Reduction Reaction. *J. Mater. Chem. A.* **2018**, *6*(8), 3642–3648. DOI: [10.1039/C7TA10342E](https://doi.org/10.1039/C7TA10342E).
- [81] Li, C.; Wang, H.; Li, Y.; Yu, H.; Yin, S.; Xue, H.; Li, X.; Xu, Y.; Wang, L. Tri-metallic PtPdAu mesoporous nanoelectrocatalysts. *Nanotechnol.* **2018**, *29*(25), 255404. DOI: [10.1088/1361-6528/aabb47](https://doi.org/10.1088/1361-6528/aabb47).
- [82] Ho, S. F.; Mendoza-Garcia, A.; Guo, S.; He, K.; Su, D.; Liu, S.; Metin, Ö.; Sun, S. A Facile Route to Monodisperse MPd (M= Co or Cu) Alloy Nanoparticles and Their Catalysis for

- Electrooxidation of Formic Acid. *Nanoscale*. 2014, 6(12), 6970–6973. DOI: [10.1039/C4NR01107D](https://doi.org/10.1039/C4NR01107D).
- [83] Liu, Y.; Wei, M.; Raciti, D.; Wang, Y.; Hu, P.; Park, J. H.; Barclay, M.; Wang, C. Electro-Oxidation of Ethanol Using Pt 3 Sn Alloy Nanoparticles. *ACS Catal.* 2018, 8(11), 10931–10937. DOI: [10.1021/acscatal.8b03763](https://doi.org/10.1021/acscatal.8b03763).
- [84] Abdinejad, M.; Subramanian, S.; Motlagh, M. K.; Noroozifar, M.; Duangdangchote, S.; Neporozhnyi, I.; Ripepi, D.; Pinto, D.; Li, M.; Tang, K. Insertion of MXene-Based Materials into Cu–Pd 3D Aerogels for Electroreduction of CO<sub>2</sub> to Formate. *Adv. Energy Mater.* 2023, 13(19), 2300402. DOI: [10.1002/aenm.202300402](https://doi.org/10.1002/aenm.202300402).
- [85] Abdinejad, M.; Motlagh, M. K.; Noroozifar, M.; Kraatz, H. B. Electroreduction of Carbon Dioxide to Formate Using Highly Efficient Bimetallic Sn–Pd Aerogels. *Mater. Adv.* 2022, 3(2), 1224–1230. DOI: [10.1039/D1MA01057C](https://doi.org/10.1039/D1MA01057C).
- [86] Xu, D.; Liu, L.; He, Z.; Yang, J.; Wu, Z.; Jing, Z. Hydrothermal Upgrading of water-insoluble Algal Biocrude over  $\gamma$ -Al<sub>2</sub>O<sub>3</sub> Supported multi-metallic Catalysts. *J. Anal. Appl. Pyrolysis*. 2019, 140, 188–194. DOI: [10.1016/j.jaap.2019.03.014](https://doi.org/10.1016/j.jaap.2019.03.014).
- [87] Epron, F.; Especel, C.; Lafaye, G.; Marécot, P. *Multimetallic Nanoparticles Prepared by Redox Processes Applied in Catalysis, Nanoparticles and Catalysis*; Wiley-VCH: Weinheim, 2008.
- [88] Sun, Q.; Wang, N.; Bing, Q.; Si, R.; Liu, J.; Bai, R.; Zhang, P.; Jia, M.; Yu, J. Subnanometric Hybrid Pd-M (OH)<sub>2</sub>, M= Ni, Co, Clusters in Zeolites as Highly Efficient Nanocatalysts for Hydrogen Generation. *Chem.* 2017, 3(3), 477–493. DOI: [10.1016/j.chempr.2017.07.001](https://doi.org/10.1016/j.chempr.2017.07.001).
- [89] Valero, M. C.; Raybaud, P. Computational Chemistry Approaches for the Preparation of Supported Catalysts: Progress and Challenges. *J. Catal.* 2020, 391, 539–547. DOI: [10.1016/j.jcat.2020.09.006](https://doi.org/10.1016/j.jcat.2020.09.006).
- [90] Wang, H.; Yang, Y.; DiSalvo, F. J.; Abruña, H. D. Multifunctional Electrocatalysts: Ru–M (M= Co, Ni, Fe) for Alkaline Fuel Cells and Electrolyzers. *ACS Catal.* 2020, 10(8), 4608–4616. DOI: [10.1021/acscatal.9b05621](https://doi.org/10.1021/acscatal.9b05621).
- [91] Wang, H.; Abruña, H. D. IrPdRu/C as H<sub>2</sub> Oxidation Catalysts for Alkaline Fuel Cells. *J. Am. Chem. Soc.* 2017, 139(20), 6807–6810. DOI: [10.1021/jacs.7b02434](https://doi.org/10.1021/jacs.7b02434).
- [92] Shen, X.; Dai, S.; Pan, Y.; Yao, L.; Yang, J.; Pan, X.; Zeng, J.; Peng, Z. Tuning electronic structure and lattice diffusion barrier of ternary Pt–In–Ni for both improved activity and stability properties in oxygen reduction electrocatalysis. *ACS Catal.* 2019, 9(12), 11431–11437. DOI: [10.1021/acscatal.9b03430](https://doi.org/10.1021/acscatal.9b03430).
- [93] Wang, L.; Zhang, Y.; Zhang, Y.; Liu, P.; Han, H.; Yang, M.; Jiang, Z.; Li, C. Hydrodesulfurization of 4, 6-DMDBT on a multi-metallic Sulfide Catalyst with Layered Structure. *Appl. Catal. A*. 2011, 394(1–2), 18–24. DOI: [10.1016/j.apcata.2010.11.043](https://doi.org/10.1016/j.apcata.2010.11.043).
- [94] Chen, Y.; Wang, L.; Liu, X.; Liu, T.; Huang, B.; Li, P.; Jiang, Z.; Li, C. Hydrodesulfurization of 4, 6-DMDBT on multi-metallic bulk catalyst NiAlZnMoW: Effect of Zn. *Appl. Catal. A*. 2015, 504, 319–327. DOI: [10.1016/j.apcata.2015.01.039](https://doi.org/10.1016/j.apcata.2015.01.039).
- [95] Lv, H.; Fan, C.; Xu, X.; Zhao, C.; Long, J. Rational Design to manganese-doped Amorphous tetra-metallic Oxides as Efficient Catalysts for LiO<sub>2</sub> Batteries. *Solid State Ionics*. 2023, 391, 116146. DOI: [10.1016/j.ssi.2023.116146](https://doi.org/10.1016/j.ssi.2023.116146).
- [96] Sagar, T. V.; Kumar, P.; Žener, B.; Šuligoj, A.; Koči, K.; Štangar, U. L. Effective Production of Formic and Acetic Acid via CO<sub>2</sub> Hydrogenation with Hydrazine by Using ZrO<sub>2</sub> Catalysts. *Mol. Catal.* 2023, 545, 113238. DOI: [10.1016/j.mcat.2023.113238](https://doi.org/10.1016/j.mcat.2023.113238).
- [97] Chen, S.; Zhang, J.; Wang, P.; Wang, X.; Song, F.; Bai, Y.; Zhang, M.; Wu, Y.; Xie, H.; Tan, Y. Effect of Vapor-phase-treatment to CuZnZr Catalyst on the Reaction Behaviors in CO<sub>2</sub> Hydrogenation into Methanol. *ChemCatChem*. 2019, 11(5), 1448–1457. DOI: [10.1002/cctc.201801988](https://doi.org/10.1002/cctc.201801988).

- [98] Zhou, Y.; Zhang, W.; Hu, J.; Li, D.; Yin, X.; Gao, Q. Inherent Oxygen Vacancies Boost Surface Reconstruction of Ultrathin Ni-Fe layered-double-hydroxides toward Efficient Electrocatalytic Oxygen Evolution. *ACS Sustain. Chem. Eng.* **2021**, *9*(21), 7390–7399. DOI: [10.1021/acssuschemeng.1c02256](https://doi.org/10.1021/acssuschemeng.1c02256).
- [99] Razmara, Z.; Razmara, F. Synthesis and Magnetic Properties of Fe-Ni-Zn, Fe-Co-Zn and Co-Ni-Zn Nanoparticles by co-precipitation Method, *Inorg. Nano-Met. Chem.* **2019**, *49*, 163–168.
- [100] Chu, C.; Chang, L.; Yin, D.; Zhang, D.; Cheng, Y.; Wang, L. Large-Sized Nickel–Cobalt–Manganese Composite Oxide Agglomerate Anode Material for Long-Life-Span Lithium-Ion Batteries. *ACS Appl. Energy Mater.* **2021**, *4*(12), 13811–13818. DOI: [10.1021/acsaem.1c02565](https://doi.org/10.1021/acsaem.1c02565).
- [101] Wang, Z.; Lin, J.; Xu, H.; Zheng, Y.; Xiao, Y.; Zheng, Y. Zr-doped NiO Nanoparticles for low-temperature Methane Combustion. *ACS Applied Nano Materials.* **2021**, *4*(11), 11920–11930. DOI: [10.1021/acsanm.1c02487](https://doi.org/10.1021/acsanm.1c02487).
- [102] Cargnello, M.; Agarwal, R.; Klein, D. R.; Diroll, B. T.; Agarwal, R.; Murray, C. B. Uniform Bimetallic Nanocrystals by high-temperature seed-mediated Colloidal Synthesis and Their Catalytic Properties for Semiconducting Nanowire Growth. *Chem. Mater.* **2015**, *27*(16), 5833–5838. DOI: [10.1021/acs.chemmater.5b02900](https://doi.org/10.1021/acs.chemmater.5b02900).
- [103] Ahmed, H. B.; Emam, H. E. Seeded Growth core-shell (Ag–Au–Pd) Ternary Nanostructure at Room Temperature for Potential Water Treatment. *Polym. Test.* **2020**, *89*, 106720. DOI: [10.1016/j.polymertesting.2020.106720](https://doi.org/10.1016/j.polymertesting.2020.106720).
- [104] Bian, T.; Sun, B.; Luo, S.; Huang, L.; Su, S.; Meng, C.; Su, S.; Yuan, A.; Zhang, H. Seed-mediated Synthesis of Au@PtCu Nanostars with Rich Twin Defects as Efficient and Stable Electrocatalysts for Methanol Oxidation Reaction. *RSC Adv.* **2019**, *9*(61), 35887–35894. DOI: [10.1039/C9RA06893G](https://doi.org/10.1039/C9RA06893G).
- [105] Xiao, X.; Jung, E.; Yu, S.; Kim, H.; Kim, H.; Lee, K.; Ahn, J.; Lim, T.; Kim, J.; Yu, T. Facile Aqueous-Phase Synthesis of Pd–FePt Core–Shell Nanoparticles for Methanol Oxidation Reaction Note: MDPI stays neutral with regard to jurisdictional claims in . . ., 2021. *Catalysts.* **2021**, *11*(1), 130. DOI: [10.3390/catal11010130](https://doi.org/10.3390/catal11010130).
- [106] Gong, Z.; Ma, T.; Liang, F. Syntheses of Magnetic blackberry-like Ni@Cu@Pd Nanoparticles for Efficient Catalytic Reduction of Organic Pollutants. *J. Alloys Compd.* **2021**, *873*, 159802. DOI: [10.1016/j.jallcom.2021.159802](https://doi.org/10.1016/j.jallcom.2021.159802).
- [107] Tang, Z.; Yeo, B. C.; Han, S. S.; Lee, T.-J.; Bhang, S. H.; Kim, W.-S.; Yu, T. Facile aqueous-phase Synthesis of Ag–Cu–Pt–Pd Quadrometallic Nanoparticles. *Nano Convergence.* **2019**, *6*(1), 1–7. DOI: [10.1186/s40580-019-0208-z](https://doi.org/10.1186/s40580-019-0208-z).
- [108] Tang, Z.; Jung, E.; Jang, Y.; Bhang, S. H.; Kim, J.; Kim, W.-S.; Yu, T. Facile aqueous-phase Synthesis of Bimetallic (AgPt, AgPd, and CuPt) and Trimetallic (AgCuPt) Nanoparticles. *Materials.* **2020**, *13*(2), 254. DOI: [10.3390/ma13020254](https://doi.org/10.3390/ma13020254).
- [109] Xi, Z.; Li, J.; Su, D.; Muzzio, M.; Yu, C.; Li, Q.; Sun, S. Stabilizing CuPd Nanoparticles via CuPd Coupling to Wo 2.72 Nanorods in Electrochemical Oxidation of Formic Acid. *J. Am. Chem. Soc.* **2017**, *139*(42), 15191–15196. DOI: [10.1021/jacs.7b08643](https://doi.org/10.1021/jacs.7b08643).
- [110] Shore, M. S.; Wang, J.; Johnston-Peck, A. C.; Oldenburg, A. L.; Tracy, J. B. Synthesis of Au(Core)/Ag(Shell) Nanoparticles and Their Conversion to AuAg Alloy Nanoparticles. *Small.* **2011**, *7*(2), 230–234. DOI: [10.1002/sml.201001138](https://doi.org/10.1002/sml.201001138).
- [111] Wang, C.; Peng, S.; Chan, R.; Sun, S. Synthesis of AuAg Alloy Nanoparticles from Core/Shell-Structured Ag/Au. *Small.* **2009**, *5*, 567–570.
- [112] Kokoh, K.; Mayousse, E.; Napporn, T.; Servat, K.; Guillet, N.; Soye, E.; Grosjean, A.; Rakotondrainibé, A.; Paul-Joseph, J. Efficient multi-metallic anode catalysts in a PEM water electrolyzer. *Int. J. Hydrogen Energy.* **2014**, *39*(5), 1924–1931. DOI: [10.1016/j.ijhydene.2013.11.076](https://doi.org/10.1016/j.ijhydene.2013.11.076).

- [113] Cui, M.; Xu, B.; Wang, L. Recent Advances in Multi-metallic-based Nanozymes for Enhanced Catalytic Cancer Therapy. *BMEMat.* **2024**, *2*, e12043.
- [114] Gao, S.; Chen, H.; Liu, Y.; Li, G.-D.; Gao, R.; Zou, X. Surface-clean, phase-pure multi-metallic Carbides for Efficient Electrocatalytic Hydrogen Evolution Reaction. *Inorg. Chem. Front.* **2019**, *6*(4), 940–947. DOI: [10.1039/C8QI01360H](https://doi.org/10.1039/C8QI01360H).
- [115] Kwon, S. G.; Hyeon, T. Formation Mechanisms of Uniform Nanocrystals via Hot-Injection and Heat-Up Methods. *Small.* **2011**, *7*(19), 2685–2702. DOI: [10.1002/sml.201002022](https://doi.org/10.1002/sml.201002022).
- [116] Sun, S.; Murray, C. B.; Weller, D.; Folks, L.; Moser, A. Monodisperse FePt Nanoparticles and Ferromagnetic FePt Nanocrystal Superlattices. *science.* **2000**, *287*(5460), 1989–1992. DOI: [10.1126/science.287.5460.1989](https://doi.org/10.1126/science.287.5460.1989).
- [117] Sun, S.; Recent Advances in Chemical Synthesis, Self-Assembly, and Applications of FePt Nanoparticles. *Adv. Mater.* **2006**, *18*(4), 393–403. DOI: [10.1002/adma.200501464](https://doi.org/10.1002/adma.200501464).
- [118] Chen, M.; Liu, J.; Sun, S. One-step Synthesis of FePt Nanoparticles with Tunable Size. *J. Am. Chem. Soc.* **2004**, *126*(27), 8394–8395. DOI: [10.1021/ja047648m](https://doi.org/10.1021/ja047648m).
- [119] Shih, K.-Y.; Wei, -J.-J.; Tsai, M.-C. One-Step Microwave-Assisted Synthesis of PtNiCo/rGO Electrocatalysts with High Electrochemical Performance for Direct Methanol Fuel Cells. *Nanomater.* **2021**, *11*(9), 2206. DOI: [10.3390/nano11092206](https://doi.org/10.3390/nano11092206).
- [120] Wang, B.; Chen, Y.; Wang, X.; Zhang, X.; Hu, Y.; Yu, B.; Yang, D.; Zhang, W. A microwave-assisted Bubble Bursting Strategy to Grow Co<sub>8</sub>FeS<sub>8</sub>/CoS Heterostructure on Rearranged Carbon Nanotubes as Efficient Electrocatalyst for Oxygen Evolution Reaction. *J. Power Sources.* **2020**, *449*, 227561. DOI: [10.1016/j.jpowsour.2019.227561](https://doi.org/10.1016/j.jpowsour.2019.227561).
- [121] Yadav, N.; Yadav, R. R.; Dey, K. K. Microwave Assisted Formation of Trimetallic AuPtCu Nanoparticles from Bimetallic nano-islands: Why It Is a Superior New Age Biocidal Agent Compared to Monometallic & Bimetallic Nanoparticles. *J. Alloys Compd.* **2022**, *896*, 163073. DOI: [10.1016/j.jallcom.2021.163073](https://doi.org/10.1016/j.jallcom.2021.163073).
- [122] Rethinasabapathy, M.; Kang, S.-M.; Haldorai, Y.; Jankiraman, M.; Jonna, N.; Choe, S. R.; Huh, Y. S.; Natesan, B. Ternary PtRuFe nanoparticles supported N-doped graphene as an efficient bifunctional catalyst for methanol oxidation and oxygen reduction reactions. *Int. J. Hydrogen Energy.* **2017**, *42*(52), 30738–30749. DOI: [10.1016/j.ijhydene.2017.10.121](https://doi.org/10.1016/j.ijhydene.2017.10.121).
- [123] Köhler, D.; Heise, M.; Baranov, A. I.; Luo, Y.; Geiger, D.; Ruck, M.; Armbrüster, M. Synthesis of BiRh Nanoplates with Superior Catalytic Performance in the Semihydrogenation of Acetylene. *Chem. Mater.* **2012**, *24*, 1639–1644.
- [124] Li, -H.-H.; Ma, S.-Y.; Fu, -Q.-Q.; Liu, X.-J.; Wu, L.; Yu, S.-H. Scalable Bromide-Triggered Synthesis of Pd@Pt Core–Shell Ultrathin Nanowires with Enhanced Electrocatalytic Performance toward Oxygen Reduction Reaction. *J. Am. Chem. Soc.* **2015**, *137*(24), 7862–7868. DOI: [10.1021/jacs.5b03877](https://doi.org/10.1021/jacs.5b03877).
- [125] Ahn, J.; Qin, D. Fabrication of Nanoscale Cage Cubes by Drilling Orthogonal, Intersected Holes through All Six Side Faces of Ag Nanocubes. *Chem. Mater.* **2019**, *31*(21), 9179–9187. DOI: [10.1021/acs.chemmater.9b03774](https://doi.org/10.1021/acs.chemmater.9b03774).
- [126] Zhu, W.; Wang, X.-B.; Li, C.; Chen, X.; Li, W.-Y.; Liu, Z.; Liang, C. Defect Engineering over Co<sub>3</sub>O<sub>4</sub> Catalyst for Surface Lattice Oxygen Activation and Boosted Propane Total Oxidation. *J. Catal.* **2022**, *413*, 150–162.
- [127] Naresh, N.; Karthik, P.; Vinoth, R.; Muthamizhchelvan, C.; Neppolian, B. Tailoring multi-metallic Nanotubes by Copper Nanowires with Platinum and Gold via Galvanic Replacement Route for the Efficient Methanol Oxidation Reaction. *Electrochim. Acta.* **2018**, *282*, 792–798. DOI: [10.1016/j.electacta.2018.06.094](https://doi.org/10.1016/j.electacta.2018.06.094).
- [128] Crockett, J. R.; Wang, M.; Doebler, J. E.; Pawale, T.; Li, X.; Bao, Y. Impact on the Formation and Catalytic Property of Pt-Based Nanocatalysts by Galvanic Reaction

- with Co-Reduction Agents. *Chem. Mater.* **2022**, *34*(20), 9282–9293. DOI: [10.1021/acs.chemmater.2c02659](https://doi.org/10.1021/acs.chemmater.2c02659).
- [129] Shahrokhian, S.; Rezaee, S. Fabrication of Trimetallic Pt–Pd–Co Porous Nanostructures on Reduced Graphene Oxide by Galvanic Replacement: Application to Electrocatalytic Oxidation of Ethylene Glycol. *Electroanalysis*. **2017**, *29*(11), 2591–2601. DOI: [10.1002/elan.201700355](https://doi.org/10.1002/elan.201700355).
- [130] Zhou, M.; Li, C.; Fang, J. Noble-metal Based Random Alloy and Intermetallic Nanocrystals. *Syntheses and Applications, Chem. Rev.* **2020**, *121*, 736–795.
- [131] Gebre, S. H.; Sendeku, M. G. Trimetallic Nanostructures and Their Applications in Electrocatalytic Energy Conversions. *J. Energy Chem.* **2022**, *65*, 329–351. DOI: [10.1016/j.jechem.2021.06.006](https://doi.org/10.1016/j.jechem.2021.06.006).
- [132] Kuang, W.-T.; Jiang, Z.-L.; Li, H.; Zhang, J.-X.; Zhou, L.-N.; Li, Y.-J. Self-Supported Composition-Tunable Au/PtPd Core/Shell Tri-Metallic Nanowires for Boosting Alcohol Electrooxidation and Suzuki Coupling. *ChemElectroChem*. **2018**, *5*(24), 3901–3905. DOI: [10.1002/celec.201801255](https://doi.org/10.1002/celec.201801255).
- [133] Xu, Y.; Zhang, B. Recent advances in porous Pt-based nanostructures: synthesis and electrochemical applications. *Chem. Soc. Rev.* **2014**, *43*(8), 2439–2450. DOI: [10.1039/c3cs60351b](https://doi.org/10.1039/c3cs60351b).
- [134] Kaur, R.; Mehta, S. Self Aggregating Metal Surfactant Complexes: Precursors for Nanostructures. *Coord. Chem. Rev.* **2014**, *262*, 37–54. DOI: [10.1016/j.ccr.2013.12.014](https://doi.org/10.1016/j.ccr.2013.12.014).
- [135] Gebre, S. H. Synthesis and Potential Applications of Trimetallic Nanostructures. *New J. Chem.* **2022**, *46*(12), 5438–5459. DOI: [10.1039/D1NJ06074K](https://doi.org/10.1039/D1NJ06074K).
- [136] Cheney, B. *Reverse Micelle Synthesis and Characterization of Supported Bimetallic Catalysts*; University of Delaware, **2010**. <https://api.semanticscholar.org/CorpusID:97688776>.
- [137] Zhang, X.; Tsang, K.-Y.; Chan, K.-Y. Electrocatalytic Properties of Supported platinum–cobalt Nanoparticles with Uniform and Controlled Composition. *J. Electroanal. Chem.* **2004**, *573*, 1–9.
- [138] Cheney, B. A.; Lauterbach, J. A.; Chen, J. G. Reverse Micelle Synthesis and Characterization of Supported Pt/Ni Bimetallic Catalysts on  $\gamma$ -Al<sub>2</sub>O<sub>3</sub>. *Appl. Catal., A*. **2011**, *394*(1–2), 41–47. DOI: [10.1016/j.apcata.2010.12.021](https://doi.org/10.1016/j.apcata.2010.12.021).
- [139] Abazari, R.; Heshmatpour, F.; Balalaie, S. Pt/Pd/Fe Trimetallic Nanoparticle Produced via Reverse Micelle Technique: Synthesis, Characterization, and Its Use as an Efficient Catalyst for Reductive Hydrodehalogenation of Aryl and Aliphatic Halides under Mild Conditions. *ACS Catal.* **2013**, *3*(2), 139–149. DOI: [10.1021/cs300507a](https://doi.org/10.1021/cs300507a).
- [140] Melo-Banda, J.; Lam-Maldonado, M.; Rodríguez-Gómez, F.; Hernández-Vega, L.; Malpica-Maldonado, J.; de la Torre, A. I. R. Ni:Fe:Mo and Ni:Co:Mo Nanocatalysts to Hydroprocessing to Heavy Crude Oil: Effect of Continue Phase in the Final Metallic Nanoparticles Size. *ACS Catal.* **2022**, *392*–393, 72–80. DOI: [10.1016/j.cattod.2021.09.018](https://doi.org/10.1016/j.cattod.2021.09.018).
- [141] Zhang, H.; Kawashima, K.; Okumura, M.; Toshima, N. Colloidal Au single-atom Catalysts Embedded on Pd Nanoclusters. *J. Mater. Chem. A*. **2014**, *2*(33), 13498–13508. DOI: [10.1039/C4TA01696C](https://doi.org/10.1039/C4TA01696C).
- [142] An, K.; Somorjai, G. A. Size and Shape Control of Metal Nanoparticles for Reaction Selectivity in Catalysis. *ChemCatChem*. **2012**, *4*(10), 1512–1524. DOI: [10.1002/cctc.201200229](https://doi.org/10.1002/cctc.201200229).
- [143] Li, C.; Pan, J.; Zhang, L.; Fang, J. Colloidal Synthesis of Monodisperse Trimetallic Pt–Fe–Ni Nanocrystals and Their Enhanced Electrochemical Performances. *Nanotechnol.* **2023**, *34*(7), 075401. DOI: [10.1088/1361-6528/aca337](https://doi.org/10.1088/1361-6528/aca337).
- [144] Wong, W. K.; Chin, J. T. Y.; Khan, S. A.; Pelletier, F.; Corbos, E. C. Robust Continuous Synthesis and in Situ Deposition of Catalytically Active Nanoparticles on Colloidal

- Support Materials in a Triphasic Flow Millireactor. *Chem. Eng. J.* **2022**, *430*, 132778. DOI: [10.1016/j.cej.2021.132778](https://doi.org/10.1016/j.cej.2021.132778).
- [145] Crawley, J. W. M.; Gow, I. E.; Lawes, N.; Kowalec, I.; Kabalan, L.; Catlow, C. R. A.; Logsdail, A. J.; Taylor, S. H.; Dummer, N. F.; Hutchings, G. J. Heterogeneous Trimetallic Nanoparticles as Catalysts. *Chem. Rev.* **2022**, *122*(6), 6795–6849. DOI: [10.1021/acs.chemrev.1c00493](https://doi.org/10.1021/acs.chemrev.1c00493).
- [146] Konuspayeva, Z.; Berhault, G.; Afanasiev, P.; Nguyen, T.-S.; Giorgio, S.; Piccolo, L. Monitoring in situ the colloidal synthesis of AuRh/TiO<sub>2</sub> selective-hydrogenation nanocatalysts. *J. Mater. Chem. A.* **2017**, *5*(33), 17360–17367. DOI: [10.1039/C7TA03965D](https://doi.org/10.1039/C7TA03965D).
- [147] Atarod, M.; Safari, J.; Tavakolizadeh, M.; Pourjavadi, A. A facile green synthesis of MgCoFe<sub>2</sub>O<sub>4</sub> nanomaterials with robust catalytic performance in the synthesis of pyrano[2,3-d]pyrimidinedione and their bis-derivatives. *Mol. Diversity.* **2021**, *25*(4), 2183–2200. DOI: [10.1007/s11030-020-10111-4](https://doi.org/10.1007/s11030-020-10111-4).
- [148] Einert, M.; Waheed, A.; Lauterbach, S.; Mellin, M.; Rohnke, M.; Wagner, L. Q.; Gallenberger, J.; Tian, C.; Smarsly, B. M.; Jaegermann, W., et al. Sol-Gel-Derived Ordered Mesoporous High Entropy Spinel Ferrites and Assessment of Their Photoelectrochemical and Electrocatalytic Water Splitting Performance. *Small.* **2023**, *19*(14), 2205412. DOI: [10.1002/sml.202205412](https://doi.org/10.1002/sml.202205412).
- [149] Ramezani, Y.; Meshkani, F.; Rezaei, M. Promotional effect of Mg in trimetallic nickel-manganese-magnesium nanocrystalline catalysts in CO<sub>2</sub> reforming of methane. *Int. J. Hydrogen Energy.* **2018**, *43*(49), 22347–22356. DOI: [10.1016/j.ijhydene.2018.09.222](https://doi.org/10.1016/j.ijhydene.2018.09.222).
- [150] D'Arienzo, M.; Scotti, R.; Di Credico, B.; Redaelli, M. Synthesis and Characterization of morphology-controlled TiO<sub>2</sub> Nanocrystals: Opportunities and Challenges for Their Application in Photocatalytic Materials, *Stud. Surf. Sci. Catal.* **2017**, *177*, 477–540.
- [151] Casillas, J.; Tzompantzi, F.; Castellanos, S.; Mendoza-Damián, G.; Pérez-Hernández, R.; López-Gaona, A.; Barrera, A. Promotion Effect of ZnO on the Photocatalytic Activity of Coupled Al<sub>2</sub>O<sub>3</sub>-Nd<sub>2</sub>O<sub>3</sub>-ZnO Composites Prepared by the Sol–Gel Method in the Degradation of Phenol. *Appl. Catal. B.* **2017**, *208*, 161–170.
- [152] Qi, S.; Yu, W.; Lonergan, W. W.; Yang, B.; Chen, J. G. General Trends in the Partial and Complete Hydrogenation of 1, 4-Cyclohexadiene over Pt–Co. *Pt–Ni and Pt–Cu Bimetallic Catalysts*, *ChemCatChem.* **2010**, *2*, 625–628.
- [153] Wang, T.; Mpourmpakis, G.; Lonergan, W. W.; Vlachos, D. G.; Chen, J. G. Effect of Oxide Supports in Stabilizing Desirable Pt–Ni Bimetallic Structures for Hydrogenation and Reforming Reactions. *Phys. Chem. Chem. Phys.* **2013**, *15*, 12156–12164.
- [154] Wang, T.; Porosoff, M. D.; Chen, J. G. Effects of Oxide Supports on the water-gas Shift Reaction over PtNi Bimetallic Catalysts: Activity and Methanation Inhibition, *Catal. Today.* **2014**, *233*, 61–69.
- [155] Ferreira, S. L. C.; Bezerra, M. A.; Santos, A. S.; Dos Santos, W. N. L.; Novaes, C. G.; de Oliveira, O. M. C.; Oliveira, M. L.; Garcia, R. L. Atomic Absorption Spectrometry – A Multi Element Technique. *TrAC Trends Anal. Chem.* **2018**, *100*, 1–6.
- [156] Zhang, M.; Song, H.; Shang, J.; Liu, X.; Qi, S.; Li, H. Spectroscopic methods for isotope analysis of heavy metal atoms: A review, *Spectrochimica Acta Part B. At. Spectrosc.* **2023**, *207*, 106740.
- [157] Planeta, K.; Kubala-Kukus, A.; Drozd, A.; Matusiak, K.; Setkowicz, Z.; Chwiej, J. The Assessment of the Usability of Selected Instrumental Techniques for the Elemental Analysis of Biomedical Samples. *Sci. Rep.* **2021**, *11*, 3704.
- [158] Bisht, N. S.; Pancholi, D.; Sahoo, N. G.; Melkani, A. B.; Mehta, S. P. S.; Dandapat, A. Effect of Ag–Fe–Cu tri-metal Loading in Bismuth Oxybromide to Develop a Novel Nanocomposite for the Sunlight Driven Photocatalytic Oxidation of Alcohols. *Catal. Sci. Technol.* **2019**, *9*, 3923–3932.

- [159] Chen, C.; Tuo, Y.; Lu, Q.; Lu, H.; Zhang, S.; Zhou, Y.; Zhang, J.; Liu, Z.; Kang, Z.; Feng, X., et al. Hierarchical Trimetallic Co-Ni-Fe Oxides Derived from core-shell Structured metal-organic Frameworks for Highly Efficient Oxygen Evolution Reaction. *Appl. Catal. B Environ.* **2021**, *287*, 119953.
- [160] Linge, K. L. Recent Developments in Trace Element Analysis by ICP-AES and ICP-MS with Particular Reference to Geological and *Environmental Samples*. *Geostandards and Geoanalytical Research.* **2005**, *29*, 7–22.
- [161] Jia, X.; Jiang, J.; Zou, S.; Han, L.; Zhu, H.; Zhang, Q.; Ma, Y.; Luo, P.; Wu, P.; Mayoral, A., et al. Library Creation of Ultrasmall Multi-metallic Nanoparticles Confined in Mesoporous MFI Zeolites. *Angew. Chem. Int. Ed.* **2021**, *60*, 14571–14577.
- [162] Balaram, V. Recent Advances in the Determination of Elemental Impurities in pharmaceuticals—Status, Challenges and Moving Frontiers, TrAC, Trends Anal. Chem. **2016**, *80*, 83–95.
- [163] Ding, H.; Wang, P.; Su, C.; Liu, H.; Tai, X.; Zhang, N.; Lv, H.; Lin, Y.; Chu, W.; Wu, X. Epitaxial Growth of Ultrathin Highly Crystalline Pt–Ni Nanostructure on a Metal Carbide Template for Efficient Oxygen Reduction Reaction. *Adv. Mater.* **2022**, *34*, 2109188.
- [164] Zhang, B.; Zheng, X.; Voznyy, O.; Comin, R.; Bajdich, M.; García-Melchor, M.; Han, L.; Xu, J.; Liu, M.; Zheng, L. Homogeneously Dispersed Multimetal oxygen-evolving Catalysts. *science.* **2016**, *352*, 333–337.
- [165] Gervasini, A. Temperature Programmed Reduction/Oxidation (TPR/TPO) Methods. *Calorimetry and Thermal Methods in Catalysis*, Springer. **2013**, *154*, 175–195.
- [166] Besselmann, S.; Freitag, C.; Hinrichsen, O.; Muhler, M. Temperature-programmed Reduction and Oxidation Experiments with V<sub>2</sub>O<sub>5</sub>/TiO<sub>2</sub> Catalysts. *Phys. Chem. Chem. Phys.* **2001**, *3*, 4633–4638.
- [167] Theofanidis, S. A.; Galvita, V. V.; Sabbe, M.; Poelman, H.; Detavernier, C.; Marin, G. B. Controlling the Stability of a Fe–Ni Reforming Catalyst: Structural Organization of the Active Components. *Appl. Catal. B.* **2017**, *209*, 405–416.
- [168] Friberg, I.; Sadokhina, N.; Olsson, L. Complete Methane Oxidation over Ba Modified Pd/Al<sub>2</sub>O<sub>3</sub>: The Effect of Water Vapor, *Appl. Catal. B.* **2018**, *231*, 242–250.
- [169] Ishii, T.; Kyotani, T. Temperature Programmed Desorption. *Mater. Sci. Eng.* **2016**, *287*–305.
- [170] Cai, C.; Liu, K.; Zhu, Y.; Li, P.; Wang, Q.; Liu, B.; Chen, S.; Li, H.; Zhu, L.; Li, H. Optimizing Hydrogen Binding on Ru Sites with RuCo Alloy Nanosheets for Efficient Alkaline Hydrogen Evolution. *Angew. Chem. Int. Ed.* **2022**, *134*, e202113664.
- [171] Bermejo-López, A.; Pereda-Ayo, B.; González-Marcos, J.; González-Velasco, J. Mechanism of the CO<sub>2</sub> Storage and in Situ Hydrogenation to CH<sub>4</sub>. Temperature and Adsorbent Loading Effects over Ru–CaO/Al<sub>2</sub>O<sub>3</sub> and Ru–Na<sub>2</sub>CO<sub>3</sub>/Al<sub>2</sub>O<sub>3</sub> Catalysts. *Appl. Catal. B.* **2019**, *256*, 117845.
- [172] Vladár, A. E.; Hodoroba, V.-D. Chapter 2.1.1 - Characterization of Nanoparticles by Scanning Electron Microscopy. In *Characterization of Nanoparticles*, Elsevier; Hodoroba, V.-D., Unger, W. E. S., Shard, A. G.; Eds.; Micro and Nano Technologies, **2020**; 7–27.
- [173] Li, G.; Zhang, H.; Han, Y. Applications of Transmission Electron Microscopy in Phase Engineering of Nanomaterials. *Chem. Rev.* **2023**, *123*, 10728–10749.
- [174] Ponce, A.; Aguilar, J. A.; Tate, J.; Yacamán, M. J. Advances in the Electron Diffraction Characterization of Atomic Clusters and Nanoparticles. *Nanoscale Adv.* **2021**, *3*, 311–325.



- [175] Jagadeesh, P.; Rangappa, S. M.; Siengchin, S. Advanced Characterization Techniques for Nanostructured Materials in Biomedical Applications. *Adv. Ind. Eng. Polym. Res.* **2024**, *7* (1), 122–143.
- [176] Vanrompay, H.; Skorikov, A.; Bladt, E.; Béch e, A.; Freitag, B.; Verbeeck, J.; Bals, S. Fast versus conventional HAADF-STEM tomography of nanoparticles: advantages and challenges. *Ultramicroscopy.* **2021**, *221*, 113191.
- [177] Liu, S.; Yin, S.; Zhang, H.; Jiao, S.; Wang, Z.; Xu, Y.; Li, X.; Wang, L.; Wang, H. Trimetallic Au@ PdPt Porous core-shell Structured Nanowires for Oxygen Reduction Electrocatalysis. *Chem. Eng. J.* **2022**, *428*, 131070.
- [178] Mourdikoudis, S.; Pallares, R. M.; Thanh, N. T. Characterization Techniques for Nanoparticles: Comparison and Complementarity upon Studying Nanoparticle Properties. *Nanoscale.* **2018**, *10*, 12871–12934.
- [179] Modena, M. M.; R uhle, B.; Burg, T. P.; Wuttke, S. Nanoparticle Characterization: What to Measure? *Adv. Mater.* **2019**, *31*, 1901556.
- [180] Shah, K.; Dai, R.; Mateen, M.; Hassan, Z.; Zhuang, Z.; Liu, C.; Israr, M.; Cheong, W. C.; Hu, B.; Tu, R. Cobalt single atom incorporated in ruthenium oxide sphere: a robust bifunctional electrocatalyst for HER and OER. *Angew. Chem. Int. Ed.* **2022**, *134*, e202114951.
- [181] Wang, H.; Ren, H.; Liu, S.; Yin, S.; Jiao, S.; Xu, Y.; Li, X.; Wang, Z.; Wang, L. Three-dimensional PdAuRu Nanospines Assemblies for Oxygen Reduction Electrocatalysis. *Chem. Eng. J.* **2022**, *438*, 135539.
- [182] Wu, R.; Tsiakaras, P.; Shen, P. K. Facile Synthesis of Bimetallic Pt-Pd symmetry-broken Concave Nanocubes and Their Enhanced Activity toward Oxygen Reduction Reaction. *Appl. Catal. B.* **2019**, *251*, 49–56.
- [183] Chen, W.; Luo, S.; Sun, M.; Tang, M.; Fan, X.; Cheng, Y.; Wu, X.; Liao, Y.; Huang, B.; Quan, Z. Hexagonal PtBi Intermetallic Inlaid with Sub-Monolayer Pb Oxyhydroxide Boosts Methanol Oxidation. *Small.* **2022**, *18*, 2107803.
- [184] Wang, X.; Xiao, H.; Li, A.; Li, Z.; Liu, S.; Zhang, Q.; Gong, Y.; Zheng, L.; Zhu, Y.; Chen, C. Constructing NiCo/Fe<sub>3</sub>O<sub>4</sub> Heteroparticles within MOF-74 for Efficient Oxygen Evolution Reactions. *J. Am. Chem. Soc.* **2018**, *140*, 15336–15341.
- [185] Deng, Y.; Xiao, Z.; Wang, Z.; Lai, J.; Liu, X.; Zhang, D.; Han, Y.; Li, S.; Sun, W.; Wang, L. The Rational Adjusting of proton-feeding by Pt-doped FeP/C Hollow Nanorod for Promoting Nitrogen Reduction Kinetics. *Appl. Catal. B.* **2021**, *291*, 120047.
- [186] Zaera, F.; New Advances in the Use of Infrared Absorption Spectroscopy for the Characterization of Heterogeneous Catalytic Reactions. *Chem. Soc. Rev.* **2014**, *43*, 7624–7663.
- [187] Venezia, A. M.; X-ray Photoelectron Spectroscopy (XPS) for Catalysts Characterization, *Catal. Today.* **2003**, *77*, 359–370.
- [188] Chen, H.-Y.; Niu, H.-J.; Han, Z.; Feng, -J.-J.; Huang, H.; Wang, A.-J. Simple Fabrication of Trimetallic platinum-nickel-cobalt Hollow Alloyed 3D Multipods for Highly Boosted Hydrogen Evolution Reaction. *J. Colloid Sci.* **2020**, *570*, 205–211.
- [189] Jia, Y.; Huang, T.-H.; Lin, S.; Guo, L.; Yu, Y.-M.; Wang, J.-H.; Wang, K.-W.; Dai, S. Stable Pd–Cu Hydride Catalyst for Efficient Hydrogen Evolution. *Nano Lett.* **2022**, *22*, 1391–1397.
- [190] Koningsberger, D. C. Principles, Applications, Techniques of EXAFS, SEXAFS and XANES. *X-ray Absorption.* **1988**. <https://cir.nii.ac.jp/crid/1571135649230758400>.
- [191] Niemantsverdriet, J. W. *Spectroscopy in Catalysis: An Introduction*; Wiley-VCH Verlag GmbH & Co. KGaA: John Wiley & Sons, **2007**.
- [192] Aksenov, V.; Kuzmin, A. Y.; Purans, J.; Tyutyunnikov, S. EXAFS spectroscopy at synchrotron-radiation beams. *Phys. Part. Nucl.* **2001**, *32*, 675–707.

- [193] Aksenov, V.; Koval'chuk, M.; Kuz'min, A. Y.; Purans, Y.; Tyutyunnikov, S. Development of Methods of EXAFS Spectroscopy on Synchrotron Radiation Beams, *Crystallogr. Rep.* **2006**, *51*, 908–935.
- [194] Iwasawa, Y. X-ray Absorption Fine Structure for Catalysts and Surfaces, World Scientific. **1996**.
- [195] Zheng, Y.; Wang, X.; Kong, Y.; Ma, Y. Two-dimensional Multimetallic Alloy Nanocrystals: Recent Progress and Challenges. *CrystEngComm.* **2021**, *23*, 6454–6469.
- [196] Lu, G.-H.; Zong, M.-H.; Li, N. Combining Electro-, Photo-, and Biocatalysis for one-pot Selective Conversion of Furfural into value-added C4 Chemicals. *ACS Catal.* **2023**, *13*, 1371–1380.
- [197] Humayun, M.; Israr, M.; Khan, A.; Bououdina, M. State-of-the-art single-atom Catalysts in Electrocatalysis: From Fundamentals to Applications. *Nano Energy.* **2023**, *113*, 108570.
- [198] Humayun, M.; Bououdina, M.; Khan, A.; Ali, S.; Wang, C. Designing single atom catalysts for exceptional electrochemical CO<sub>2</sub> reduction. *Chin. J. Struct. Chem.* **2024**, *43*, 100193.
- [199] Abdinejad, M.; Dao, C.; Deng, B.; Dinic, F.; Voznyy, O.; Zhang, X.-A.; Kraatz, H.-B. Electrocatalytic Reduction of CO<sub>2</sub> to CH<sub>4</sub> and CO in Aqueous Solution Using Pyridine-Porphyrins Immobilized onto Carbon Nanotubes. *ACS Sustainable Chem. Eng.* **2020**, *8*, 9549–9557.
- [200] Abdinejad, M.; Dao, C.; Deng, B.; Sweeney, M. E.; Dielmann, F.; Zhang, X.-A.; Kraatz, H. B. Enhanced Electrochemical Reduction of CO<sub>2</sub> to CO upon Immobilization onto Carbon Nanotubes Using an Iron-Porphyrin Dimer. *ChemistrySelect.* **2020**, *5*, 979–984.
- [201] Abdinejad, M.; Yuan, T.; Tang, K.; Duangdangchote, S.; Farzi, A.; Iglesias van Montfort, H.-P.; Li, M.; Middelkoop, J.; Wolff, M.; Seifitokaldani, A., et al. Electroreduction of Carbon Dioxide to Acetate using Heterogenized Hydrophilic Manganese Porphyrins, *Chemistry. Chem. Eur. J. Chemistry.* **2023**, *29*(14), e202203977.
- [202] Zang, W.; Kou, Z.; Pennycook, S. J.; Wang, J. Heterogeneous Single Atom Electrocatalysis, Where “Singles” are “Married. *Adv. Energy Mater.* **2020**, *10*, 1903181.
- [203] Zhu, S.; Qin, X.; Wang, Q.; Li, T.; Tao, R.; Gu, M.; Shao, M. Composition-dependent CO<sub>2</sub> Electrochemical Reduction Activity and Selectivity on Au–Pd core-shell Nanoparticles. *J. Mater. Chem. A.* **2019**, *7*, 16954–16961.
- [204] Abdinejad, M.; Ferrag, C.; Hossain, M. N.; Noroozifar, M.; Kerman, K.; Kraatz, H. B. Capture and Electroreduction of CO<sub>2</sub> Using Highly Efficient Bimetallic Pd–Ag Aerogels Paired with Carbon Nanotubes. *J. Mater. Chem. A.* **2021**, *9*, 12870–12877.
- [205] Cheng, H.; Wu, X.; Feng, M.; Li, X.; Lei, G.; Fan, Z.; Pan, D.; Cui, F.; He, G. Atomically Dispersed Ni/Cu Dual Sites for Boosting the CO<sub>2</sub> Reduction Reaction. *ACS Catal.* **2021**, *11*, 12673–12681.
- [206] Yang, Z.; Wang, H.; Fei, X.; Wang, W.; Zhao, Y.; Wang, X.; Tan, X.; Zhao, Q.; Wang, H.; Zhu, J. MOF Derived Bimetallic CuBi Catalysts with ultra-wide Potential Window for high-efficient Electrochemical Reduction of CO<sub>2</sub> to Formate. *Appl. Catal. B.* **2021**, *298*, 120571.
- [207] Pei, J.; Wang, T.; Sui, R.; Zhang, X.; Zhou, D.; Qin, F.; Zhao, X.; Liu, Q.; Yan, W.; Dong, J. N-Bridged CO–N–Ni: New Bimetallic Sites for Promoting Electrochemical CO<sub>2</sub> Reduction. *Energy Environ. Sci.* **2021**, *14*, 3019–3028.
- [208] Chen, M.; Wan, S.; Zhong, L.; Liu, D.; Yang, H.; Li, C.; Huang, Z.; Liu, C.; Chen, J.; Pan, H. Dynamic Restructuring of Cu-Doped SnS<sub>2</sub> Nanoflowers for Highly Selective Electrochemical CO<sub>2</sub> Reduction to Formate. *Angew. Chem. Int. Ed.* **2021**, *60*, 26233–26237.

- [209] Helal, A.; Shah, S. S.; Usman, M.; Khan, M. Y.; Aziz, M. A.; Rahman, M. M. Potential Applications of Nickel-Based Metal-Organic Frameworks and their Derivatives. *Chem. Rec.* **2022**, *22*(7), e202200055.
- [210] Xiong, L.; Zhang, X.; Yuan, H.; Wang, J.; Yuan, X.; Lian, Y.; Jin, H.; Sun, H.; Deng, Z.; Wang, D. Breaking the Linear Scaling Relationship by Compositional and Structural Crafting of Ternary Cu–Au/Ag Nanoframes for Electrocatalytic Ethylene Production. *Angew. Chem. Int. Ed.* **2021**, *133*, 2538–2548.
- [211] Wang, Y.; Cao, L.; Libretto, N. J.; Li, X.; Li, C.; Wan, Y.; He, C.; Lee, J.; Gregg, J.; Zong, H. Ensemble Effect in Bimetallic Electrocatalysts for CO<sub>2</sub> Reduction. *J. Am. Chem. Soc.* **2019**, *141*, 16635–16642.
- [212] Yang, Q.; Wu, Q.; Liu, Y.; Luo, S.; Wu, X.; Zhao, X.; Zou, H.; Long, B.; Chen, W.; Liao, Y. Novel Bi-Doped Amorphous SnOx Nanoshells for Efficient Electrochemical CO<sub>2</sub> Reduction into Formate at Low Overpotentials. *Adv. Mater.* **2020**, *32*, 2002822.
- [213] Lamaison, S.; Wakerley, D.; Blanchard, J.; Montero, D.; Rouse, G.; Mercier, D.; Marcus, P.; Taverna, D.; Giaume, D.; Mougél, V. High-current-density CO<sub>2</sub>-to-CO Electroreduction on Ag-alloyed Zn Dendrites at Elevated Pressure. *Joule.* **2020**, *4*, 395–406.
- [214] Chen, Y.; Fan, Z.; Wang, J.; Ling, C.; Niu, W.; Huang, Z.; Liu, G.; Chen, B.; Lai, Z.; Liu, X. Ethylene Selectivity in Electrocatalytic CO<sub>2</sub> Reduction on Cu Nanomaterials: A Crystal phase-dependent Study. *J. Am. Chem. Soc.* **2020**, *142*, 12760–12766.
- [215] Dai, L.; Qin, Q.; Wang, P.; Zhao, X.; Hu, C.; Liu, P.; Qin, R.; Chen, M.; Ou, D.; Xu, C. Ultrastable Atomic Copper Nanosheets for Selective Electrochemical Reduction of Carbon Dioxide. *Sci. Adv.* **2017**, *3*, e1701069.
- [216] Ren, W.; Tan, X.; Yang, W.; Jia, C.; Xu, S.; Wang, K.; Smith, S. C.; Zhao, C. Isolated diatomic Ni-Fe metal–nitrogen sites for synergistic electroreduction of CO<sub>2</sub>. *Angew. Chem. Int. Ed.* **2019**, *58*, 6972–6976.
- [217] Ren, D.; Ang, B. S.-H.; Yeo, B. S. Tuning the Selectivity of Carbon Dioxide Electroreduction toward Ethanol on oxide-derived Cu X Zn Catalysts. *ACS Catal.* **2016**, *6*, 8239–8247.
- [218] Herzog, A.; Bergmann, A.; Jeon, H. S.; Timoshenko, J.; Kühl, S.; Rettenmaier, C.; Luna, M. L.; Haase, F. T.; Cuenya, B. R. Operando Investigation of Ag-Decorated Cu<sub>2</sub>O Nanocube Catalysts with Enhanced CO<sub>2</sub> Electroreduction toward Liquid Products. *Angew. Chem. Int. Ed.* **2021**, *60*, 7426–7435.
- [219] Xing, Y.; Kong, X.; Guo, X.; Liu, Y.; Li, Q.; Zhang, Y.; Sheng, Y.; Yang, X.; Geng, Z.; Zeng, J. Bi@ Sn core–shell Structure with Compressive Strain Boosts the Electroreduction of CO<sub>2</sub> into Formic Acid. *Adv. Sci.* **2020**, *7*, 1902989.
- [220] Zhang, W.; Qin, Q.; Dai, L.; Qin, R.; Zhao, X.; Chen, X.; Ou, D.; Chen, J.; Chuong, T. T.; Wu, B., Electrochemical Reduction of Carbon Dioxide to Methanol on Hierarchical Pd/SnO<sub>2</sub> Nanosheets with Abundant Pd–O–Sn Interfaces, *Angew. Chem. Int. Ed.*, **57** (2018) 9475–9479
- [221] Chen, Y.; Ji, S.; Chen, C.; Peng, Q.; Wang, D.; Li, Y. Single-atom Catalysts: Synthetic Strategies and Electrochemical Applications. *Joule.* **2018**, *2*, 1242–1264.
- [222] Zhou, A.; Guo, W.-J.; Wang, Y.-Q.; Zhang, J.-T. The Rapid Preparation of Efficient MoFeCo-Based Bifunctional Electrocatalysts via Joule Heating for Overall Water Splitting. *J. Electrochem.* **2022**, *28*, 4.
- [223] Sun, H.; Li, L.; Humayun, M.; Zhang, H.; Bo, Y.; Ao, X.; Xu, X.; Chen, K.; Ostrikov, K. K.; Huo, K. Achieving Highly Efficient pH-universal Hydrogen Evolution by Superhydrophilic amorphous/crystalline Rh (OH) <sub>3</sub>/NiTe Coaxial Nanorod Array Electrode. *Appl. Catal. B Environ.* **2022**, *305*, 121088.

- [224] Qin, M.; Chen, L.; Zhang, H.; Humayun, M.; Fu, Y.; Xu, X.; Xue, X.; Wang, C. Achieving Highly Efficient pH-universal Hydrogen Evolution by Mott-Schottky Heterojunction of CO<sub>2</sub>P/Co<sub>4</sub>N. *Chem. Eng. J.* **2023**, *454*, 140230.
- [225] Xu, X.; Ullah, H.; Humayun, M.; Li, L.; Zhang, X.; Bououdina, M.; Debecker, D. P.; Huo, K.; Wang, D.; Wang, C. Fluorinated Ni-O-C Heterogeneous Catalyst for Efficient Urea-Assisted Hydrogen Production. *Adv. Funct. Mater.* **2023**, *33*, 2303986.
- [226] Wang, H.-F.; Chen, L.; Pang, H.; Kaskel, S.; Xu, Q. MOF-derived Electrocatalysts for Oxygen Reduction, Oxygen Evolution and Hydrogen Evolution Reactions. *Chem. Soc. Rev.* **2020**, *49*, 1414–1448.
- [227] Liu, G.; Zhou, W.; Chen, B.; Zhang, Q.; Cui, X.; Li, B.; Lai, Z.; Chen, Y.; Zhang, Z.; Gu, L. Synthesis of RuNi Alloy Nanostructures Composed of Multilayered Nanosheets for Highly Efficient Electrocatalytic Hydrogen Evolution. *Nano Energy.* **2019**, *66*, 104173.
- [228] Lu, J.; Tang, Z.; Luo, L.; Yin, S.; Shen, P. K.; Tsiakaras, P. Worm-like S-doped RhNi Alloys as Highly Efficient Electrocatalysts for Hydrogen Evolution Reaction. *Appl. Catal.* **2019**, *255*, 117737.
- [229] Shin, D.; Kim, H. J.; Kim, M.; Shin, D.; Kim, H.; Song, H.; Choi, S.-I. Fe X Ni<sub>2-x</sub> P Alloy Nanocatalysts with Electron-Deficient Phosphorus Enhancing the Hydrogen Evolution Reaction in Acidic Media. *ACS Catal.* **2020**, *10*, 11665–11673.
- [230] Wang, G.; Chen, W.; Chen, G.; Huang, J.; Song, C.; Chen, D.; Du, Y.; Li, C.; Ostrikov, K. K. Trimetallic Mo–Ni–Co Selenides Nanorod Electrocatalysts for highly-efficient and ultra-stable Hydrogen Evolution. *Nano Energy.* **2020**, *71*, 104637.
- [231] Zheng, Y.; Shang, P.; Pei, F.; Ma, G.; Ye, Z.; Peng, X.; Li, D. Achieving an Efficient Hydrogen Evolution Reaction with a Bicontinuous Nanoporous PtNiMg Alloy of Ultralow Noble-metal Content at an Ultrawide Range of Current Densities. *Chem. Eng. J.* **2022**, *433*, 134571.
- [232] Gao, L.; Yang, Z.; Sun, T.; Tan, X.; Lai, W.; Li, M.; Kim, J.; Lu, Y. F.; Choi, S. I.; Zhang, W. Autocatalytic Surface Reduction-Assisted Synthesis of PtW Ultrathin Alloy Nanowires for Highly Efficient Hydrogen Evolution Reaction. *Adv. Energy Mater.* **2022**, *12*, 2103943.
- [233] Kim, T.; Roy, S. B.; Moon, S.; Yoo, S.; Choi, H.; Parale, V. G.; Kim, Y.; Lee, J.; Jun, S. C.; Kang, K. Highly Dispersed Pt Clusters on F-Doped Tin (IV) Oxide Aerogel Matrix: An Ultra-Robust Hybrid Catalyst for Enhanced Hydrogen Evolution. *ACS Nano.* **2022**, *16*, 1625–1638.
- [234] Mu, X.; Gu, J.; Feng, F.; Xiao, Z.; Chen, C.; Liu, S.; Mu, S., RuRh Bimetallene Nanoring as High-efficiency pH-Universal Catalyst for Hydrogen Evolution Reaction, *Adv. Sci.* **8** (2021) 2002341
- [235] Wang, M.; Wang, J. Q.; Xi, C.; Cheng, C. Q.; Kuai, C. G.; Zheng, X. L.; Zhang, R.; Xie, Y. M.; Dong, C. K.; Chen, Y. J. Valence-State Effect of Iridium Dopant in NiFe (OH) 2 Catalyst for Hydrogen Evolution Reaction. *Small.* **2021**, *17*, 2100203.
- [236] Shan, A.; Teng, X.; Zhang, Y.; Zhang, P.; Xu, Y.; Liu, C.; Li, H.; Ye, H.; Wang, R. Interfacial electronic structure modulation of Pt-MoS<sub>2</sub> heterostructure for enhancing electrocatalytic hydrogen evolution reaction. *Nano Energy.* **2022**, *94*, 106913.
- [237] Yang, D.; Li, P.; Gao, X.-Y.; Han, J.; Liu, Z.-Y.; Yang, Y.-P.; Yang, J.-H. Modulating Surface Segregation of Ni<sub>2</sub>P-Ru<sub>2</sub>P/CCG Nanoparticles for Boosting Hydrogen Evolution Reaction in pH-universal. *Chem. Eng. J.* **2022**, *432*, 134422.
- [238] Tu, K.; Tranca, D.; Rodríguez-Hernández, F.; Jiang, K.; Huang, S.; Zheng, Q.; Chen, M. X.; Lu, C.; Su, Y.; Chen, Z. A Novel Heterostructure Based on RuMo Nanoalloys and N-doped Carbon as an Efficient Electrocatalyst for the Hydrogen Evolution Reaction. *Adv. Mater.* **2020**, *32*, 2005433.

- [239] Zhang, F.; Zhu, Y.; Chen, Y.; Lu, Y.; Lin, Q.; Zhang, L.; Tao, S.; Zhang, X.; Wang, H. RuCo alloy bimodal nanoparticles embedded in N-doped carbon: a superior pH-universal electrocatalyst outperforms benchmark Pt for the hydrogen evolution reaction. *J. Mater. Chem. A*. **2020**, *8*, 12810–12820.
- [240] Jin, M.; Zhang, X.; Shi, R.; Lian, Q.; Niu, S.; Peng, O.; Wang, Q.; Cheng, C. Hierarchical CoP@ Ni<sub>2</sub>P Catalysts for pH-universal Hydrogen Evolution at High Current Density. *Appl. Catal. B*. **2021**, *296*, 120350.
- [241] Li, M.; Sun, H.; Yang, J.; Humayun, M.; Li, L.; Xu, X.; Xue, X.; Habibi-Yangjeh, A.; Temst, K.; Wang, C. Mono-coordinated Metallocene Ligands Endow metal-organic Frameworks with Highly Efficient Oxygen Evolution and Urea Electrolysis. *Chem. Eng. J*. **2022**, *430*, 132733.
- [242] Chen, B.; Humayun, M.; Li, Y.; Zhang, H.; Sun, H.; Wu, Y.; Wang, C. Constructing Hierarchical Fluffy CoO–Co<sub>4</sub>N@ NiFe-LDH Nanorod Arrays for Highly Effective Overall Water Splitting and Urea Electrolysis. *ACS Sustainable Chem. Eng*. **2021**, *9*, 14180–14192.
- [243] Xie, M.; Bian, J.; Humayun, M.; Qu, Y.; Feng, Y.; Jing, L. The Promotion Effect of Surface Negative Electrostatic Field on the Photogenerated Charge Separation of BiVO<sub>4</sub> and Its Contribution to the Enhanced PEC Water Oxidation. *Chem. Commun*. **2015**, *51*, 2821–2823.
- [244] Zhang, X.; Cui, H.; Humayun, M.; Qu, Y.; Fan, N.; Sun, X.; Jing, L. Exceptional Performance of Photoelectrochemical Water Oxidation of single-crystal Rutile TiO<sub>2</sub> Nanorods Dependent on the Hole Trapping of Modified Chloride. *Sci. Rep*. **2016**, *6*, 21430.
- [245] Song, Z.; Zhang, L.; Doyle-Davis, K.; Fu, X.; Luo, J. L.; Sun, X. Recent Advances in MOF-derived Single Atom Catalysts for Electrochemical Applications. *Adv. Energy Mater*. **2020**, *10*, 2001561.
- [246] Zhang, J.; Qian, J.; Ran, J.; Xi, P.; Yang, L.; Gao, D. Engineering Lower Coordination Atoms onto NiO/Co<sub>3</sub>O<sub>4</sub> Heterointerfaces for Boosting Oxygen Evolution Reactions. *ACS Catal*. **2020**, *10*, 12376–12384.
- [247] Zhao, Y.; Wang, Y.; Dong, Y.; Carlos, C.; Li, J.; Zhang, Z.; Li, T.; Shao, Y.; Yan, S.; Gu, L. Quasi-two-dimensional earth-abundant bimetallic electrocatalysts for oxygen evolution reactions. *ACS Energy Lett*. **2021**, *6*, 3367–3375.
- [248] Qiu, L.; Zheng, G.; He, Y.; Lei, L.; Zhang, X. Ultra-small Sn-RuO<sub>2</sub> nanoparticles supported on N-doped carbon polyhedra for highly active and durable oxygen evolution reaction in acidic media. *Chem. Eng. J*. **2021**, *409*, 128155.
- [249] Alharthy, M.; Suliman, M. H.; Al-Betar, A.-R.; Wang, Y.; Tian, Z.; Drmish, Q. A.; Yamani, Z. H.; Qamar, M. Reaping the Catalytic Benefits of Both Surface (Ni<sub>2</sub>O<sub>4</sub>) and Underneath (Ni<sub>3</sub>Fe) Layers for the Oxygen Evolution Reaction. *Sustain Energy Fuels*. **2021**, *5*, 2704–2714.
- [250] Suliman, M.; Al Ghamdi, A.; Baroud, T.; Drmish, Q.; Rafatullah, M.; Yamani, Z.; Qamar, M. Growth of Ultrathin Nanosheets of Nickel Iron Layered Double Hydroxide for the Oxygen Evolution Reaction. *Int. J. Hydrogen Energy*. **2022**, *47*, 23498–23507.
- [251] Li, R.; Wang, Y.; Chen, B.; Zhang, H.; Yan, C.; Xu, X.; Humayun, M.; Debecker, D. P.; Wang, C. Core-shell Structured Co (OH) F@ FeOOH Enables Highly Efficient Overall Water Splitting in Alkaline Electrolyte. *Int. J. Hydrogen Energy*. **2024**, *51*, 1292–1302.
- [252] Huang, Y.; Zhang, S. L.; Lu, X. F.; Wu, Z. P.; Luan, D.; Lou, X. W. Trimetallic Spinel NiCO<sub>2</sub>-xFe<sub>x</sub>O<sub>4</sub> Nanoboxes for Highly Efficient Electrocatalytic Oxygen Evolution. *Angew. Chem. Int. Ed*. **2021**, *133*, 11947–11952.
- [253] Solomon, G.; Landström, A.; Mazzaro, R.; Jugovac, M.; Moras, P.; Cattaruzza, E.; Morandi, V.; Concina, I.; Vomiero, A. NiMoO<sub>4</sub>@ Co<sub>3</sub>O<sub>4</sub> core-shell Nanorods: In Situ

- Catalyst Reconstruction toward High Efficiency Oxygen Evolution Reaction. *Adv. Energy Mater.* **2021**, *11*, 2101324.
- [254] Yu, L.; Zhang, G.; Chen, H.; Zeng, J.; Liu, Y.; Yang, Q.; Zhong, L.; Qiu, Y. Ultrathin hollow hemisphere-carbon-anchored Ni<sub>3</sub>FeN nanoparticles as nanoreactors facilitating the formation of NiC<sub>x</sub> with long-term durability for the oxygen evolution reaction. *J. Mater. Chem. A*. **2022**, *10*, 7911–7919.
- [255] Xue, Y.; Fang, J.; Wang, X.; Xu, Z.; Zhang, Y.; Lv, Q.; Liu, M.; Zhu, W.; Zhuang, Z. Sulfate-Functionalized RuFeOx as Highly Efficient Oxygen Evolution Reaction Electrocatalyst in Acid. *Adv. Funct. Mater.* **2021**, *31*, 2101405.
- [256] Lin, X.; Cao, S.; Chen, H.; Chen, X.; Wang, Z.; Zhou, S.; Xu, H.; Liu, S.; Wei, S.; Lu, X. Boosting Oxygen Evolution Reaction of Hierarchical Spongy NiFe-PBA/Ni<sub>3</sub>C (B) Electrocatalyst. *Interfacial Engineering with Matchable Structure, Chem. Eng. J.* **2022**, *433*, 133524.
- [257] Liu, C.; Han, Y.; Yao, L.; Liang, L.; He, J.; Hao, Q.; Zhang, J.; Li, Y.; Liu, H. Engineering Bimetallic NiFe-Based Hydroxides/Selenides Heterostructure Nanosheet Arrays for Highly-Efficient Oxygen Evolution Reaction. *Small*. **2021**, *17*, 2007334.
- [258] Zhang, Y.; Wang, X.; Luo, F.; Tan, Y.; Zeng, L.; Fang, B.; Liu, A. Rock Salt Type NiCO<sub>2</sub>O<sub>3</sub> Supported on Ordered Mesoporous Carbon as a Highly Efficient Electrocatalyst for Oxygen Evolution Reaction. *Appl. Catal. B*. **2019**, *256*, 117852.
- [259] Xu, S.; Gao, X.; Deshmukh, A.; Zhou, J.; Chen, N.; Peng, W.; Gong, Y.; Yao, Z.; Finkelstein, K. D.; Wan, B. Pressure-promoted Irregular CoMoP<sub>2</sub> Nanoparticles Activated by Surface Reconstruction for Oxygen Evolution Reaction Electrocatalysts. *J. Mater. Chem. A*. **2020**, *8*, 2001–2007.
- [260] Li, T.; Hu, Y.; Pan, X.; Yin, J.; Li, Y.; Wang, Y.; Zhang, Y.; Sun, H.; Tang, Y. N-carbon Supported Hierarchical Ni/Ni<sub>0.2</sub>Mo<sub>0.8</sub>N Nanosheets as high-efficiency Oxygen Evolution Electrocatalysts. *Chem. Eng. J.* **2020**, *392*, 124845.
- [261] Huang, W.-H.; Li, X.-M.; Yang, X.-F.; Zhang, H.-Y.; Liu, P.-B.; Ma, Y.-M.; Lu, X. CeO<sub>2</sub>-embedded Mesoporous CoS/MoS<sub>2</sub> as Highly Efficient and Robust Oxygen Evolution Electrocatalyst. *Chem. Eng. J.* **2021**, *420*, 127595.
- [262] Wang, K.; Huang, B.; Zhang, W.; Lv, F.; Xing, Y.; Zhang, W.; Zhou, J.; Yang, W.; Lin, F.; Zhou, P. Ultrathin RuRh@(RuRh)<sub>2</sub>O<sub>3</sub> Core@ Shell Nanosheets as Stable Oxygen Evolution Electrocatalysts. *J. Mater. Chem. A*. **2020**, *8*, 15746–15751.
- [263] Chen, S.; Huang, H.; Jiang, P.; Yang, K.; Diao, J.; Gong, S.; Liu, S.; Huang, M.; Wang, H.; Chen, Q. Mn-doped RuO<sub>2</sub> nanocrystals as highly active electrocatalysts for enhanced oxygen evolution in acidic media. *ACS Catal.* **2019**, *10*, 1152–1160.
- [264] Zhang, J.; Fu, X.; Xia, F.; Zhang, W.; Ma, D.; Zhou, Y.; Peng, H.; Wu, J.; Gong, X.; Wang, D. Core-Shell Nanostructured Ru@ Ir–O Electrocatalysts for Superb Oxygen Evolution in Acid. *Small*. **2022**, *18*, 2108031.
- [265] Wang, J.; Kim, J.; Choi, S.; Wang, H.; Lim, J. A Review of Carbon-supported Nonprecious Metals as Energy-related Electrocatalysts. *Small Methods*. **2020**, *4*, 2000621.
- [266] Ge, Y.; Wang, X.; Huang, B.; Huang, Z.; Chen, B.; Ling, C.; Liu, J.; Liu, G.; Zhang, J.; Wang, G. Seeded Synthesis of Unconventional 2H-phase Pd Alloy Nanomaterials for Highly Efficient Oxygen Reduction. *J. Am. Chem. Soc.* **2021**, *143*, 17292–17299.
- [267] Sanad, M. F.; Puente Santiago, A. R.; Tolba, S. A.; Ahsan, M. A.; Fernandez-Delgado, O.; Shawky Adly, M.; Hashem, E. M.; Mahrous Abodouh, M.; El-Shall, M. S.; Sreenivasan, S. T. Co–Cu bimetallic metal organic framework catalyst outperforms the Pt/C benchmark for oxygen reduction. *J. Am. Chem. Soc.* **2021**, *143*, 4064–4073.
- [268] Liu, S.; Ren, H.; Yin, S.; Zhang, H.; Wang, Z.; Xu, Y.; Li, X.; Wang, L.; Wang, H. Defect-rich Ultrathin AuPd Nanowires with Boerdijk–Coxeter Structure for Oxygen Reduction Electrocatalysis. *Chem. Eng. J.* **2022**, *435*, 134823.

- [269] Chen, Z.; Su, X.; Ding, J.; Yang, N.; Zuo, W.; He, Q.; Wei, Z.; Zhang, Q.; Huang, J.; Zhai, Y. Boosting Oxygen Reduction Reaction with Fe and Se dual-atom Sites Supported by nitrogen-doped Porous Carbon. *Appl. Catal. B.* **2022**, *308*, 121206.
- [270] Zhang, X.; Wang, J.; Zhang, M.; Yue, X.; Du, W.; Fan, W.; Xia, H. S-doped AuPd Aerogels as High Efficiency Catalysts for the Oxygen Reduction Reaction by Balancing the Ratio between Bridging S 2 2- and Apical S 2- Ligands. *J. Mater. Chem. A.* **2022**, *10*, 7800–7810.
- [271] Zhang, Z.-N.; Miao, B.-Q.; Wu, Z.-Q.; Chen, P.; Xiao, X.; Li, S.-N.; Chen, Y. Carbon Nanobowl Supported Chemically Functionalized PtRh Nanocrystals: A Highly Active and Methanol Tolerant Electrocatalyst Towards the Oxygen Reduction Reaction. *J. Mater. Chem. A.* **2021**, *9*, 25621–25628.
- [272] Gupta, S.; Qiao, L.; Zhao, S.; Xu, H.; Lin, Y.; Devaguptapu, S. V.; Wang, X.; Swihart, M. T.; Wu, G. Highly Active and Stable Graphene Tubes Decorated with FeCoNi Alloy Nanoparticles via a Template-free Graphitization for Bifunctional Oxygen Reduction and Evolution. *Adv. Energy Mater.* **2016**, *6*, 1601198.
- [273] Yin, S.; Liu, S.; Jiao, S.; Zhang, H.; Xu, Y.; Wang, Z.; Li, X.; Wang, L.; Wang, H. Tannic Acid Decorated AuPd lavender-like Nanochains for Enhanced Oxygen Reduction Electrocatalysis. *J. Mater. Chem. A.* **2021**, *9*, 15678–15683.
- [274] Sahoo, L.; Garg, R.; Kaur, K.; Vinod, C.; Gautam, U. K. Ultrathin Twisty PdNi Alloy Nanowires as Highly Active ORR Electrocatalysts Exhibiting Morphology-Induced Durability over 200 K Cycles. *Nano Lett.* **2022**, *22*, 246–254.
- [275] Xue, Q.; Sun, H.-Y.; Li, Y.-N.; Zhong, M.-J.; Li, F.-M.; Tian, X.; Chen, P.; Yin, S.-B.; Chen, Y. Au@ Ir core-shell Nanowires Towards Oxygen Reduction Reaction. *Chem. Eng. J.* **2021**, *421*, 129760.
- [276] Ithisuphalap, K.; Zhang, H.; Guo, L.; Yang, Q.; Yang, H.; Wu, G. Photocatalysis and Photoelectrocatalysis Methods of Nitrogen Reduction for Sustainable Ammonia Synthesis. *Small Methods.* **2019**, *3*, 1800352.
- [277] Wan, Y.; Xu, J.; Lv, R. Heterogeneous Electrocatalysts Design for Nitrogen Reduction Reaction under Ambient Conditions, *Mater. Today.* **2019**, *27*, 69–90.
- [278] Chen, G. F.; Ren, S.; Zhang, L.; Cheng, H.; Luo, Y.; Zhu, K.; Ding, L. X.; Wang, H. Advances in electrocatalytic N<sub>2</sub> reduction—strategies to tackle the selectivity challenge. *Small Methods.* **2019**, *3*, 1800337.
- [279] Li, M.; Huang, H.; Low, J.; Gao, C.; Long, R.; Xiong, Y. Recent progress on electrocatalyst and photocatalyst design for nitrogen reduction. *Small Methods.* **2019**, *3*, 1800388.
- [280] Yan, D.; Li, H.; Chen, C.; Zou, Y.; Wang, S. Defect Engineering Strategies for Nitrogen Reduction Reactions under Ambient Conditions. *Small Methods.* **2019**, *3*, 1800331.
- [281] Shi, M. M.; Bao, D.; Wulan, B. R.; Li, Y. H.; Zhang, Y. F.; Yan, J. M.; Jiang, Q. Au Subnanoclusters on TiO<sub>2</sub> toward Highly Efficient and Selective Electrocatalyst for N<sub>2</sub> Conversion to NH<sub>3</sub> at Ambient Conditions. *Adv. Mater.* **2017**, *29*, 1606550.
- [282] Zhou, J.-H.; Zhang, Y.-W. Metal-based Heterogeneous Electrocatalysts for Reduction of Carbon Dioxide and Nitrogen: Mechanisms, Recent Advances and Perspective. *Reaction Chem. Eng.* **2018**, *3*, 591–625.
- [283] Wang, H.; Mao, Q.; Yu, H.; Wang, S.; Xu, Y.; Li, X.; Wang, Z.; Wang, L. Enhanced electrocatalytic performance of mesoporous Au-Rh bimetallic films for ammonia synthesis. *Chem. Eng. J.* **2021**, *418*, 129493.
- [284] Wang, P.; Nong, W.; Li, Y.; Cui, H.; Wang, C. Strengthening Nitrogen Affinity on CuAu@ Cu core-shell Nanoparticles with Ultrathin Cu Skin via Strain Engineering and Ligand Effect for Boosting Nitrogen Reduction Reaction. *Appl. Catal. B.* **2021**, *288*, 119999.

- [285] Liu, P.-Y.; Shi, K.; Chen, W.-Z.; Gao, R.; Liu, Z.-L.; Hao, H.; Wang, Y.-Q. Enhanced Electrocatalytic Nitrogen Reduction Reaction Performance by Interfacial Engineering of MOF-based Sulfides FeNi<sub>2</sub>S<sub>4</sub>/NiS hetero-interface. *Appl. Catal. B.* **2021**, *287*, 119956.
- [286] Wang, X.; Luo, M.; Lan, J.; Peng, M.; Tan, Y. Nanoporous Intermetallic Pd<sub>3</sub>Bi for Efficient Electrochemical Nitrogen Reduction. *Adv. Mater.* **2021**, *33*, 2007733.
- [287] Tong, Y.; Guo, H.; Liu, D.; Yan, X.; Su, P.; Liang, J.; Zhou, S.; Liu, J.; Lu, G. Q.; Dou, S. X. Vacancy Engineering of Iron-doped W<sub>18</sub>O<sub>49</sub> Nanoreactors for Low-barrier Electrochemical Nitrogen Reduction. *Angew. Chem. Int. Ed.* **2020**, *132*, 7426–7431.
- [288] Zhao, R.; Wang, G.; Mao, Y.; Bao, X.; Wang, Z.; Wang, P.; Liu, Y.; Zheng, Z.; Dai, Y.; Cheng, H. Li-intercalation Boosted Oxygen Vacancies Enable Efficient Electrochemical Nitrogen Reduction on Ultrathin TiO<sub>2</sub> Nanosheets. *Chem. Eng. J.* **2022**, *430*, 133085.
- [289] Tan, Y.; Yan, L.; Huang, C.; Zhang, W.; Qi, H.; Kang, L.; Pan, X.; Zhong, Y.; Hu, Y.; Ding, Y. Fabrication of an Au<sub>25</sub>-Cys-Mo Electrocatalyst for Efficient Nitrogen Reduction to Ammonia under Ambient Conditions. *Small.* **2021**, *17*, 2100372.
- [290] Liu, W.; Han, L.; Wang, H.-T.; Zhao, X.; Boscoboinik, J. A.; Liu, X.; Pao, C.-W.; Sun, J.; Zhuo, L.; Luo, J. FeMo sub-nanoclusters/single atoms for neutral ammonia electrosynthesis. *Nano Energy.* **2020**, *77*, 105078.
- [291] Zhao, L.; Liu, X.; Zhang, S.; Zhao, J.; Xu, X.; Du, Y.; Sun, X.; Zhang, N.; Zhang, Y.; Ren, X. Rational Design of Bimetallic Rh 0.6 Ru 0.4 Nanoalloys for Enhanced Nitrogen Reduction Electrocatalysis under Mild Conditions. *J. Mater. Chem. A.* **2021**, *9*, 259–263.
- [292] Tong, W.; Huang, B.; Wang, P.; Li, L.; Shao, Q.; Huang, X. Crystal-phase-engineered PdCu Electrocatalyst for Enhanced Ammonia Synthesis. *Angew. Chem. Int. Ed.* **2020**, *132*, 2671–2675.
- [293] Zhang, J.; Ji, Y.; Wang, P.; Shao, Q.; Li, Y.; Huang, X. Adsorbing and Activating N<sub>2</sub> on Heterogeneous Au–Fe<sub>3</sub>O<sub>4</sub> Nanoparticles for N<sub>2</sub> Fixation. *Adv. Funct. Mater.* **2020**, *30*, 1906579.
- [294] Guo, C.; Liu, X.; Gao, L.; Kuang, X.; Ren, X.; Ma, X.; Zhao, M.; Yang, H.; Sun, X.; Wei, Q. Fe-doped Ni<sub>2</sub>P Nanosheets with Porous Structure for Electroreduction of Nitrogen to Ammonia under Ambient Conditions. *Appl. Catal. B.* **2020**, *263*, 118296.
- [295] Zhang, X.; Feizpoor, S.; Humayun, M.; Wang, C. Urea Oxidation Reaction Electrocatalysts: Correlation of Structure, Activity, and Selectivity. *Chem. Cat.* **2024**, *4* (2), 100840.
- [296] Qiu, Y.; Zhang, J.; Jin, J.; Sun, J.; Tang, H.; Chen, Q.; Zhang, Z.; Sun, W.; Meng, G.; Xu, Q. Construction of Pd-Zn Dual Sites to Enhance the Performance for Ethanol electro-oxidation Reaction. *Nat. Commun.* **2021**, *12*, 1–9.
- [297] Luo, S.; Chen, W.; Cheng, Y.; Song, X.; Wu, Q.; Li, L.; Wu, X.; Wu, T.; Li, M.; Yang, Q. Trimetallic Synergy in Intermetallic PtSnBi Nanoplates Boosts Formic Acid Oxidation. *Adv. Mater.* **2019**, *31*, 1903683.
- [298] Yu, Z.-Y.; Lang, C.-C.; Gao, M.-R.; Chen, Y.; Fu, Q.-Q.; Duan, Y.; Yu, S.-H. Ni–Mo–O nanorod-derived Composite Catalysts for Efficient Alkaline water-to-hydrogen Conversion via Urea Electrolysis. *Energy Environ. Sci.* **2018**, *11*, 1890–1897.
- [299] Li, F.; Chen, J.; Zhang, D.; Fu, W.-F.; Chen, Y.; Wen, Z.; Lv, X.-J. Heteroporous MoS<sub>2</sub>/Ni<sub>3</sub>S<sub>2</sub> Towards Superior Electrocatalytic Overall Urea Splitting. *Chem. Commun.* **2018**, *54*, 5181–5184.
- [300] Wu, F.; Ou, G.; Yang, J.; Li, H.; Gao, Y.; Chen, F.; Wang, Y.; Shi, Y. Bifunctional Nickel oxide-based Nanosheets for Highly Efficient Overall Urea Splitting. *Chem. Commun.* **2019**, *55*, 6555–6558.
- [301] King, R. L.; Botte, G. G. Investigation of multi-metal catalysts for stable hydrogen production via urea electrolysis. *J. Power Sources.* **2011**, *196*, 9579–9584.